UCLA
UCLA Electronic Theses and Dissertations

Title
The cribriform plate: Evolution of mammalian olfaction written in bone

Permalink
https://escholarship.org/uc/item/37334238

Author
Bird, Deborah Jean

Publication Date
2017

Supplemental Material
https://escholarship.org/uc/item/37334238#supplemental

Peer reviewed|Thesis/dissertation

eScholarship.org Powered by the California Digital Library
University of California

UNIVERSITY OF CALIFORNIA

Los Angeles

The cribriform plate:

Evolution of mammalian olfaction written in bone

A dissertation submitted in partial satisfaction of the requirements for the degree Doctor of Philosophy in Biology

by

Deborah Jean Bird

2017

© Copyright by

Deborah Jean Bird

2017

ABSTRACT OF THE DISSERTATION

The cribriform plate:

Evolution of mammalian olfaction written in bone

by

Deborah Jean Bird

Doctor of Philosophy in Biology

University of California, Los Angeles, 2017

Professor Blaire Van Valkenburgh, Chair

Deep inside the snout of nearly every mammal is a small, perforated bone that separates the nasal cavity from the brain case. It is called the cribriform plate (CP). Its holes, or foramina, usher olfactory nerve bundles on their path from nasal epithelium to the olfactory bulb of the brain. The imprint left in the CP bone by these nerves is the subject of this study. The size of the imprint describes the relative olfactory innervation in a given animal's nose and varies under ecological and evolutionary pressures across all mammal species. As a well-preserved, quantifiable feature of skull morphology, the CP is a potentially informative tool for comparing olfactory capacity in extant as well as extinct species. However, in general, the CP is overlooked and understudied. This study developed novel digital methods to conduct a comprehensive comparative analysis of CP morphology across species from all mammalian superorders. I further analyzed relative CP

size in the context of skull morphology, olfactory genomics, habitat, and behavior, to test the hypothesis that the CP is a valid proxy of olfactory function. I found a tight covariance between the surface area of the CP and the olfactory-related ethmoid and nasal turbinal bones. Results further revealed a strong positive relationship between relative CP size and the number of olfactory receptor genes in a species' genome. I confirmed the near or total loss of the CP in the bottlenose dolphin (*Tursiops truncatus*) and reported an unsurpassed expansion in the relative CP size of the African elephant (*Loxodonta africana*), paralleling its highly expanded OR gene repertoire. Finally, this study discovered that within Carnivora, aquatic species, which are known to forage underwater without odor cues, have significantly smaller relative CPs than their terrestrial relatives. Within the aquatic carnivoran pinnipeds and sea otter, I found that relative CP size is inversely correlated with both diving depth and duration, suggesting that secondary adaptation to life underwater, especially at depth, favored the loss of olfactory function and morphology. In summary, the morphological, molecular and ecological coherence found in this study reinforces the CP as a stand-alone proxy of olfactory capacity that can be applied to living and extinct species, allowing us to document the evolution of olfactory function within mammals over geologic time.

The dissertation of Deborah Jean Bird is approved.

Michael Alfaro

Michael McNitt-Gray

Blaire Van Valkenburgh, Committee Chair

University of California, Los Angeles

2017

DEDICATION

I dedicate this to Bill. There is no one on Earth I would rather talk science with.

TABLE OF CONTENTS

LIST OF FIGURES

LIST OF TABLES

ACKNOWLEDGEMENTS

Thank you, Dr. Blaire Van Valkenburgh, for your mentoring. I became a scientist on your watch. I am grateful and amazed in equal measure. Tony Friscia summed up graduate school perfectly on my first day in, “It is the best of times and it is the worst of times.” Thank you, Blaire, for giving me the skills to navigate the best and the worst of times. Your guidance came in the form of lightning fast feedback, shared knowledge and libraries, statistical insights, critical scientific discussions and the crucial shaping of manuscripts, talks and posters, to list just a few. It also came in the form of encouragement, perspective and a big, wide sense of humor. More than anything, I want to thank you for choosing me as a graduate student. It was an uncommon and non-traditional choice. I appreciate this.

Thanks to the rest of my committee members; Michael Alfaro for never letting me get away with assuming statistical independence when there isn’t any; Michael McNitt-Gray for fitting elephants and walruses in between patients; Robert Wayne for delivering a page full of welcome and grounding questions at my orals; David Jacobs for always pulling up a chair and asking me about my work, engaging me in wide open science talk and for asking the questions no one else does.

I am lucky to have shared space in the Van Valkenburgh lab with a most excellent army of labmates. Abigail Curtis, Caitlin Brown, Benison Pang, Mairin Balisi, Graham Slater and Tony Friscia. Thank you for talking over projects one-on-one, for the track changes, R secrets, dumplings, for co-conspiring, for making me laugh so, so hard. Abbie, you are my inspiration. I could never have not become a scientist with you sitting right next to me. Greer Dolby, thank

you for talking work and wild science into the late late evenings with me. Thank you, Tony, for making it the best of times.

In order to complete my study, I needed so many skulls and so much generosity from four collections managers and curators, Chris Conroy, Kathy Molina, James Dines and David Janiger. In scanning the skulls, I relied on the guidance of Megan Faillace, Rebecca Rudolph and Jeffrey Urbanski. Thanks to you all.

Finally, to Jocelyn Yamadera, Tessa Villaseñor, Ora Rutherford-Green, Ruth Olivas, Jonathan Rodgers, thank you for administering every bit of my progress. An awed thank you to the Department of Ecology and Evolutionary Biology, UCLA, Sigma Xi and the National Science Foundation for funding my study and making this science happen.

VITA

EDUCATION

1981 Bachelors of Science, University of Wisconsin, Madison
1974 Vordiplom, Karl Eberhardt Universität Tübingen, Biology

FELLOWSHIPS, HONORS AND AWARDS

2009-2013 National Science Foundation Graduate Research Fellowship
2011 Sigma Xi Grants-in-Aid
2011-2015 Graduate Research Support, Department of Ecology Evolutionary Biology
2013 Research Travel Grant, UCLA
2016 Dissertation Year Fellowship, UCLA

PUBLICATIONS

Bird D., Amirkhanian A., Pang B., Van Valkenburgh B. 2014. Quantifying the cribriform plate: influences of allometry, function and phylogeny. *The Anatomical Record*. **297,** 2080-2092.

Winegard, T., Herr, J., Mena, C., Lee, B., Dinov, I., Bird, D., Bernards Jr, M., Hobel, S., Van Valkenburgh, B., Toga, A. and Fudge, D., 2014. Coiling and maturation of a high-performance fibre in hagfish slime gland thread cells. *Nature communications*, 5:3534.

Van Valkenburgh B., Pang B., Bird D., Curtis A., Yee K., Wysocki C., Craven B. 2014. Respiratory and olfactory turbinals in Feliform and Caniform carnivorans. *The Anatomical Record*. **297**, 2065-2079.

Green, P., Van Valkenburgh, B., Pang, B., Bird, D., Rowe, T., Curtis, A., (2012), Respiratory and olfactory turbinal size in canid and arctoid carnivorans, *Journal of Anatomy,* 221 (3) 609-621; DOI: 10.1111/j.1469-7580.2012.01570.x

Van Valkenburgh, B., Curtis, A., Samuels, J.X., Bird, D., Fulkerson, B., Meachen-Samuels, J., Slater, G.J. (2011), Aquatic adaptations in the nose of carnivorans: evidence from the turbinates, *Journal of Anatomy,* 218 (3) 298-310

PRESENTATIONS

2016 Talk: "The bones and genes of smell: Cribriform morphology and olfactory receptor gene repertoires." International Congress of Vertebrate Morphology meeting, Washington, D.C.
2016 Talk: "The anatomy of smell: the bones and genes of it." Environmental Sciences Colloquium, UCLA.

2015 Poster: “Visualizing the olfactory imprint within mammal skull: 3D imaging and the cryptic cribriform plate.” Society of Vertebrate Paleontology meeting, Dallas, TX.
2013 Talk: “The cribriform plate as a proxy for olfactory innervation in Carnivora.” International Congress of Vertebrate morphology meeting, Barcelona, ES.
2013 Poster: “Cribriform Plate Morphology as Proxy for Olfactory Innervation in Felids and Canids,” Society of Integrative and Comparative Biology annual meeting, San Francisco
2011 Poster: “Does Cribriform Morphology Predict Olfactory Function?” Society of Integrative and Comparative Biology annual meeting, Salt Lake City
2011 Poster: “The Evolution of the Cribriform Plate in Mammals,” Ecology and Evolutionary Biology Research Symposium
2012 Poster: “The Effect of Dietary Behavior on Cribriform Plate Morphology in Canidae,” The Society of Mammalogists annual meeting.
2012 Talk, “Cribriform Morphology and Olfactory Function: A Comparative and Molecular Study,” presented at departmental bimonthly seminar.

THE ANATOMICAL RECORD 297:2080–2092 (2014)

Quantifying the Cribriform Plate: Influences of Allometry, Function, and Phylogeny in Carnivora

DEBORAH J. BIRD,* ARSINEH AMIRKHANIAN, BENISON PANG, AND BLAIRE VAN VALKENBURGH
Department of Ecology and Evolutionary Biology, UCLA, Los Angeles, California

ABSTRACT

The small, perforated bony cup of the anterior cranial fossa called the cribriform plate (CP) is perhaps the best-preserved remnant of olfactory anatomy in fossil mammal skulls. The CP and its myriad foramina record the passage of peripheral olfactory nerves from nasal cavity to olfactory bulb. Previous work has suggested that CP surface area reflects aspects of olfactory capacity (as inferred from habitat and observed behavior) in mammals. To further explore the utility of CP as a proxy for olfactory function, we designed novel, nondestructive digital methods to quantify CP morphology from dry skulls. Using CT scans and 3-D imaging software, we quantified CP features from 42 species of Carnivora, a group that represents a wide spectrum of ecologies and sensory demands. Two metrics, CP surface area (CPSA) and cumulative CP foramina area (FXSA), scaled to skull length with negative allometry, and differed between aquatic and terrestrial species, with the former having reduced areas. Number of foramina (NF) was not correlated with skull length but tended to be greater in caniforms than feliforms. Both CPSA and FXSA are well correlated with ethmoturbinal surface area, a known osteological correlate of olfactory function. This suggests that CPSA and FXSA are useful proxies for olfactory ability, especially when studying fossils or skulls in which turbinals are not preserved. Total area of CP foramina (FXSA), an exacting measure of olfactory nerve endocasts, is tightly correlated with CPSA. Because of this, it may be desirable to use CPSA alone as a proxy given that it is easier to measure than FXSA.
Anat Rec, 297:2080–2092, 2014. © 2014 Wiley Periodicals, Inc.

Key words: cribriform plate; olfaction; Carnivora; turbinal; turbinate; olfactory function

INTRODUCTION

We know little about the olfactory ecology of extinct mammals largely because we do not have an osteological proxy for olfactory ability that is likely to be preserved in fossils and that can be accessed without damaging specimens. Previous workers have relied on the relative size of the ethmoturbinal bones to infer olfactory function, or reliance on olfaction, in extant mammals (Allen, 1882; Negus, 1958; Maier, 1993; Maier et al., 1996; Smith et al., 2004; Van Valkenburgh et al., 2004, 2011; Green et al., 2012), but turbinals are fragile and rarely preserved in fossil skulls. A second possible metric, olfactory bulb vol-

Additional Supporting Information may be found in the online version of this article.

Grant sponsor: NSF Graduate Research Fellowship Program; Grant number: DGE-1144087; Grant sponsor: NSF; Grant numbers: IOB-0517748, IOS-1119768.

*Corresponding to: Deborah Bird, Department of Ecology and Evolutionary Biology, University of California, Los Angeles 90095, CA. Fax: 310-206-3987. E-mail: dbirdseed@gmail.com

Received 24 June 2014; Accepted 25 June 2014.

DOI 10.1002/ar.23032
Published online in Wiley Online Library (wileyonlinelibrary.com).

© 2014 WILEY PERIODICALS, INC.

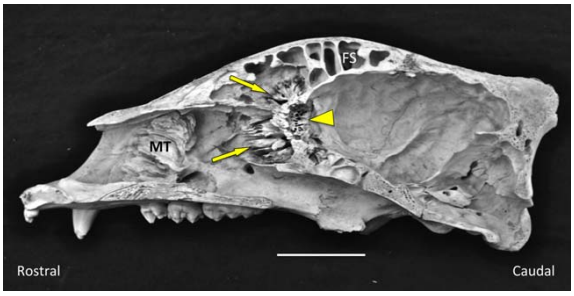

Fig. 1. Cribriform plate shown in the sagittally sectioned skull of a grizzly bear (*Ursus arctos*). Arrowhead: Caudal aspect of cribriform plate. Arrows: ethmoturbinals; MT: maxilloturbinals; FS: frontal sinus. Skull courtesy of George Stevenson and Montana Fish, Wildlife and Parks. Scale bar: 5 cm.

ume, can be approximated from fossil cranial endocasts (Gittleman, 1991), but estimates may be unreliable, as the boundaries of the olfactory bulb cavity are inconsistent (Smith and Rossie, 2006). A third metric, the relative size of the cribriform plate (CP), is more promising. CP surface area has been shown to correlate with aspects of olfactory function (Bhatnagar and Kallen, 1974; Pihlström et al., 2005) and does preserve in fossils (Joeckel et al., 1997; Hoch, 2000; Kielan-Jaworowska, 2004; Garcia et al., 2007; Godfrey et al., 2013).

The CP, or lamina cribrosa, is a perforated cup of ethmoid bone that separates the nasal chamber from the olfactory bulb in mammals (Fig. 1). The myriad CP foramina are the only points of passage for axons from olfactory sensory neurons streaming from snout to brain and so provide an osseous imprint of peripheral olfactory innervation (Farbman, 1992). Tissue passing through the CP includes small amounts of connective tissue, circulating cerebrospinal fluid, and an occasional small vessel but is predominantly made up of axon fascicles (Doucette, 1991; Silver et al., 2002; Kavoi et al., 2010). For this reason, the CP and its foramina might be a reasonable proxy for the relative number of olfactory neurons transmitting information from the nose to the olfactory bulb (Paulli, 1900; Negus, 1958).

CP morphology, specifically its size and shape as well as the distribution, number and size of its foramina, varies markedly across mammalian taxa. It is the assumption of this article that the CP is an informative feature of olfactory anatomy, that aspects of the variation in CP morphology reflect differences in olfactory function (Allen, 1882; Negus, 1958). Olfactory capabilities of mammals can be defined in many ways and have been described variously as detection sensitivity (Marshall et al., 1981; Doty et al., 1984; Meisami, 1989), odor discrimination (Friedrich, 2006), and breadth of odor reception (Saito et al., 2004). For this study we have chosen to define olfactory capacity in terms of relative reliance on olfaction, something that can best be inferred from an animal's habitat and observed behavior (Kruuk, 1972; Estes, 1989; Ewer, 1998). Previous studies have begun to link CP morphology to ecology. It has been established that the CP, a trait unique to mammals, is secondarily reduced or lost altogether in obligate aquatic species. In the toothed cetaceans or Odontoceti, for example, the CP is present as anlage in the fetus but is entirely absent in the adult animal (Buhl and Oelschläger, 1988; Oelschläger, 1992, 2000; Colbert et al., 2005). Similarly, the adult mysticetes, or baleen whales, have lost all but a very rudimentary CP (Oelschläger, 1989). In the platypus (*Ornithorynchus anatinus*), an aquatic monotreme, the signature multitude of CP foramina has devolved into a single opening, while the closely related echidna (*Tachyglossus aculeatus*) maintains a fully formed CP (Kuhn, 1971; Zeller, 1988). Among terrestrial mammals, one clade known for its developed visual anatomy, the anthropoid primates, have exceptionally small CPs (Pihlström et al., 2005; Nummela et al., 2013). Diet may also be linked to CP morphology, as one comparative study of 40 bat species showed that frugivorous bats have a higher density of CP foramina than do insectivorous species (Bhatnagar and Kallen, 1974).

In order to clarify the relationship between CP morphology and behavioral ecology and infer the relationship between CP morphology and olfactory function in living and extinct species, we need to first establish rigorous, accurate methods of quantifying variation in the CP. Previous workers have focused on the surface area of the plate and number of foramina, using internal molds or direct measurements from sectioned skulls (Bhatnagar and Kallen, 1974; Pihlström et al., 2005). However, neither of these approaches is likely to be useful for fossil specimens. The CP is located in the anterior cranial fossa and can only be seen clearly by removing the calvaria, or skull roof. The cranial and nasal cavities of a fossilized skull are typically filled with matrix, making direct access to the plate even more problematic. Previous methods of studying CP size have additional limitations. Estimates of surface area calculated from linear measurements alone may be inaccurate, because CP shape is irregular and highly variable in most dimensions. Additionally, it is impossible to quantify the finer CP features, such as the total cross-sectional area of its foramina from direct measurements. However, the CP can now be visualized using computed tomography (CT) and imaging software, thus allowing quantification of variation in CP morphology, close examination of novel features, and the potential for studying olfactory anatomy in extinct taxa.

Before attempting to infer olfactory function in fossil mammals from CP surface area and/or foramina size and number, it is essential to understand the variation in these parameters across a broad sample of living species of known ecologies and body size. Not only do we need to know how CP size and foramina dimensions vary with body size and phylogeny, but we also need to understand the relationship among the three parameters: CP surface area, total cross-sectional area of CP foramina, and foramina count. This baseline information is needed to establish expected scaling relationships and thereby allow us to identify species that deviate from the expected, presumably due to olfactory adaptations.

Here, we present the first comparative analysis of CP morphology based on CT scans across a diverse sample of mammal species, all within the order Carnivora. We chose this order in part due to the ready availability of previously scanned skulls (Van Valkenburgh et al., 2004, 2011; Green et al., 2012), but also because carnivorans vary widely in body size and CP morphology and represent disparate ecologies with differing olfactory demands (Estes, 1991; Ewer, 1998; Wilson and Mittermeier, 2009).

TABLE 1. Sample species with associated skull length (orbit to occipital condyle length: OOL), cribriform plate surface area (CPSA), total cross-sectional area of CP foramina (FXSA), total number of CP foramina (NF), and olfactory turbinal surface area (OTSA)

Code	Species	Sex	OOL: orbit to occipital length (mm)	CPSA: CP surface area (mm^2)	FXSA: foramina cross-sectional area (mm^2)	NF: number of CP foramina	OTSA: olfact. turbinal surface area (mm^2)
MME	*Mephitis mephitis*	M	56.49	334.65		338	13374.8
		F	50.05	279.35	64.08	356	7153.8
ELU	*Enhydra lutris*	M	113.93	418.79	65.44	208	6182.24
		F	106.29	373.53	53.72	274	7523.26
GGU	*Gulo gulo*	M	103.6	889.60	146.12	454	71642.28
		F	100.78	813.88	150.16	502	52550.38
LCA	*Lontra canadensis*	M	87.14	223.29	56.06	328	8299.78
		F	89.24	280.77	55.78	410	10995.26
MFR	*Mustela frenata*	M	39.05	70.43	15.06	298	1695.08
		F	31.67	49.50	11.68	270	3018.24
NVI	*Neovison vison*	M	59.96	125.09	30.74	368	4713.96
TTA	*Taxidea taxus*	M	78.09	558.62			23246.96
		F	86.3	664.17	123.36	652	22955.14
PFL	*Potos flavus*	M	66.76	268.54	67.88	308	11385.12
		F	64.56	228.84	44.46	248	12854.3
PLO	*Procyon lotor*	M	75.53	353.08	66.00	314	19399.32
		F	77.94	412.00	85.74	394	22357.16
HLE	*Hydrurga leptonyx*	M	254.23	992.41	148.94	248	65081.22
		F	273.88	973.30			42075.5
MAN	*Mirounga angustirostris*	F	181.51	388.51	41.6	94	9189.19
MTR	*Monachus tropicalis*	M	187.09	510.89			21230.51
		F	170.38	406.99	50.02	86	18048.2
ZCA	*Zalophus californianus*	M	214.3	868.25	149.30	216	17527.7
		F	155.72	599.72	105.1	236	9323.76
UAM	*Ursus americanus*	M	196.6	1607.41	486.34	606	
		F	129.79	1339.36		590	72682.8
UAR	*Ursus arctos*	U	194.8	1467.82	487.618	826	
		F	205.65	2317.92		664	143929.5
UMA	*Ursus maritimus*	M	266.74	2800.14			254792
		F	232.1	2453.58	865.22	804	
CLA	*Canis latrans*	M	105.11	918.24	144.17	540	40071.5
		F	99.9	826.96	123.46	516	46420.34
CLU	*Canis lupus*	M	135.87	1045.53	194.126	572	116248.6
		F	122.37	946.09	193.704	578	
CME	*Canis mesomelas*	U	94.17	732.03	121.046		
CSI	*Canis simensis*	U	105.64	928.92	143.244		
LPI	*Lycaon pictus*	M	114.97	799.46	162.358	450	
		F	112.9	813.55	198.072	540	70391.68
NPR	*Nyctereutes procyonoides*	M	73.98	446.45	72.39	368	16364.9
		F	68.63	391.83	78.522	392	17934.82
OME	*Otocyon megalotis*	M	73.46	332.72	64.288	350	10671.5
		F	70.24	308.27	61.04	372	13394.84
SVE	*Speothos venaticus*	M	94.5	380.41	92.724	354	19668.1
UCI	*Urocyon cinereoargenteus*	M	73.72	290.80	46.24	352	10008.84
		F	73.46	296.33	61.44	428	13855.94
VLA	*Vulpes lagopus*	M	95.76	585.36	107	604	33182.98
		F	73.73	572.38	117.68	644	27662.68
VMA	*Vulpes macrotis*	M	64	349.05	62.28	612	12824.28
		F	76.43	356.02	69.778	646	14059.76
VVU	*Vulpes vulpes*	M	84.84	636.29	193.43	578	35840.3
		F	80.06	644.19	173.128	582	33264.32
CCR	*Crocuta crocuta*	M	155.53	1074.06	175.06	244	48966.68
		F	151.54	1157.79	165.70	260	73130.6
PBR	*Parahyaena brunnea*	M	146.46	1167.44	188.88	252	89789.1
		U	151.07	1322.74	172.538	196	99297.46
HHY	*Hyaena hyaena*	M	132.92	1057.66	235.428	240	64866.06
PCR	*Proteles cristata*	F	88.09	325.32	57.692	258	12361.48
GSA	*Galerella sanguinea*	M	48.53	101.82	26.44	206	2539.22
		F	46.14	87.25	18.58	170	1526.82
SSU	*Suricata suricatta*	M	40.55	81.05	17.58		1055.72
		F	41.52	95.30	23.94		1689.46
PPA	*Panthera pardus*	M	159.66	712.55	125.14	158	73781.4
LPA	*Leopardus pardalis*	M	98.76	293.326	83.184	192	21192.06

TABLE 1. (continued).

Code	Species	Sex	OOL: orbit to occipital length (mm)	CPSA: CP surface area (mm^2)	FXSA: foramina cross-sectional area (mm^2)	NF: number of CP foramina	OTSA: olfact. turbinal surface area (mm^2)
		F	100.92	315.17			
LRU	*Lynx rufus*	M	79.13	196.54	51.01	148	14852.92
		F	94.69	184.14	49.95	170	13479.12
AJU	*Acinonyx jubatus*	M	120.46	433.79	117.98	128	43846.78
		F	112.07	369.54	96.52	116	22123.96
PCO	*Puma concolor*	M	127.47	906.49	178.12	244	85849.7
		F	124.36	686.83	154.16	220	60988.42
FSY	*Felis silvestris*	M	67.27	178.51	43.81	214	11151.94
		F	62.45	145.75	37.56	178	6309.66
PLE	*Panthera leo*	M	209.79	1046.5	242.56	216	114745.3
		F	173.97	1041.53	219.42	264	79182.04
NNE	*Neofelis nebulosa*	M	120.58	479.04	84.942	112	

The code column is a guide to species abbreviations used to identify data points on the graphs in Figs. 7–9. Gaps in the data for the finer parameters (FXSA, NF) are due to the insufficient resolution of some existing scans.

Our study had four objectives, the first of which was to establish methodologies for quantifying three key features of CP morphology (CP surface area, total cross-sectional area of foramina, total number of foramina) using high-resolution CT scans and imaging software. This proved to be a significant challenge given the intricate and complex anatomy of CPs; a single foramen on the caudal aspect may represent the confluence of multiple foramina on the rostral aspect, and the level of CT scan resolution required to visualize such minute features was difficult to achieve in our largest skulls. Having measured the three parameters, our next objective was to study the relationship among them. Does foramina number or size increase linearly with CP surface area? Does one parameter predict another? Such questions are especially important in cases where features of the CP are damaged or scan quality is poor. Our-third objective was to understand how each of the parameters scaled with body mass, and our fourth was to explore the relationship between CP data and a previously established osteological correlate of olfaction, ethmoturbinal surface area. New methods secured from this study open the door to close examination of CP morphology in both fresh heads and fossil skulls embedded in matrix. While this article does not tackle questions of olfactory function, CP data gathered from animals representing divergent olfactory ecologies provide the basis for just such studies in the future.

MATERIAL AND METHODS

Sample

We sampled 77 skulls from 42 species and six families of carnivorans (Table 1). With the exception of the tropical monk seal (*Monachus tropicalis)*, all species are extant. The sample spans a wide range of body sizes (<1 to >500 kg) and represents a cross-section of behavioral ecologies. Availability permitting, we sampled two wild-caught adult specimens, one male, one female, for each species. Most skulls were scanned at the University of Texas High-Resolution CT Scanning Facility (http://www.ctlab.geo.utexas.edu). The field of view for each scan was restricted to the CP and surrounding ethmoturbinals in order to maximize resolution. Slice thickness ranges from 15 to 250 μm. Resolution for the large ursids was not sufficient to measure the small and complex CP foramina, so these species were rescanned on the phoenix v|tome|x s^{TM} scanner at General Electric Inspection Technologies Facilities (http://www.ge-mcs.com/en/inspection-technologies.html). Slice thickness was reduced and scan resolution improved, by an order of magnitude. All University of Texas scans are available through Digimorph (http://www.digimorph.org).

A three-dimensional digital model of the CP was made from each of the scans (Fig. 2). To do so, the scan was first imported into the visualization software package Mimics 15.0 (Materialise). A threshold was chosen that best delineated bone from nonbone. Using segmentation, bone that included the CP and the most posterior ethmoturbinals was selected and committed to a 2-D mask (Fig. 2B), which was then reconstructed as a 3-D model (Fig. 2C). Once rendered, these models could be rotated and magnified, allowing close access to any feature of the CP from any vantage point.

The first metric, CP surface area (CPSA), is defined here as the area of the CP perforated by olfactory foramina. It excludes the lateral section that is perforated only by the ethmoid foramen, a large passageway for the nasociliary branch of the trigeminal nerve. Establishing an accurate measure of CP bone surface within a complex latticework of openings is prohibitively difficult (Fig. 3A), so we first create a continuous surface in Mimics 15.1 using a wrapping function that fills the foramina in the 3-D model virtually (Fig. 2B). We import the wrapped model into a second imaging program, 3-matic 7.0.1 (Materialise) and select the area (Fig. 3C). Surface area is then isolated and calculated in 3-matic based on the number of triangles selected.

The second metric, total cross-sectional area of CP foramina (FXSA), is an estimate of the relative area occupied by peripheral olfactory nerves crossing the CP from snout to brain. We devised a unique metric that quantifies a surface not of bone but of missing bone. Specifically, we applied a "necklace" or spline of coordinate points along the perimeter of each foramen in the 3-D model (Fig. 4B). Splines from all foramina are imported into Rhinoceros 4, a NURBS-based 3-D modeling software (McNeel and Associates). Rhinoceros then calculates the area of each foramen as a nonplanar

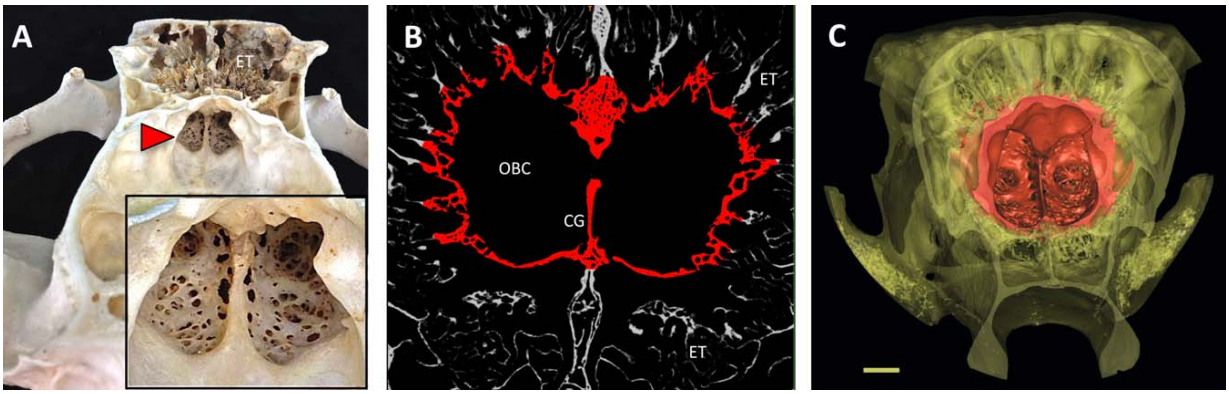

Fig. 2. Cribriform plate (CP), from bone to digital reconstruction. (**A**) Skull of grizzly bear *(Ursus arctos)* with calavaria removed, viewed from caudal aspect. Arrowhead: CP. Inset: close-up of caudal surface and foramina of CP. (**B**) Segmentation: CT scan of CP and surrounding turbinals (in coronal view) is imported into Mimics 15.0; CP bone (red) is selected and committed to 2-D mask. Scan produced on phoenix v|tome|x s^{TM} high-resolution scanner. (**C**) Reconstructed 3-D model of CP (red) seen from caudal aspect inside skull matrix (yellow). CG: crista galli; ET: Ethmoturbinals; OBC: olfactory bulb cavity. Scale bar: 1 cm.

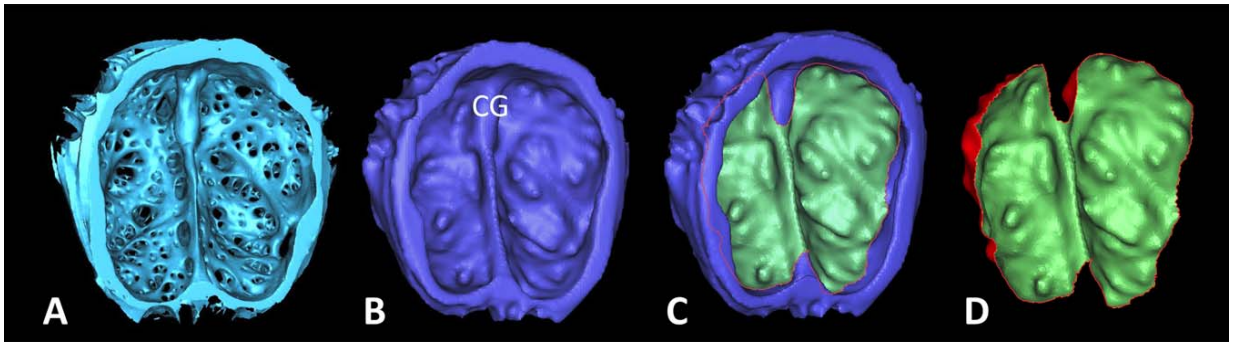

Fig. 3. Measuring CP surface area. (**A**) 3-D CP model from North American river otter (*Lontra canadensis)* made in Mimics 15.0, as viewed from caudal aspect. (**B**) A continuous surface is created in Mimics by virtually filling foramina with a wrap function. (**C**) Wrapped model is imported into 3-matic 7.0.1. Surface area of perforate zone in CP is selected. (**D**) CP surface is isolated and area calculated. CG: Crista galli.

surface between coordinate points within a voxel matrix and then totals them, giving us FXSA (Fig. 4C). In nearly all cases, splines were applied to single foramina, but wherever one foramen on the caudal aspect was made up of several foramina feeding into it from the rostral side, the single, caudal-most foramen was measured (Fig. 4B). This ensured that the cross-sectional area was measured at the narrowest passage through the bone, this being the maximum diameter available for nerve tissue crossing the CP at this point. Of our three metrics, FXSA is perhaps the closest representation of olfactory nerve bundles, but it presents two practical limitations. In addition to being time-intensive, measuring FXSA requires extra high-resolution scans. Due to the uneven quality of some of our older CT scans, FXSA data do not exist for some specimens in our sample.

To count the total number of CP foramina (NF) in each specimen, we assigned numbered points to each opening on the 3-D model and totaled these. Perforation patterns differ among species. In most cases a single opening guides a single axon bundle through the bone, but in some animals a single opening is made up of multiple foramina, all housing smaller nerve bundles that converge from anterior to posterior. Wherever the latter was the case, all converging foramina were counted (Fig. 4A).

The body size proxy used for this study was skull length as described by the distance between the anterior extent of the orbit to the posterior extent of the occipital condyle (OOL). We chose skull length over body mass because our sample included pinnipeds whose body mass is exaggerated due to their large stores of fat. Additionally, our skull length metric (OOL), which includes only the cranium, avoids the confounding effect of highly variable snout lengths among our sample species, particularly an issue among felids and canids (Van Valkenburgh, 1990). Basicranial length is often used for this same purpose. We chose to not use this metric, as it relies on sutures as its boundaries, and sutures are often fully fused and thereby difficult to delineate in adult mustelids. Skull length (OOL) was measured on 3-D digital models of full skulls. Where full skull scans

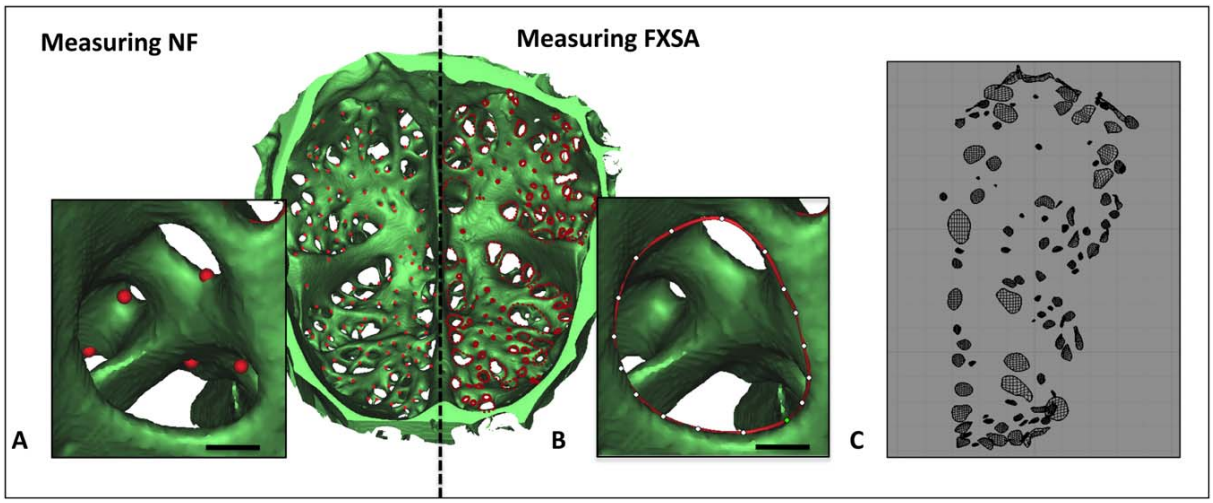

Fig. 4. Measuring foramina on a digital model of an American mink *(Neovison vison)* cribriform plate made in Mimics 15.0. Left side**:** Numbered points are assigned to all openings to quantify total number of foramina (NF). (Inset **A**) If multiple foramina converge onto a single opening, all foramina are counted. Right side: Coordinate points in a voxel matrix (splines) are drawn along the perimeter of all openings to measure foramina cross-sectional area (FXSA). (Inset **B**) if a single foramen is made up of several feed-ins, it alone is measured. Scale bar for Inserts A and B: 20 μm. (**C**) Splines are imported into imaging program Rhinoceros 4.0 where nonplanar surface areas are calculated and tallied.

did not exist for specimens, OOL was measured directly from the skulls with mechanical calipers. To test consistency, we applied both methods to two different specimens and found no significant difference.

Finally, estimates of olfactory turbinal surface area (OTSA) used in this study are taken directly from published data (Green et al., 2011; Van Valkenburgh et al., this volume). In these articles as well as ours, olfactory turbinals are defined to include the nasoturbinal bones as well as all ethmoturbinals and frontoturbinals located outside the respiratory pathway.

Statistical Analysis

Species means were derived for FXSA, NF, CPSA and olfactory turbinal surface area (OTSA) as well as the body size proxy, OOL. With the exception of the number of foramina (NF), all species means were log transformed to normalize the data. To view the scaling relationships between the CP features and body size, each CP measure was plotted against OOL. Linear regressions between each of the olfactory variables were performed to determine whether the CP and turbinal data reinforce each other. In all cases, generalized least squares (GLS) regressions were performed in R (R Code Team, 2012).

To account for phylogenetic relatedness and covariance among taxa, we constructed a time-calibrated phylogeny specific to this study. For this, we trimmed taxa from a recently constructed Carnivora phylogeny (Slater and Friscia, unpublished), an extension of the caniform phylogeny published by Slater et al. (2012). We then performed phylogenetic generalized least squares (PGLS) analyses (R Caper package) to reexamine relationships between all variables. If CP morphology has evolved under the significant influence of phylogeny, we expect that Pagel's lambda will not be significantly different from one. As all of the variables are shown to be under strong phylogenetic influence, slope and correlation r^2 values reported in the text are derived from regressions in which phylogeny is accounted for (PGLS). For visualization purposes, however, GLS plots are shown in Figs. 7–9.

RESULTS

Qualitative Observations

Using high-resolution CT scans and imaging software we transformed the CPs of 76 carnivorans into discrete digital 3-D models within virtual skull matrices. Visible from every vantage point and measurable with new digital applications, these 3-D reconstructions give us an accurate picture of the gross and fine comparative anatomy of the CP. Close examination of the 3-D models allowed us to define general features of CP morphology in Carnivora. In all specimens observed, the CP can be described as a perforated concavity in the ethmoid bone at the posterior most extent of the nasal cavity. Struts of imperforate bone reinforce the perforated surface from lateral to medial. On the rostral aspect, the plate is bisected along the midline by the perpendicular ethmoid bone of the nasal septum, on the caudal side by the crista galli. On either side of the crista galli is a distinctly linear series of large foramina (Fig. 5). Generally, one or two pairs of these medial most foramina open into deeper tunnels of bone that project into the nasal chamber. Multiple foramina converge from anterior to posterior into these paired tunnels. The location of these tunnel-like foramina within the dorsal half of the CP is intriguing because it matches early illustrations and descriptions of the specific point at which axon bundles streaming from the vomeronasal organ cross from the nasal septum to the cranium (McCotter, 1912).

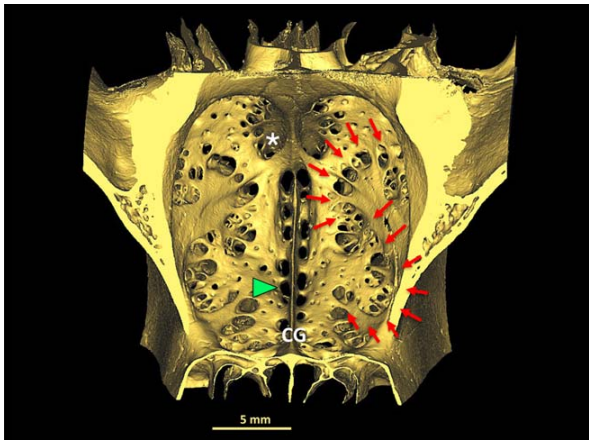

Fig. 5. Foramina distribution patterns shown in an aardwolf *(Proteles cristata)* cribriform plate. The crista galli (CG) divides the CP bilaterally. Two rows of foramina line either side of midline in all carnivoran CP (green arrowhead). Cribriform plates are often perforated along the dorsomedial midline by a pair of deep tunneling foramina (asterix). These openings extend rostrally in osseous canals that straddle the perpendicular ethmoid plate of the nasal septum. All feliform CP share a sigmoidal pattern of foramina (red arrows).

Determining with certainty whether any of the CP foramina are dedicated exclusively to vomeronasal nerves will require concurrent dissection and modeling of CP from fresh heads in a future study.

Several general patterns of variation in CP morphology stood out in our initial qualitative observations of the 3-D models. In contrast to its enduring description as a plate, CP shape appears in fact to be highly variable in all dimensions. Within the constraints of bilateral symmetry, the shape defined by the caudal surface area of the CP is irregular and ranges from deep (anterior to posterior) and roughly spherical in the polar bear (*Ursus maritimus)* to shallow and kidney-shaped in the elephant seal (*Mirounga angustirostris)*, showing just two examples (Fig. 6A-C). The crista galli, a ridge marking the division between the two lobes of the olfactory bulb (OB), is morphologically diverse as well. Wide enough to fully separate the OB lobes in the elephant seal (Fig. 6B), the crista galli is nearly absent in some carnivorans, such as the slender mongoose (*Galerella sanguinea)*. Perhaps the most variable aspect of CP morphology is the pattern of its perforations, that is, the size, number and distribution of its foramina. Qualitative observations suggest that CP in closely related species tend to have similar patterns of foramina distribution. Canid CP, for example, appear to have a characteristically dense distribution of foramina, many of which are relatively small, while feliform plates share a lower density pattern of larger holes distributed in a sigmoidal pattern along its lateral aspect (Fig. 5). In exceptional cases, closely related species have markedly different CP shape and foramina distribution. For example, the contrast between the wolverine's (*Gulo gulo*) deeply cupped, highly perforated CP and the flattened, sparsely perforated plate of the sea otter (*Enhydra lutris*) likely reflect differences in olfactory capacity and/or skull shape constraints.

Scaling CP Metrics With Body Size

Inferring olfactory function from our three CP metrics is beyond the scope of this article, but as a first step in this direction, we examine the scaling relationships between each of the variables and body size. The total area of the CP foramina (FXSA) scales to our body size proxy, orbit to occipital condyle length (OOL), with negative allometry ($r^2 = 0.67$, slope = 1.70). The slope is significantly less than expected under geometric similarity and indicates that larger animals have relatively smaller CP for their size (Fig. 7A). Surface area (CPSA) appears to scale to OOL ($r^2 = 0.77$) with slightly less negative allometry and a slope of 1.80 (Fig. 7B). Much of the noise, or scatter in these two plots can be attributed to the low CPSA and FXSA values for the phocid pinnipeds, the elephant seal (MAN, *M. angustirostris*), tropical monk seal, (MTR, *Monachus tropicalis*) and leopard seal, (*HLE, Hydrurga leptononyx*), and very high FXSA values for the grizzly bear (UAR, *Ursus arctos*), polar bear (UMA, *Ursus maritimus*), black bear (UAM, *Ursus americanus*) and red fox (VVU, *Vulpes vulpes*; Fig. 7A,B). Scatter is more pronounced for FXSA than CPSA, particularly evident in the spread between the largest caniforms, the pinnipeds and ursids (Fig. 7A). In both FXSA and CPSA plots, the caniforms tend to ride above the regression line with the exception of the aquatic and semi-aquatic species. In contrast, the feliforms tend to fall below the regression line with the exception of the three carnivorous hyaenids (CCR, HHY, PBR) and the mountain lion (PCO, *Puma concolor*). Finally, among our three metrics, total number of CP foramina (NF) stands out for its weak relationship to skull length ($r^2 = 0.15$, $P = 0.007$). Disregarding the scant correlation to skull length, we can see that absolute NF values separate caniforms into aquatic and nonaquatic in concordance with the other two parameters, but that in contrast to FXSA and CPSA, NF values rank all feliforms together as sharing CP morphology with relatively few perforations (Fig. 7C).

Relationships Among the CP Metrics

Each of the three CP variables was viewed in relationship to one another.

What first stands out among these comparisons is the strong positive correlation between CPSA and the totaled area of its foramina (FXSA), with 90% of the variation in FXSA explained by CPSA (Fig. 8A). CP surface area predicts the total area of its foramina. Interestingly, some of the same species deviate from the expected as those that do when FXSA is regressed against skull length, two ursids (UAM, UMA) and two phocid pinnipeds (MAN, MTR). Plotting the total number of CP foramina (NF) against CPSA (Fig. 8C) shows a far weaker, yet significant, relationship ($r^2 = 0.30$ $P < 0.001$). A slightly stronger correlation exists between NF and FXSA, with approximately 35% of the variation in NF

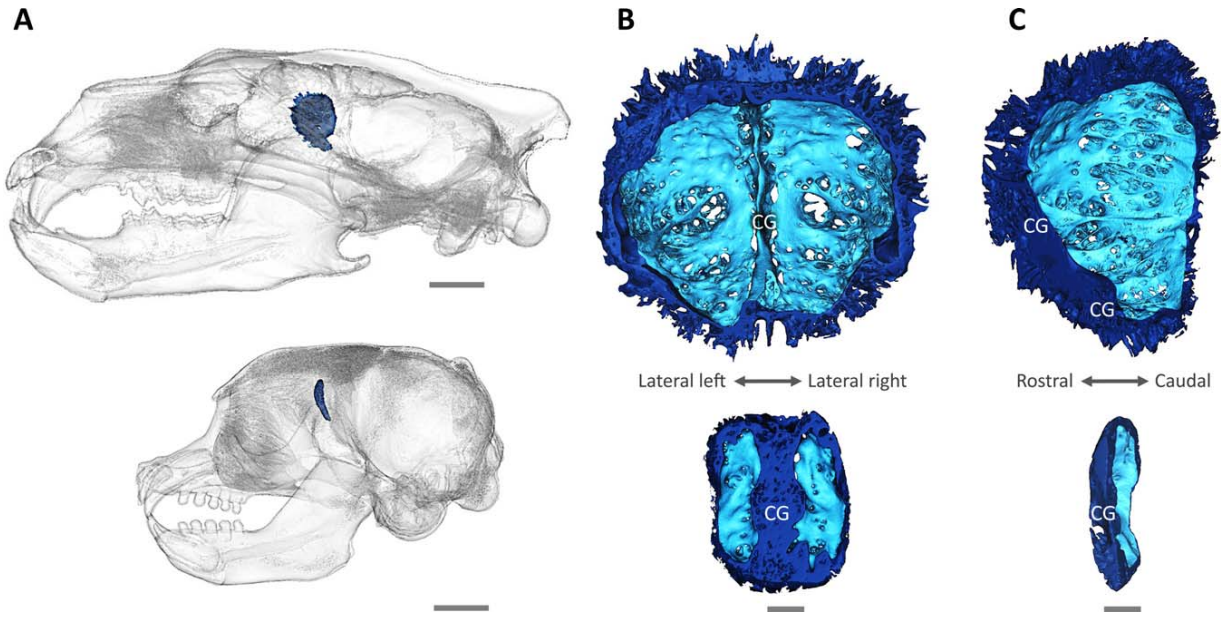

Fig. 6. Examples of CP shape variability. Top row: polar bear *(Ursus maritimus*); bottom row: elephant seal *(Mirounga angustirostris)*. (Left column **A**) Cribriform plate (dark blue) viewed within the skull. (Middle column **B**) Caudal view of CP showing the concave housing for the olfactory bulb. Dark blue: rostral aspect of plate with attached turbinal fragments; light blue: caudal CP surface. Polar bear CP (top) is 23.22 mm at its widest from crista galli to lateral extent. Elephant seal (bottom) CP is 5.56 mm at its widest from crista galli to lateral extent. (Right column **C**) Sagittally sectioned CP as viewed from the midline (CG: crista galli). The polar bear CP cavity is deep (24.66 mm rostral-caudal) and roughly semispherical; the elephant seal CP is shallow (7.72 mm rostral-caudal) and roughly kidney shaped. Irregularity in CP shape suggests that CP surface is more accurately captured by digital methods than previous linear measurements. Scale bars: (A) 20 mm; (B, C) 5 mm.

explained by FXSA (Fig. 8B). In both NF plots, all feliforms, including the hyaenids, tend to group with the aquatic caniforms as having reduced NF relative to the terrestrial caniforms (Fig. 8A,B).

Olfactory Turbinals

Finally, we investigated the relationship between the CP and an established osteological correlate of olfactory capacity, the ethmoturbinal surface area (Van Valkenburgh et al., 2004, 2011; Green et al., 2012). Developmentally related as two components of one ethmoid bone (De Beer, 1937; Rowe et al., 2005), the CP and the ethmoturbinals are functionally connected as well. Scrolls of turbinal bones on the anterior surface of the CP are covered in part by olfactory epithelium, a carpet of olfactory sensory neurons that send fascicles of axons through the CP foramina to the brain. For our PGLS regressions we use published data on the total surface area of fronto-ethmoturbinals and nasoturbinals in carnivorans (OTSA; Van Valkenburgh et al., 2004, 2011; Green et al., 2012). Among our regressions we find a tight correlation between total foramina area (FXSA) and OTSA ($r^2 = 0.87$, Fig. 9A). Ursids stand out as having higher FXSA than might be expected from the turbinal data. A very similar tight relationship exists between CP surface area (CPSA) and OTSA ($r^2 = 0.88$, Fig. 9B). Here, the California sea lion (ZCA, *Zalophus californianus)* is anomalous with an unexpectedly large CP surface area in relationship to OTSA. We can conclude that both FXSA and CPSA can be estimated from olfactory turbinal surface area in these carnivorans. CP surface area and FXSA scale to OTSA with strong negative allometry (Table 2). This relationship might be expected, as FXSA and CPSA more directly represent the presence of olfactory tissue than OTSA (turbinals are only partially covered in olfactory epithelium), and because sensory tissue is known to scale with extreme negative allometry across large body size ranges (Jerison, 1973; Menco, 1980; Nummela, 1995). Of the three CP variables, number of foramina (NF) has the weakest relationship to turbinal surface area, with only 36% of the variation in NF explained by turbinal surface area (Fig. 9C). This mirrors the previous pattern in which NF is decoupled from other CP metrics (Fig. 8B,C).

DISCUSSION

Qualitative Observations

Often the stepchild of olfactory anatomy, the CP is rarely described in the literature (Allen, 1882; McCotter, 1912; Radinsky, 1969; Kuhn, 1971; Wall, 1980; Rowe et al., 2005; Zeller, 1988; Smith and Rossie, 2006). Even rarer are comparative studies of specific features of CP morphology over a large number of taxa (Bhatnagar and Kallen, 1974; Pihlström et al., 2005). Results from the present study have created the basis for consistent, close examination of CP morphology across many species of living as well as extinct mammals. Our study confirms that variation in CP morphology is pronounced and that this variation is measurable using a nondestructive, digital approach. Novel methods established in our study

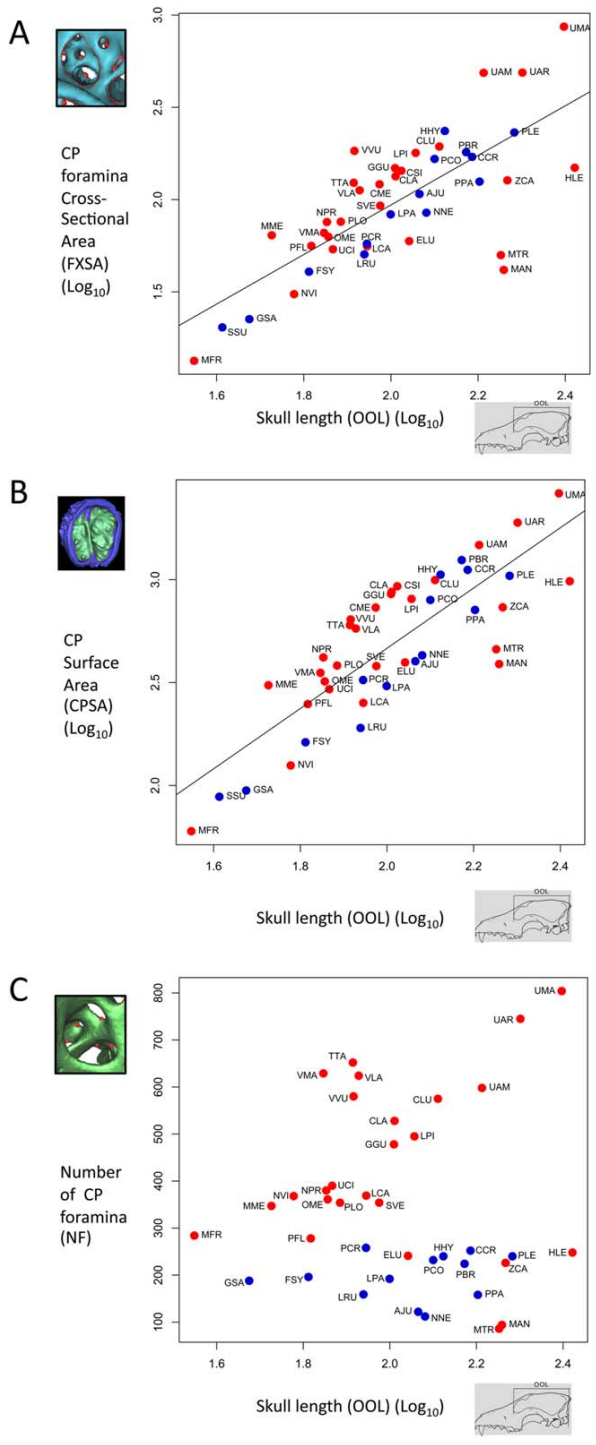

Fig. 7. Generalized least squares regression plots of cribriform plate (CP) parameters against estimated body size. Skull length (orbit to occipital condyle length: OOL) is used as a proxy for body size. All parameters in (A)–(C) are log_{10}-transformed with the exception of number of foramina (NF). Red circles are caniforms; blue circles feliforms. See Table 1 for species codes and Table 2 for summary statistics.

enabled both full visualization of CP gross anatomy and the quantification of its finer-scaled features. This work was performed on 42 carnivoran species of known ecologies and body size as a first step toward establishing CP metrics as proxies for olfactory function.

Our general observations of CP gross anatomy contradict earlier assumptions about CP shape. Beyond shared bilateral symmetry and concave caudal surface, CP shape does not appear to be generalizable. This has a bearing on which methods most accurately measure CP size, specifically CP surface area. Previous estimates of CP surface area, calculated from linear measurements alone, relied on an assumption that the CP could be summarized as an oblate ellipsoid (Pihlström et al., 2005). Our CPSA values were consistently higher than Pihlström et al.'s among the 17 species found in both our studies, with increases ranging from a factor of 0.25–1.57. One might expect this, as measurements taken from digital reconstructions account for the specific shape profile of each CP, while linear estimates are derived from equations that fit a single gross shape. While we do not attempt to quantify shape differences in this article, it is evident from initial examination of 77 CP models made from CT scans that CP morphology is irregular in all dimensions and as such is most accurately quantified using a digital approach.

The CP belies its given name. It is far from flattened or plate shaped. Instead it has dimensionality. In some species, as in the ursids, the CP is a pronounced concavity while in others it is a shallower trough. But in all cases it is a kind of cup surrounding the olfactory bulbs. If anything, the CP might be better named "cribriform cup" or "cribriform calyx."

Establishing Digital Methods

With the aid of CT scans and imaging software, we designed digital methods that made possible for the first time nondestructive quantification of two features of CP morphology, the number of CP foramina (NF) and their cumulative cross-sectional area (FXSA). One previous study successfully counted CP foramina in 40 bat species, but because of the limitations of direct measurement, the cryptically located CP had to first be removed, thereby compromising the future research potential of the skulls (Bhatnagar and Kallen, 1974). Likewise, an earlier effort to quantify the area of CP foramina was restricted to an analysis of photographs taken from sectioned skulls (Kalmey et al., 1998). In contrast to both of these methods, we used as our reference digital 3-D models of CPs rendered directly from the voxel matrices of CT scans. In this way, CP foramina were measured from coordinate points we placed along the perimeter of each opening within the model, a method that can be performed on a large number of animals with no damage to the original specimens. The nondestructive methods developed in this study for visualizing and quantifying all dimensions of CP foramina are a necessary advance if we are to conduct comparative studies on CP morphology from museum specimens, rare species and fossils.

Relationship Among Three CP Metrics

If we expect variation in CP morphology to reflect aspects of olfactory capacity, as is asserted in the

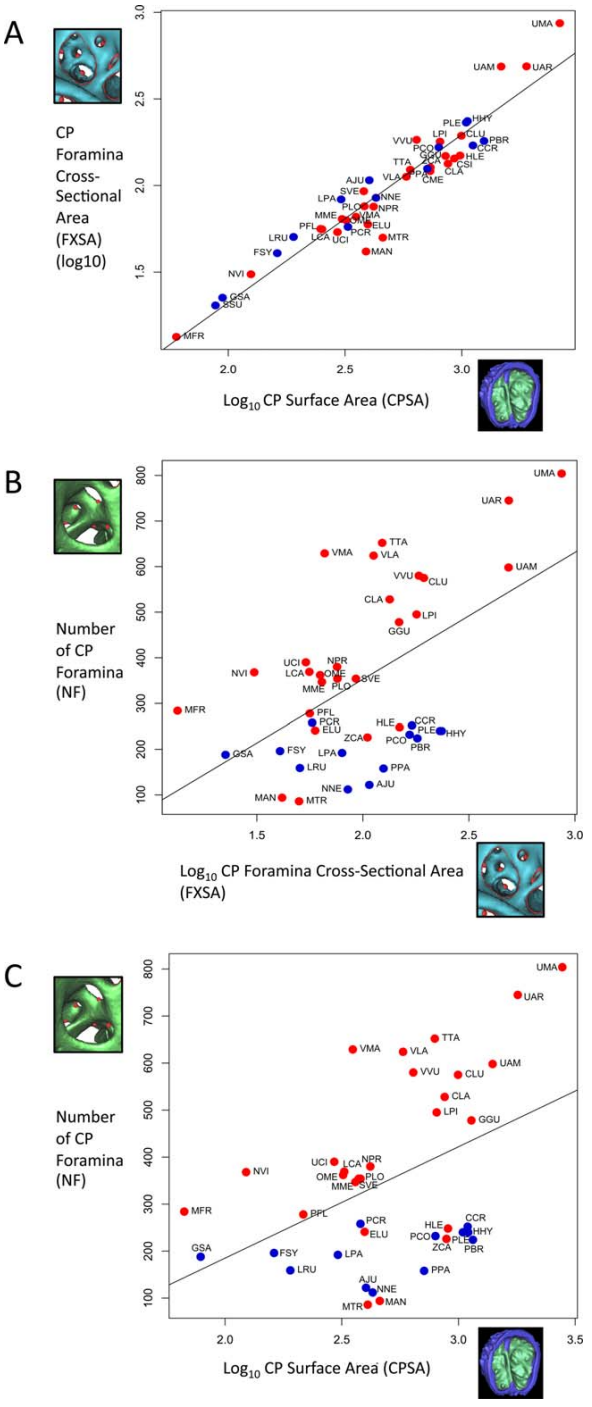

Fig. 8. Pair-wise regression plots of three cribriform plate (CP) metrics. Surface area variables (FXSA, CPSA) are $\log_{10}$-transformed; number of foramina (NF) is not. Red circles are caniforms; blue circles feliforms. See Table 1 for species codes and Table 2 for summary statistics.

literature (Negus, 1958; Bhatnagar and Kallen, 1974; Kalmey et al., 1998; Pihlström et al., 2005), we might in turn expect the three variables measured in this study, CPSA, FXSA and NF, to be strongly correlated and to predict one another. In fact, the relationships between the three metrics are not equally strong. While the metrics all reinforce each other, the only truly predictive relationship is between CP surface area and foramina cross-sectional area with 90% of the variation in FXSA explained by surface area. The relationship between NF and the other two variables is significant but far weaker. The strong correlation between CPSA and FXSA is notable for several reasons. First, as a collective endocast of the nerve fibers coursing through the CP, FXSA might be considered to be a more direct representation of peripheral olfactory innervation and function, and as such a more informative metric than either CP surface area or olfactory turbinal surface area. Supporting this is the fact that material contained in CP foramina is made up almost exclusively of nervous tissue, specifically olfactory axon fascicles, ensheathing cells, cerebrospinal fluid, and an occasional very small vessel (Doucette, 1991; Farbman, 1992; Silver et al., 2002; Kavoi et al., 2010). Relative size of axon bundles crossing the plate corresponds to the area and density of olfactory sensory neurons (OSN) found on the olfactory nasal epithelium, and in turn, OSN density is known to determine olfactory sensitivity (Apfelbach et al., 1991; Kandel et al., 2000). With its direct relationship to olfactory nerve tissue, FXSA might be viewed as a more rigorous metric of olfactory function than plate size. Whether this is the case remains to be tested in future functional studies, but it is evident from this study that the finer-scaled FXSA reinforces the coarser-scaled CPSA across our entire sample of carnivorans. Second, this strong relationship between FXSA and CPSA is important when considering undertaking large-scale comparative studies of CP morphology. In contrast to the relatively simple steps of determining CP surface area, securing an accurate measurement of the cumulative foramina area is a labor- and time-intensive process that demands particularly high-resolution scans. Such scans can be expensive and data-rich as well, making them somewhat cumbersome to work with. Our results here suggest that in future studies we can rely largely on quantifying CPSA and reinforce this with FXSA quantification in a smaller number of specimens. This is the approach we are currently using in a study we have begun on the relationship between CP morphology and olfactory gene repertoire, in which a number of the sample species, such as the armadillo (*Dasypus novemcinctus*) and cow (*Bos taurus)*, have exceptionally intricate and numerous foramina. Finally, and most importantly, our results indicate that when we apply our methods to CP morphology in fossils, CPSA can be substituted for FXSA wherever plates are damaged or foramina obscured by matrix.

The weak relationship between NF and the other two variables confounds any easy assumption that the total number of CP foramina alone predicts olfactory ability. The relationship between NF and FXSA makes sense in light of the general perforation patterns observed in the CP. Not all foramina are created equal. For example, in our study, wherever numerous rostral openings converged onto a single caudal foramen, we counted all

TABLE 2. Summary statistics for phylogenetic least squares regressions between all parameters

Regression	Analysis	r^2	Slope	*P* value	Pagel's lambda	Lambda lower bound = 0	Lambda upper bound = 0
FXSA vs. OOL	PGLS	0.67	1.7	<0.001	0.96	<0.001	0.35
CPSA vs. OOL	PGLS	0.77	1.8	<0.001	1.00	<0.001	1.00
NF vs. OOL	PGLS	0.15	284	0.007	1.00	<0.001	1.00
FXSA vs. CPSA	PGLS	0.90	0.93	<0.001	0.64	0.02	0.003
NF vs. FXSA	PGLS	0.35	201	<0.001	1.00	<0.001	1.00
NF vs. CPSA	PGLS	0.30	198	<0.001	1.00	<0.001	1.00
FXSA vs. OTSA	PGLS	0.87	0.68	<0.001	0.60	0.015	<0.001
CPSA vs. OTSA	PGLS	0.88	0.69	<0.001	1.00	0.001	1.00
NF vs. OTSA	PGLS	0.36	155	<0.001	1.00	<0.001	1.00

All correlations were significant at the 0.05 level. Pagel's lambda values are relative measures of phylogenetic influence on the data, ranging from zero (no influence) to one (strongest influence). Lower and upper bound *P* values indicate whether lambda values are significantly different from lower bound zero or upper bound one. Phylogeny has a strong influence on all parameters.

foramina toward the NF total but we only measured the caudal-most foramen for the FXSA total, as this foramen area best describes the space constraint for axons crossing the CP at this particular point. Two equal cross-sectional areas can be comprised of one or many foramina.

Using NF as a proxy for olfactory function proves to be problematic for two additional reasons. In some species, especially within the nonaquatic caniforms, there is a small swath of bone in the CP perforated by unusually small foramina (on the order of 10–25 μm in diameter). Whether these particularly small foramina serve a function separate from axon transport, such as drainage of cerebrospinal fluid (Silver, et al., 2002), remains to be seen and can only be solved with a much needed histological examination of the CP. These myriad little perforations amount to negligible cross-sectional area but contribute a sizable number to NF total and so partially account for an inflated NF relative to FXSA in terrestrial caniforms (Fig. 8B). This problem might be alleviated by not counting foramina under a certain size. There was a second obstacle to collecting consistent NF data. Because the smallest foramina can only be visualized in scans of very high resolution, it is possible that foramina in some specimens were undercounted solely due to inadequate scan quality. Intraspecific variation was pronounced in our NF results and may be attributable to this issue. This can only be tested by conducting a future CP study across a number of individuals of a single species.

The relationship between total number and total area of CP foramina is particularly weak within the feliforms. On the one hand, NF in all four species of hyaenids is similar to that among fellow feliforms, in which all share a common pattern of low foramina density. But in their FXSA and CPSA, the three carnivorous hyaenids rank among the canids and stand apart from other feliforms, even their own closest relative, the insectivorous aardwolf (Fig. 7A,B). This suggests that NF is determined by phylogeny, as much or more than function. High lambda values in all PGLS regressions involving NF suggest this may be the case (Table 2), but this needs further investigation.

Relationship Between CP and Olfactory Turbinals

To test assumptions that CP morphology reflects olfactory function (Negus, 1958; Bhatnagar and Kallen, 1974; Pihlström et al., 2005) we viewed all three CP metrics in relationship to an established osteological correlate of olfactory capacity, olfactory turbinal surface area (Van Valkenburgh et al., 2004, 2011; Green et al., 2012). Results show a tight correlation between olfactory turbinal surface area and two of the CP metrics, suggesting that both CP surface area (CPSA) and foramina cross-sectional area (FXSA) might be used as additional proxies for olfactory capacity. When conducting comparative studies of olfactory function among living mammals, it might be preferable to consider all aspects of nasal skull morphology, turbinals as well as CP features, but among extinct mammals this is rarely an option. Fragile turbinals are most often broken or missing in fossils skulls, leaving the relatively robust CP as the best-preserved feature of olfactory skull morphology. Our results show a strong correlation between olfactory turbinal surface area and CP surface area and foramina, reinforcing the prospects of studying olfactory function from fossils in which turbinals are destroyed and only the CP is intact.

Future Work

This study examined scaling relationships for the three CP metrics to skull length as a way to begin evaluating how CP morphology varies across species. The variation in CP morphology evident in Fig. 6A–C will be tested against what we know about the olfactory behavior, ecology and genomics of species. Using parameters established in this study, we will compare CP morphology in ecological groupings that reflect a spectrum of olfactory demands, such as aquatic and terrestrial species. Already our results appear to differ sharply from conclusion drawn by Pihlström and colleagues, from their 2005 study, that the CP surface area of the pinniped species in his sample do not markedly deviate from that of terrestrial mammals. The data from our article need further analysis to quantitatively test this conclusion. As a way of comparing olfactory behavior we will study the CP morphology among predators that use disparate hunting strategies, one more reliant on scent (for example, canids) and the other on sight (for example, felids). Finally, we are beginning to explore the relationship between the olfactory genomics and CP morphology in mammal species whose olfactory gene repertoires are known (Olender et al., 2003; Niimura and Nei, 2005, 2007; Kishida et al., 2007; Hayden et al., 2010).

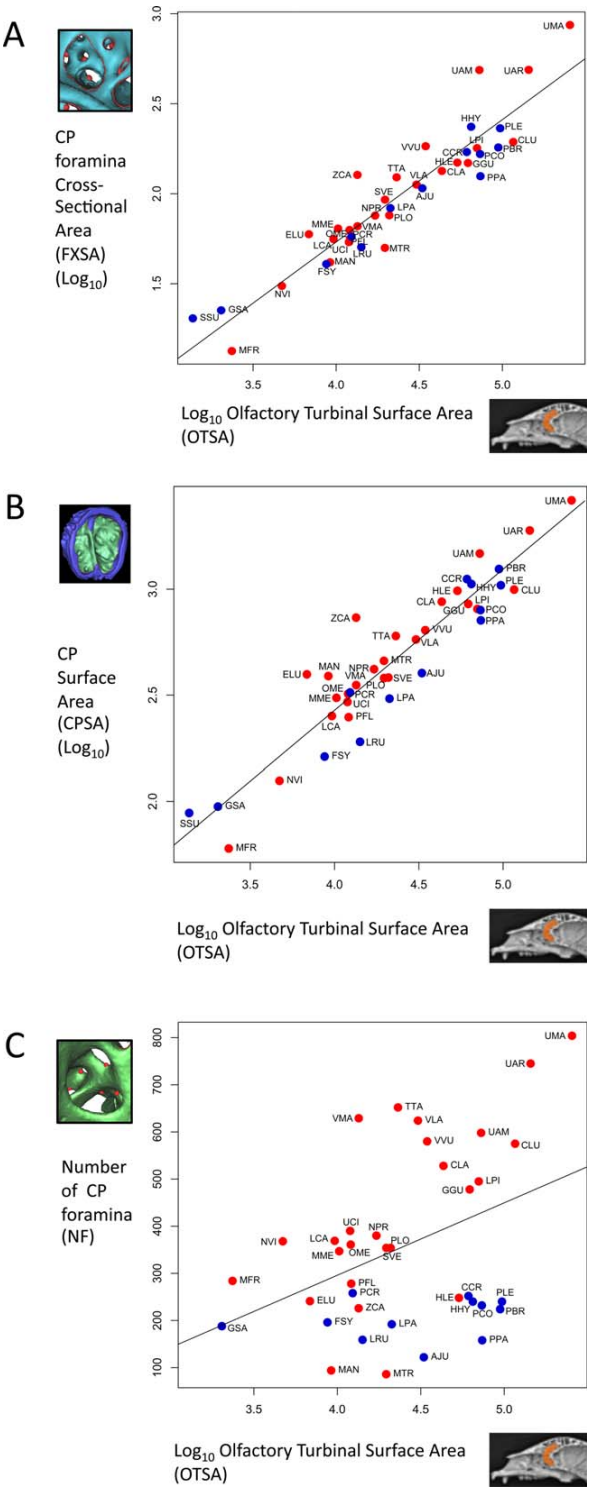

Fig. 9. Generalized least squares regression plots of cribriform plate CP) parameters against olfactory turbinal surface area (OTSA). Surface area variables (FXSA, CPSA) are $\log_{10}$-transformed; number of oramina (NF) is not. Red circles are caniforms; blue circles feliforms. See Table 1 for species codes and Table 2 for summary statistics.

A sense of smell is critical for most mammals. Olfactory systems have evolved to operate in distinct ecologies: as lineages, landscapes and chemical stimuli change over evolutionary time, species have acquired and lost particular traits of olfactory anatomy. Living animals offer us tissue with which to study these gathered olfactory adaptations, extinct species only the imprint of that tissue in the bone. Yet this bone is informative. The CP is the only feature that explicitly documents the trail left by olfactory nerves. This trail is quantifiable and comparable across extant species whose olfactory behavior and genomics we can witness. If such functional studies in living mammals establish CP morphology as a proxy for olfactory capacity, we can use novel digital methods developed in these study to examine CP features in detail in fossils. In this way, CP morphology might offer us a new osteological insight into the olfactory ecology of extinct animals.

ACKNOWLEDGMENTS

We thank M. Colbert, R. Ketcham, and J. Maisano of the University of Texas HRCT Digital Morphology group for their skill and care in producing CT scans, M. Faillace, R. Rudolph, and J. Urbanski of General Electric Inspection Technologies for their assistance, patience, and precision in producing high-res CT scans, George and Jana Stevenson for the loan of bear skulls, curators, and collection managers who lent us skulls; for scanning, G. Slater and A. Friscia for their carnivoran phylogeny, and finally L. Rosales, Y. Davydov, N. Goody, and P. Green for their cumulative years of data collection.

LITERATURE CITED

Allen H. 1882. On a revision of the ethmoid bone in the Mammalia, with special reference to the description of this bone and of the sense of smelling in the Cheiroptera. Cambridge: Harvard University Press.

Apfelbach R, Russ D, Slotnick BM. 1991. Ontogenetic changes in odor sensitivity, olfactory receptor area and olfactory receptor density in the rat. Chem Senses 16:209–218.

Bhatnagar KP, Kallen FC. 1974. Cribriform plate of ethmoid, olfactory bulb and olfactory acuity in forty species of bats. J Morphol 142:71–89.

Buhl H. and Oelschläger HA. 1988. Morphogenesis of the brain in the harbour porpoise. J Comp Neurol 277:109–125.

Colbert MW, Racicot R, Rowe T. 2005. Anatomy of the cranial endocast of the bottlenose dolphin, *Tursiops truncatus*, based on HRXCT. J Mamm Evol 12:195–207.

De Beer SG. 1937. The development of the vertebrate skull. Oxford: Clarendon Press.

Doucette R. 1991. PNS-CNS transitional zone of the first cranial nerve. J Comp Neurol 312:451–466.

Doty RL, Shaman P, Dann M. 1984. Development of the University of Pennsylvania smell identification test: a standardized microencapsulated test of olfactory function. Physiol Behav 32: 489–502.

Estes JA. 1989. Adaptations for aquatic living by carnivores. In: Gittleman JL, editor. Carnivore behavior, ecology, and evolution. Ithaca: Cornell University Press. p 242–282.

Estes RD. 1991. The behavior guide to African mammals: including hoofed mammals, carnivores, primates. Berkeley: University of California Press.

Ewer RF. 1998. The carnivores. Ithaca: Cornell University Press.

Farbman A. 1992. Cell biology of olfaction. Cambridge: Cambridge University Press.

Friedrich RW. 2006. Mechanisms of odor discrimination: neurophysiological and behavioral approaches. Trends Neurosci 29: 40–47.

Garcia N, Santos E, Arsuaga JL, Carretero JM. 2007. Endocranial morphology of the *Ursus deningeri* von Reichenau 1904 from the Sima de Los Huesos (Sierra de Atapuerca) Middle Pleistocene site. J Vert Paleontol 27:1007–1017.

Gittleman JL. 1991. Carnivore olfactory bulb size: allometry, phylogeny, and ecology. J Zool 225:253–272.

Godfrey SJ, Geisler J, Fitzgerald EM. 2013. On the olfactory anatomy in an archaic whale (Protocetidae, Cetacea) and the minke whale *Balaenoptera acutorostrata* (Balaenopteridae, Cetacea). Anat Rec 296:257–272.

Green PA, Valkenburgh B, Pang B, Bird D, Rowe T, Curtis A. 2012. Respiratory and olfactory turbinal size in canid and arctoid carnivorans. J Anat 221:609–621.

Hayden S, Bekaert M, Crider TA, Mariani S, Murphy W, Teeling E. 2010. Ecological adaptation determines functional mammalian olfactory subgenomes. Genome Res 20:1–9.

Hoch E. 2000. Olfaction in whales: evidence from a young odontocete of the Late Oligocene North Sea. Hist Biol 14:67–89.

Jerison HJ. 1973. Evolution of the brain and intelligence. New York: Academic Press.

Joeckel RM, Bond HW, Kabalka GW. 1997. Internal anatomy of the snout and paranasal sinuses of Hyaenodon (Mammalia, Creodonta). J Vert Paleontol 17:440–446.

Kalmey JK, Thewissen JGM, Dluzen DE. 1998. Age-related size reduction of foramina in the cribriform plate. Anat Rec 251:326–329.

Kandel ER, Schwartz JH, Jessell TM. 2000. Principles of neural science. New York: McGraw-Hill.

Kavoi B, Makanya A, Hassanali J, Carlsson HE, Kiama S. 2010. Comparative functional structure of the olfactory mucosa in the domestic dog and sheep. Ann Anat 192:329–337.

Kielan-Jaworowska Z. 2004. Mammals from the age of dinosaurs: origins, evolutions, and structure. New York: Columbia University Press.

Kishida T, Kubota S, Shirayama Y, Fukami H. 2007. The olfactory receptor gene repertoires in the secondary-adapted marine vertebrates: evidence for reduction of the functional proportions in cetaceans. Biol Lett 3:428–430.

Kruuk H. 1972. The spotted hyena: a study of predation and social behavior. Chicago: University of Chicago Press.

Kuhn HJ. 1971. Die Entwicklung und Morphologie des Schädels von *Tachyglossus aculeatus*. Abhandlungen der Senckenbergischen naturforschenden Gesellschaft 528:226.

Maier W. 1993. Cranial morphology of the therian common ancestor, as suggested by the adaptations of neonate marsupials. In: Szalay FS, Novacek MJ, McKenna MC, editors. Mammal phylogeny. New York: Springer Verlag. p 165–181.

Maier W, Heever JD, Durand F. 1996. New therapsid specimens and the origin of the secondary hard and soft palate of mammals. J Zoological Systematics and Evol Res 34:9–19.

Marshall DA, Blumer L, Moulton, DG. 1981. Odor detection curves for n-pentanoic acid in dogs and humans. Chem Senses 6: 445–453.

Meisami E. 1989. A proposed relationship between increases in the number of olfactory receptor neurons, convergence ratio and sensitivity in the developing rat. Devel Brain Res 46: 9–19.

Menco BPM. 1980. Qualitative and quantitative freeze-fractured studies on olfactory and nasal respiratory structures of frog, ox, rat and dog. Cell Tiss Res 207:183–209.

McCotter RE. 1912. The connection of the vomeronasal nerves with the accessory olfactory bulb in the opossum and other mammals. Anat Rec 6:299–318.

Negus SV. 1958. The comparative anatomy and physiology of the nose and paranasal sinuses. Edinburgh: Livingstone.

Niimura Y, Nei M. 2005. Comparative evolutionary analysis of olfactory receptor gene clusters between humans and mice. Gene 346:13–21.

Niimura Y, Nei M. 2007. Extensive gains and losses of olfactory receptor genes in mammalian evolution. PLoS ONE 2:e708.

Nummela S. 1995. Scaling of the mammalian middle ear. Hear Res 85:18–30.

Nummela S, Pihlström H, Puolamäki K, Fortelius M, Hemilä S, Reuter T. 2013. Exploring the mammalian sensory space: co-operations and trade-offs among senses. J Comp Physiol A 199: 1077–1092.

Oelschläger HA. 1989. Early development of the olfactory and terminalis systems in baleen whales. Brain Behav Evol 34:171–183.

Oelschläger HA. 1992. Development of the olfactory and terminalis systems in whales and dolphins. In: Doty RL, Muller-Schwarze D editors. Chemical signals in vertebrates. Vol. 6. New York: Plenum Press. p 141–147.

Oelschläger HA. 2000. Morphological and functional adaptations of the toothed whale head to aquatic life. Hist Biol 14:33–39.

Olender T, Fuchs T, Linhart C, Shamir R, Adams M, Kalush F, Khen M, Lancet D. 2003. The canine olfactory subgenome. Genomics 83:361–372.

Paulli S. 1900. Über die Pneumaticität des Schädels bei den Säugetieren; eine morphologische Studie. Morphol Jahrb 28:147–178.

Pihlström H, Fortelius M, Hemilä S, Forsman R, Reuter T. 2005. Scaling of mammalian ethmoid bones can predict olfactory organ size and performance. Proc Royal Soc B 272:957–962.

Radinsky LB. 1969. Outlines of canid and felid evolution. Ann N Y Acad Sci 167:277–288.

Rowe TB, Eiting TP, Macrini TE, Ketcham, RA, 2005. Organization of the olfactory and respiratory skeleton in the nose of the gray short-tailed opossum *Monodelphis domestica*. J Mamm Evol 12: 303–336.

Saito H, Kubota M, Roberts RW, Chi Q, Matsunami H. 2004. RTP family members induce functional expression of mammalian odorant receptors. Cell 119: 679–691.

Slater GJ, Harmon LJ, Wegmann D, Joyce P, Revell LJ, Alfaro ME, 2012. Fitting models of continuous trait evolution to incompletely sampled comparative data using approximate Bayesian computation. Evolution 66: 752–762.

Smith TD, Bhatnagar KP, Tuladhar P, Burrows AM. 2004. Distribution of olfactory epithelium in the primate nasal cavity: are microsmia and macrosmia valid morphological concepts? Anat Rec 281: 1173–1181.

Smith TD, Rossie J. 2006. Primate olfaction: anatomy and evolution. In: Warrick B, Castle D, Pantelis C, editors. Olfaction and the brain. New York: Cambridge University Press. p 135–166.

Silver I, Kim C, Mollanji R, Johnston M. 2002. Cerebrospinal fluid outflow resistance in sheep: impact of blocking cerebrospinal fluid transport through the cribriform plate. Neuropathol Appl Neurobiol 28:67–74.

Van Valkenburgh B. 1990. Skeletal and dental predictors of body mass in carnivores. In: Damuth J, MacFadden B, editors. Body size in mammalian paleobiology: estimation and biological implication. Cambridge: Cambridge University Press.

Van Valkenburgh B, Theodor J, Friscia, A, Rowe T. 2004. Respiratory turbinates of canids and felids: a quantitative comparison. J Zool 264:281–293.

Van Valkenburgh B, Curtis A, Samuels JX, Bird D, Fulkerson B, Meachen-Samuels J, Slater GJ. 2011. Aquatic adaptations in the nose of carnivorans: evidence from the turbinates. J Anat 218: 298–310.

Wall WP. 1980. Cranial evidence for a proboscis in Cadurcodon and a review of snout structure in the family Amynodontidae (Perissodactyla, Rhinocerotoidea). J Paleontol 54:968–977.

Wilson DE, Mittermeier RA. 2009. Handbook of the mammals of the world. Vol. 1. Barcelona: Lynx.

Zeller U. 1988. The lamina cribrosa of *Ornithorynchus* (Monotremata, Mammalia). Anat Embryol 178:513–519.

CHAPTER 2

Olfaction written in bone: Cribriform plate size parallels olfactory receptor gene repertoires in Mammalia

Deborah J. Bird[1]*, William J. Murphy[2], Lester Fox-Rosales[1], Iman Hamid[1], Blaire Van Valkenburgh[1]

Affiliations:

[1]Department of Ecology and Evolutionary Biology, University of California Los Angeles, 610 Charles E. Young Dr. S., Los Angeles, CA 90095-8347, USA. [2]Department of Veterinary Integrative Biosciences, Texas A&M University, College Station, Texas 77843-4458, USA

Abstract

The evolution of the mammalian olfactory system is reflected in the striking diversity of gene repertoires, neuroanatomy, and skull morphology across living species. Olfactory receptor gene (ORG) repertoires range from a mere handful to several thousand genes. Because each ORG is expressed by a unique population of nasal olfactory sensory neurons (OSN), each newly evolved ORG likely generates new OSNs. Expanded OSN populations then leave enhanced and quantifiable impressions in the foramina of the bony cribriform plate (CP), the skull's only passageway for OSN axons crossing from snout to brain. Despite this structural and developmental connection, the relationship between ORG repertoire size and CP morphology is poorly resolved. We report here a striking linear correlation between relative CP size and number of functional ORGs across all mammalian superorders. This correlation confirms the strong developmental links in the olfactory pathway between genes, neurons, and skull morphology. The molecular and morphological coherence found here establishes CP size as a metric of olfactory function, applicable to extinct and modern species.

Introduction

Reliance on olfaction for existence varies widely across mammal species. Mammalian olfactory systems have acquired and lost olfactory traits in response to shifts in chemosensory demands over evolutionary time, resulting in extensive genomic and anatomical diversity. The

keen sense of smell shared by most mammals is mediated by the olfactory receptor gene (ORG) superfamily (Buck and Axel, 1991). Through repeated gene duplication, gene loss, and pseudogenization, ORG repertoires have diverged (Niimura and Nei, 2007) and the number of ORGs (functional as well as pseudogenes) now spans approximately two orders of magnitude across living taxa (Niimura et al., 2014; Hayden et al., 2010).

Inside the mammalian nose, or snout, ORGs are the primary agents of odor detection. Each functional ORG encodes a specific odorant receptor that is expressed in the membrane of olfactory sensory neurons (OSN) (Buck and Axel, 1991). Each OSN expresses a single ORG (Chess et al., 1994), and each ORG is carried by its own unique population of thousands of OSNs (Mombaerts et al., 1996; Bressel et al., 2015). Multiple ORG-specific populations of neurons contribute to the olfactory epithelium, which is variable in size across species (Miyamichi, 2005; Pihlström et al., 2005). The olfactory pathway is completed via axonal projections from all OSN populations that travel from the periphery through the perforate bone of the cribriform plate (CP), to reach their first relay station in the brain, the olfactory bulb (Farbman, 1992).

The CP (Figs. 2-1, 2-2) is a part of the ethmoid bone that forms early in development to surround assembling olfactory nerves (Miller et al., 2010) and is the only passageway to the brain for OSN axons in adult mammals. Consequently, its foramina, or holes, are a high-fidelity imprint of the relative innervation within an animal's snout (Bird et al., 2014) (Supplementary movie). The CP is a signature trait of the mammal lineage (Rowe, et al., 2011) and is present in all crown species, with the exception of odontocetes (toothed whales), where it is thought to have been lost (Oelschläger and Buhl, 1985). Two CP metrics, surface area and the cumulative cross-sectional area of foramina, are highly correlated and covary widely across species (Fig. 2-1),

likely reflecting the relative importance of olfaction (Bird et al., 2014). Previous studies have established a correlation between CP size and other olfactory structures, such as the surface areas of both the turbinal bones and the olfactory epithelium that covers the turbinals (Bird et al., 2014; Pihlström et al., 2005; Bhatnagar and Kallen, 1974).

The expression of individual ORGs by distinct populations of OSNs and the development of the CP bone to surround OSN axon bundles, suggest that evolutionary gains or losses in functional ORG repertoires will be manifest in skull morphology as an expansion or reduction of relative CP size. However, the relationship between CP morphology and ORG repertoire size is poorly resolved. The first and only paper to explore this relationship found a significant but weak positive correlation between absolute CP surface area and total number of ORGs that disappeared when CP size was adjusted for body size (Garrett and Steiper, 2014). One limitation of this pioneering study was its sole reliance on linear measurements to estimate the surface area of the irregularly shaped CP. Here we revisit the link between CP skull morphology and the number of olfactory receptor genes, both functional and pseudogenized (Niimura and Nei, 2007; Niimura et al., 2014; Hayden et al., 2010; Matsui et al., 2010; Montague et al., 2014; Hughes et al., 2013). We use high-resolution CT scans of skulls and 3D imaging software to carefully map only the perforate surface of the CP (Fig. 2-3) in 27 genome species with identified ORG repertoires (Supplementary Fig. 2-1, Supplementary Table 2-S1). Residuals from the regression of estimated CP surface area on body mass are used to define relative CP size, thereby correcting for effects of body size. These methods allow us to better test the hypothesis that the developmental relationship between olfactory receptor genes and olfactory sensory neurons is witnessed in skull morphology. Specifically, CP size is expected to covary with number of functional OR genes. Additionally, because a number of studies have used the percentage of OR

pseudogenes within species' genomes to infer relative olfactory function (Rouquier et al., 2000; Gilad et al., 2007; Kishida et al., 2007), we examined the relationship between pseudogenes (fraction as well as the absolute number) and CP size. Finally, we apply our new osteological metric of relative CP size to a fossil skull to produce an estimate of ORG repertoire for the extinct mammal species, sabertooth cat (*Smilodon fatalis)* and to infer *Smilodon's* reliance on olfaction compared with extant felids.

Materials and Methods

Specimen collection We sampled skulls from 27 living species with annotated genomes and OR subgenomes, plus one extinct species (sabertooth cat, *Smilodon fatalis*) without molecular data (Supplementary Fig. 2-S1). Species ranged in body mass from < 0.1 kg (little brown bat, *Myotis lucifugus*) to >2900 kg (African elephant, *Loxodonta africana*) and covered 14 mammalian orders and all four superorders (Meredith et al., 2011; Foley et al, 2016). Body mass data were taken from the primary literature for the living species (Supplementary Table 2-S1). Availability permitting, we selected two (preferably one male and one female) wild-caught, adult specimens for each species from museum collections (Supplementary Table 2-S4). We recognize that the per-species sample size is low, but limited availability, high scan costs, and labor-intensive data collection prohibited a deeper sampling.

Morphological data With the exception of the elephant, all skulls were scanned on high-resolution industrial CT scanners (Phoenix's v|tome|x s^{TM}, nanotom s and m^{TM}, and NSI^{TM}). Field of view was confined to the area surrounding the CP for maximal resolution and, with the exception of three specimens, voxel size ranged from .008 - 0.045 mm. Because of its size, the

elephant skull could only be accommodated by a Definition AS64^{TM} medical scanner (Siemens Healthineers, Forchheim, Germany) and thus captured at somewhat lower resolution (voxel = .5 mm). All CT scans were imported into the visualization software package Mimics (v. 15.0-18.0, Materialise, Leuven, Belgium), segmented into 2D masks, then rendered as 3D models. Each CP was individually segmented and reconstructed as a 3D model. CP surface area was defined to include only the portion of the CP perforated by foramina that carry peripheral olfactory nerves (Fig. 2-3). CP surface area was quantified from 3D models after applying a wrapping function in imaging program 3-matic (v. 7.0.1, Materialise) that digitally fills the openings and generates a continuous surface. For further details, see Methods (Bird et al., 2014). Although we determined that the bottlenose dolphin (*Tursiops truncata*) ethmoid bone has branched foramina that connect the nasal passage to the brain (Supplementary Fig. 2-S7), we cannot establish the presence of olfactory sensory neurons (OSN) or vestigial CP until we can test the tissue in the foramina for olfactory marker protein (OMP), and so omit the dolphin from our quantitative analysis.

Genomic data Olfactory receptor (OR) gene data were retrieved from published studies (Niimura and Nei, 2007; Niimura et al., 2014; Hayden et al., 2010; Matsui et al., 2010; Montague et al., 2014; Hughes et al., 2013) (Supplementary Table 2-S1). Wherever possible, high-coverage genome sequences were used; however, in order to assemble a sufficient sample, OR gene data from some low-coverage assemblies were included in our study, including eight species with <6x draft genomes. OR genes are identified from whole genome sequences (Niimiura, 2012) and categorized as functional genes and pseudogenes, the latter of which are assumed to be non-functional (Nei et al., 2008). Genomic metrics for this study include: 1) total number of OR genes, 2) number of functional OR genes, 3) number of OR pseudogenes, and 4)

percentage of OR pseudogenes. For details on how functional and pseudogenes were defined in the source studies used for our OR data, see Supplementary Information.

Statistical analysis Species means were derived for each morphological and genomic metric. Values were log-transformed in the analysis of linear relationships because the data covered several orders of magnitude. Genomic data do not correlate with body size (Supplementary 2-S 8) and are therefore presented here without scaling to body mass. To determine CP size relative to body size, CP surface area was regressed against body mass values taken from the literature (Supplementary Table 2-S1) using generalized least squares regression. The resulting residuals (Fig. 2-4) were used as relative CP size values in all subsequent analyses. When investigating the relationship between relative CP size and OR gene variables, we used reduced major axis (RMA) regressions in order to enable us to invert predictor and response variables and establish mutual prediction lines. Correlation coefficients and confidence intervals were derived from bootstrapped resampling of the data. To estimate a probable OR gene repertoire for the sabertooth cat (*Smilodon*), we applied *Smilodon* relative CP size as new data to the regression equation derived from the relationship of number of functional OR gene to relative CP size in our larger sample. An estimated ORG range for *Smilodon* was calculated within the 95% confidence intervals around the regression line, which were derived by bootstrap resampling of the data. Finally, to account for phylogenetic relatedness and covariance in all relationships between variables, we performed phylogenetic least squares (PGLS) analysis (R Caper package) (Orme et al., 2013) with a time-calibrated mammal phylogeny (Fritz et al., 2009). Summary statistics for PGLS are given in Supplementary Table 2-S2 but non-PGLS plots are shown for

purposes of visualization (Figs. 4-7). All analyses were conducted in R v. 3.3.1 (R Development Core Team, 2016).

Results

Cribriform plate size as function of OR gene repertoire Because CP area is closely coupled to body mass (Fig. 2-4, $r^2 = 0.82$, $P < 0.001$), the relationship between CP and ORGs only comes into focus when relative CP surface areas, defined as the residuals from the regression of CP area on body mass, are considered. We found a strong positive linear correlation between relative CP size (RelCP) and the number of functional ORGs across our sample (Fig. 2-5, $r^2 = 0.76$, $P < 0.001$) (Supplementary Table 2-S2). After removing phylogenetic dependence with a phylogenetic generalized least squares (PGLS) regression (Orme et al., 2013; Fritz et al., 2009), the correlation remained robust (PGLS $r^2 = 0.75$, $P < 0.001$). A similarly strong linear correlation exists between relative CP size and the total number of ORG, which includes functional as well as pseudogenes ($r^2 = 0.68$, $P < 0.001$; PGLS $r^2 = 0.68$, $P < 0.001$) (Supplementary Fig. 2-S2). Without correcting for body size, absolute CP surface area and number of functional ORG are only weakly correlated ($r^2 = 0.22$, $P = 0.015$) (Supplementary Fig. 2-S3), and this correlation disappears if data for the greatest absolute CP, belonging to the largest species, the elephant (*Loxodonta africana*), is removed (Supplementary Table 2-S2).

Unlike the strong linear relationship between RelCP and number of functional OR genes, the association between RelCP and OR pseudogenes is complex. First, the relationship between relative CP size and *absolute number* of pseudogenes appears to have two distinct trends (Fig. 2-6). Among species with the fewest pseudogenes, there is no relationship between RelCP and number of pseudogenes. However, above ~500 OR pseudogenes, RelCP appears linearly

related to the number of pseudogenes. To further investigate this dichotomous pattern, we partitioned the sample data at an inflection point using the data-partitioning R (R Development Core Team, 2016) package "rpart" (Therneau et al., 2010) and tested each correlation separately. In species with ≤ 498 pseudogenes there is a negligible negative correlation between RelCP and pseudogenes ($r^2 = 0.23$, $P = 0.04$; $n = 19$) that disappears with phylogenetic correction (PGLS $r^2 = 0.020$, $P = 0.49$), and in species with ≥ 498 pseudogenes there is a strong positive correlation ($r^2 = 0.83$, $P < 0.001$; PGLS $r^2 = 0.82$, $P = 0.005$; $n = 7$).

Second, we found no linear correlation between RelCP and the *percentage* of pseudogenes ($r^2 = 0.12$, $P = 0.09$). Further examination of the data using a maximal information-based nonparametric exploration (MINE) statistic (Reshef et al., 2011) in R-package "minerva" (Albanese et al., 2013), suggests a significant nonlinear correlation [Maximal Information Coefficient (MIC) = 0.67, $\underline{P} = 0.002$]. The pattern is somewhat V-shaped, as species with the largest (elephant) and smallest (platypus, among others) RelCPs have similarly high proportions of pseudogenes (Supplementary Fig. 2-S4).

Morphological and genomic diversity Our sample of species includes outstanding examples of olfactory disparity. The African elephant (*Loxodonta africana*) possesses the largest CP ever recorded, a deep concavity with ~1,000 nerve passageways (Fig. 2-2). This is consistent with reports that elephants have undergone extreme expansion of their OR gene repertoire[3]. Surprisingly, the nine-banded armadillo (*Dasypus novemcinctus*) has the second largest RelCP, far outranking even the domestic dog (*Canis familiaris*) (Figs. 2-1a,b; 2-5, Supplementary Table 2-S1). All large apes share coupled reductions in ORG and CP morphology. The smallest RelCP in our sample belongs to the Philippine tarsier (*Tarsius syrichta*), a species with a

concordantly small repertoire of functional ORG (~90 compared to the ~781 estimated for the MRCA of placental mammals) (Hayden et al., 2010; Niimura et al., 2014). The notable outlier, the bottlenose dolphin (*Tursiops truncatus*), has only ~12 functional ORG (Hayden et al., 2010) and has likewise lost all obvious CP landmarks. Closer inspection of digital skull models, however, revealed a pair of foramina in the ethmoid bone that connect nasal passages to cranium but whose function is not certain (Supplementary Fig. 2-S7).

Predicting olfactory function in extinct mammal The linear correlation between functional ORG number and relative CP size apparent in our sample of living species was used to estimate a likely repertoire of functional ORGs for an extinct mammal species, For this we chose the Pleistocene sabertooth cat (*Smilodon fatalis*) from the Rancho La Brea tar seeps, for which a CT scan was available (Stock and Harris, 1992). With the aid of a high-resolution CT scan and 3D imaging software, we distinguished CP bone from its surrounding asphaltum matrix and quantified a fossil CP surface area for the first time. Relative CP size (RelCP) was estimated as the residual from the regression of CP surface area against body mass among all sample species (Supplementary Fig. 2-S5). Based on RelCP, *Smilodon* is predicted to have had ~ 598 (521, 685; 95% confidence interval) functional ORGs (Fig. 2-7), a number similar to that identified for the only other felid in our sample, the domestic cat (*Felis catus*) (Montague et al., 2014). When viewed in the context of existing morphological data from ten living felids (Bird et al., 2014), CP surface area of *Smilodon* falls well within the range of variation found among these cats, but also has a relatively smaller RelCP size than all species but the cheetah (*Acinonyx* jubatus) and the fishing cat (*Prionailurus viverrinus)* (Supplementary Fig. 2-S6, Supplementary Table 2-S3)

Discussion

Our study places the cribriform plate (CP) at an intersection of olfactory genomics, development, and evolution. The strong linear correlation between number of functional ORGs and relative CP size (Fig. 2-5) supports the hypothesis that skull morphology and ORGs are linked via the olfactory sensory neurons (OSNs), whose axon fascicles are recorded in the CP bone. Previous studies have established that each individual ORG is expressed by thousands of olfactory sensory neurons (OSNs), which together contribute to size of the olfactory epithelium (Mombaerts et al., 1996; Bressel et al., 2015). Additional research has shown that olfactory epithelium and cribriform plate (CP) surface areas are correlated (Pihlström et al., 2005). Results from our study bridge these findings by establishing a direct, linear biological relationship between the size of the OR subgenomes and the relative size of the CP (RelCP).

Our results contradict previous research that found no correlation between ORG and CP surface area adjusted to body mass (Garrett and Steiper, 2014), although the authors did find a weak correlation between ORG repertoire size and absolute CP surface area. In large part, the differences here can be explained by our contrasting approaches to the confounding factor of body size. CP size increases with body size, making comparisons across a diversity of species and body weights difficult. For example, the absolute CP surface area is far smaller in the rat than the gorilla, yet the former has an ORG repertoire that greatly exceeds that of the latter (Hayden et al., 2010; Niimura et al., 2014). This suggests that a correlation between CP size and ORG number needs to be viewed relative to body size. Residuals from the regression of CP area on body mass better resolve the relationship between morphology and genomic data (Figs. 2-4, 2-5). Our ability to recover this relationship also benefited from the application of precise digital methods to estimate CP surface area from high-resolution CT scans.

Nevertheless, there is some scatter in the plot of RelCP size against ORG repertoire (Fig. 2-5, Supplementary Fig. 2-S2) that deserves attention. An important factor contributing to the scatter is likely the inclusion of a number of low-coverage draft genomes in our sample (Supplementary Fig. 2-S9). Identification of ORGs is less reliable in low-coverage genomes owing to inherent sequencing gaps as well as over-collapse in regions with segmental duplications (Lindblad-Toh et al., 2005; Hayden et al., 2010). Because intact functional ORGs are more likely to be misidentified as truncated and generally undercounted (Hayden et al., 2010), we expect their number to increase in the low-coverage species as genome assemblies are improved. We note here four cases (elephant, rabbit, dog and cat) in which we can compare the number of functional ORGs when based on low coverage (1.5-2x) to the same species when it has high coverage (≥ 6x) (Hayden et al., 2010, Niimura et al., 2014; Montague et al., 2014). In each case, the genomes rendered an average of 41.5% more functional ORGs with the higher coverage genomes than from the initial (1.5-2x) draft genomes. This measure of increase, applied to the 12 low-coverage species in our sample, strengthens the correlation between number of functional ORGs and RelCP ($r^2 = 0.84$, PGLS $r^2 = 0.81$, $P < 0.001$, Supplementary Fig. 2-S10 compared with $r^2 = 0.76$, Fig. 2-5, Supplementary Fig. 2-S9). Similarly, when we omit the twelve low-coverage species, the correlation between OR genes and CP tightens further ($r^2 = 0.89$, PGLS $r^2 = 0.82$, $P < 0.001$; Supplementary Fig. 2-S11).

An OR pseudogene is defined as having disruptive mutations (e.g. indels) and/or premature stop codons present within the ORG-specific conserved region and so are not expected to produce a functioning receptor (Niimura and Nei, 2007). For this reason it was surprising to find a distinct association between CP morphology and the absolute number of OR pseudogenes. Unlike the above strong linear correlation between CP size and functional ORGs,

this association is complex, with what appear to be two separate trends (Fig. 2-6). First, a very weak association spans a wide range of RelCP sizes in species with fewer than 498 pseudogenes which disappears when accounting for phylogeny (Supplementary Table 2-S2). Second, for species with greater than 498 pseudogenes the RelCP significantly increases with the number of pseudogenes. This trend appears to be exponential, due to the strong influence of the armadillo and elephant. This distinct pattern raises the question why most species with high numbers of pseudogenes in their ORG repertoires have the largest RelCPs? Or, asked a different way, when the axes are inverted (Supplementary Fig. 2-S12), why do species with the largest RelCPs have high concentrations of pseudogenes? Here we consider alternative evolutionary scenarios for this pattern. First, lineages leading to large-CP species may have undergone fairly recent ORG expansions generated by repeated gene duplication events. Although a fraction of new ORGs may have been conserved under adaptive pressure (e.g., to enhance detection of specific odorants), one would predict that many duplicates would degenerate by random mutations, due to relaxed selective pressure (Nei et al., 2008), and may have persisted in the genomes for short periods of time before degenerating to sequences no longer recognized as ORGs. (Schrider et al., 2009). This is consistent with the observation that species with relatively high numbers of OR pseudogenes also have some of the largest repertoires of functional ORG (Supplementary Fig. 2-S13). Alternatively, the pattern of high pseudogene concentration in large-CP species may signal a constraint in either CP size or ORG repertoire size and a concomitant increase in pseudogenization of ORGs generated by gene duplication. A large ORG repertoire is costly, as each gene prompts the proliferation of ever-regenerating OSNs (Ma et al., 2014). Similarly, a large CP carries a structural risk, in that densely perforated bone is thinner and more easily fractured than surrounding cranial bone (Pease et al., 2014). Notably, the two largest CPs occur

in skulls with features that, while otherwise adaptive, may offer secondary reinforcement to the fragile CP, for example dermal armor in the armadillo (Chen et al., 2011) and a thick periphery (up to 250mm) of highly pneumatized bone surrounding the brain in the elephant (Shoshani et al., 2006) (Supplementary Fig. 2-S14). Finally, we consider the possibility that OR pseudogenes, traditionally assumed to be functionally inert and neutral (Gilad et al., 2007; Nei et al., 2008), may be biologically active long non-coding RNAs (lncRNAs), and are therefore conserved in species with expanded olfactory systems. As demonstrated for the tumor-suppressor *PTEN* gene, non-coding pseudogene transcripts can act as decoys for microRNAs (miRNA) that target the parent gene, thereby mitigating the effects of translational repression mediated by the miRNAs (Poliseno et al., 2010). A potential role for OR-derived lncRNA transcripts as miRNA sponges might be investigated, particularly in light of recent findings that coding ORG transcripts in mice have lost many miRNA binding sites, effectively reducing the modulatory impact of miRNAs on expression levels (Shum et al, 2015).

Numerous researchers have sought to link olfactory loss with the fraction of pseudogenes in ORG repertoires (Hayden et al., 2010; Rouquier et al., 2000, Gilad et al., 2007; Kishida et al., 2007). However, our study found no significant linear correlation between the percent pseudogenes and the RelCP (Supplementary Fig. 2-S4). These results substantiate the argument that the percentage of pseudogenes is a poor predictor of olfactory function (Niimura et al., 2014; Matsui et al., 2010).

The strong link documented here across a wide dynamic range of ORG repertoires and skull morphology invites us to examine the olfactory ecology of individual taxa within this range. Our sample offers outstanding examples of olfactory expansion and reduction that might be explained by differences in the dependence on olfaction in life history. For example, the

African elephant possesses by far the largest RelCP and ORG repertoire (Niimura et al., 2014) of any mammal studied, suggesting that elephants are heavily reliant on olfaction for their survival. This is consistent with the elephant's numerous unparalleled olfactory specializations, among them, extremely dense ethmoid turbinals (for a visual comparison of elephant and hyrax turbinals see Supplementary Fig. 2-S15), compact multiple layers of glomeruli in the olfactory bulb (Ngwenya et al., 2011), and its signature mobile proboscis. Consistent with these anatomical features, behavioral experiments reveal a striking complexity of odor recognition among elephants. Specifically, they can recognize up to 30 individuals within their kin group from urine cues alone (Bates et al., 2008) and can differentiate between two ethnic groups of humans by sniffing odor cues from worn garments Bates et al., 2007).

Interestingly, we found that nine-banded armadillo (*Dasypus novemcinctus*) has one of the largest olfactory systems in our sample (Fig. 2-5). Although it is generally assumed to be scent-oriented, based on its foraging habit of rooting under leaf litter and its poor vision (McDonough and Loughry, 2013), the armadillo's high rank in this data set supports a closer examination of its chemical ecology, particularly in the context of the closely related, understudied and ecologically diverse xenarthrans.

Domestic dogs (*Canis familiaris*) are thought to have a well developed sense of smell and are reliable drug sniffers and olfactory scouts (Browne, et al., 2006). However they are surpassed by five other species in RelCP as well as ORG count. Conceivably, the breeds chosen for our sample may have variably influenced the estimated CP size for the dog. Of the four, only the dachshund is considered a scent hound, whereas two (borzoi and saluki) are considered sight hounds and one is brachycephalic, or short-snouted (French bulldog). It has not yet been established whether selection for keen sightedness or a foreshortened snout imposes any

constraint on CP morphology or ORG repertoires. A more focused examination of the CP/ORG relationship among dog breeds is a necessary next step. Additionally, we might consider that behavioral traits selected for in dogs, such as tameness and trainability (Turcsán et al., 2011) , may play a significant role in dogs' success as keen odor detectives. Interestingly, the domestic dog has a smaller CP for its size than does the gray wolf (*Canis lupus*) (Supplementary Fig. 2-S16) (Bird et al., 2014), whose ORG repertoire is presently unknown. Based on its larger RelCP, the wolf is expected to have a larger ORG repertoire than the dog, but confirmation awaits the analysis of new genomic data (Fan et al., 2016).

Several of our sampled species with exceptionally small CPs and ORG repertoires rely on well-developed sensory modalities other than olfaction. For example, the tarsier, a nocturnal primate with pronounced visual specializations, such as enormous eyes and an enlarged primary visual cortex (Collins et al., 2005), has only a negligible CP (Fig. 2-2, Supplementary Fig. 2-S17). Similarly, the simplified CP of the semi-aquatic platypus (Fig. 2-2) may in part have been shaped by preferential reliance on an elaborate sensory system of electroreception during underwater foraging (Pettigrew, 1999). The most striking example of olfactory loss and sensory trade-off is the bottlenose dolphin, a fully aquatic odontocete that relies on echolocation instead of odor cues to locate prey. Studies variously report that CP foramina, present in fetal odontocetes, fully close in adults or that a few remain open and carry fibers not from OSN but from the terminal nerve, a cranial nerve thought to play a role in pheromone response (Oelschäger and Buhl, 1985; Ridgeway, 1987). Our digital models of adult dolphin skulls confirmed that there are indeed openings connecting the nasal passages to the brain in the ethmoid area (Supplementary Fig. 2-S7). Given that the dolphin has retained a small repertoire

of ~12 functional OR genes, tests need to be conducted on nasal tissue in order to fully exclude the vestigial presence of OSNs and other olfactory anatomy in this odontocete.

An important goal of this study was to establish the cribriform plate as an osteological correlate of olfactory function, a metric applicable to extinct species. Here we used the linear relationship between RelCP and ORG to predict the likely number of functional ORG in the extinct sabertooth cat (*Smilodon fatalis*) from its CP morphology. *Smilodon's* CP, and predicted ORG count, positions the Pleistocene felid close to, but slightly below, the domestic cat in our olfactory scale (Fig. 2-7). When compared with ten other living felids, *Smilodon* has, for its body size, a smaller CP than all but the fishing cat (*Prionailurus viverrinus*, Supplementary Figure 2-S6). *Smilodon* appears to have been less reliant on olfaction than the similarly large, extant felid, the African lion (*Panthera leo*). If so, it would be interesting to estimate *Smilodon's* relative reliance on alternative sensory modalities (e.g. hearing, vision) to determine if there is any evidence of compensatory adaptations.

Conclusion

In summary, the strong relationship we observed between cribriform plate morphology and OR genes contributes to our understanding of olfactory biology in several ways. First, the RelCP/ORG correlation illuminates an underlying developmental intersection of genes, neuroanatomy, and skull morphology along the peripheral olfactory pathway from nose to brain. Further, these results suggest that the coupling of genes and morphology provides a coherent molecular-morphological metric, with which we can make strong inferences about the relative olfactory reliance in individual mammal species. Finally, cribriform plate size is reinforced here as a stand-alone proxy of olfactory function that can be applied to extinct species, from which

molecular data can no longer be extracted, thereby allowing us to document the evolution of olfactory function within mammals over geologic time

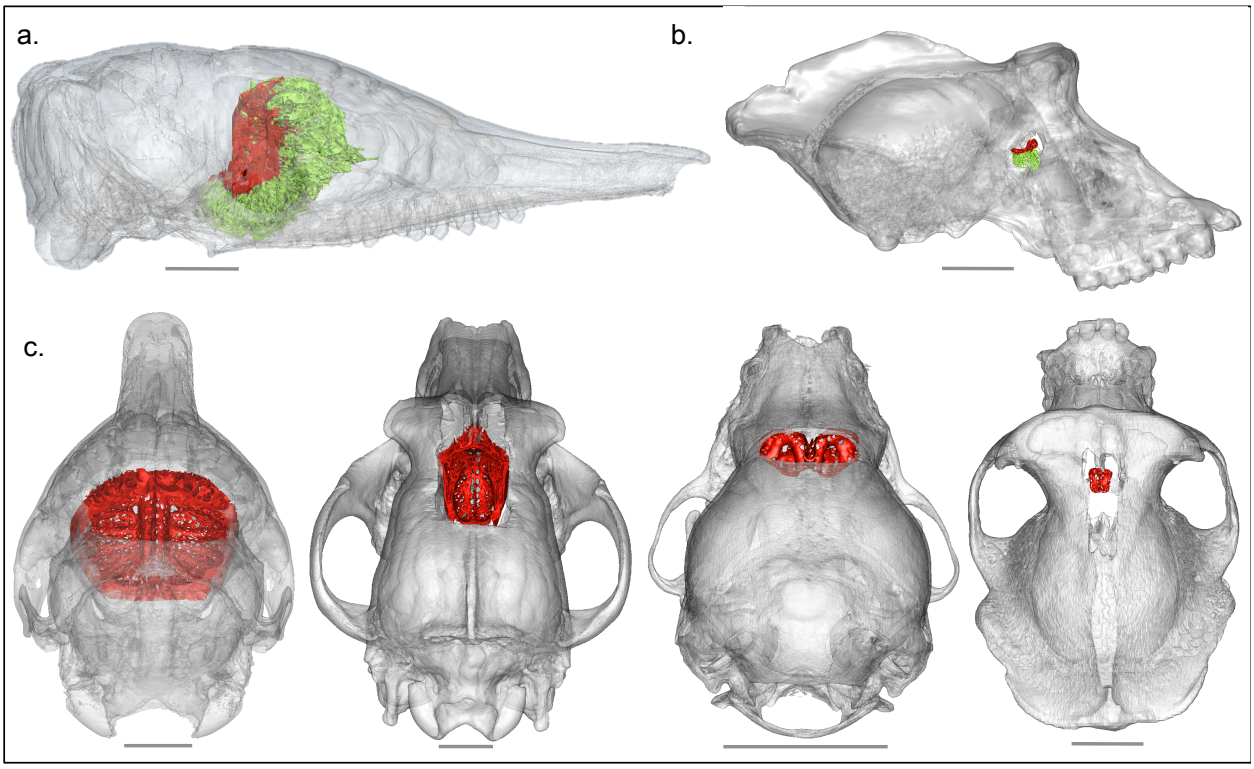

Figure 2-1. Size range of the cribriform plate. **a**, Lateral view of nine-banded armadillo (*Dasypus novemcinctus*) skull. Scale bar: 10 mm. **b**, Lateral view of gorilla (*Gorilla gorilla*). Scale bar: 50 mm. **c**, Dorsoposterior view of armadillo. Scale bar: 10 mm. **d**, Dorsoposterior view of dog (*Canis familiaris*, saluki). Scale bar: 15 mm. **e,** Dorsoposterior view of little brown bat (*Myotis lucifugus*). Scale bar: 5 mm. **f,** Dorsoposterior view of gorilla. Scale bar: 50 mm. Red: cribriform plate (CP). Green: Ethmoid, frontal, nasal turbinal bones and partial nasal septum (only viewable without obstruction in lateral view).

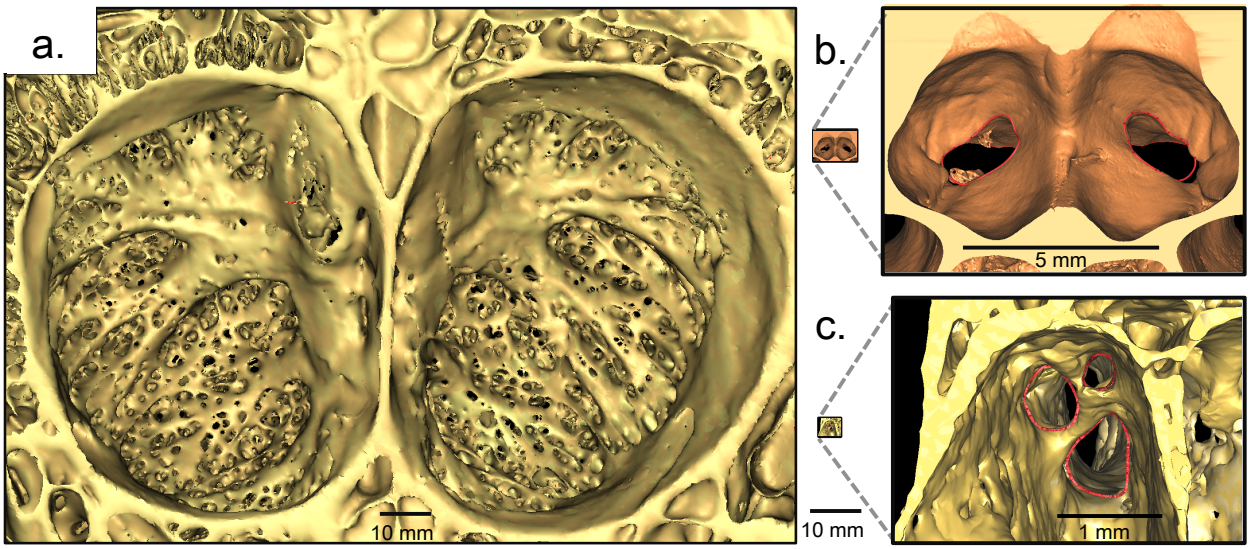

Figure 2-2. Foramina number and distribution in CP. **a**, CP of the African elephant (*Loxodonta africana*) with ~ 1,000 foramina. **b,** Platypus (*Ornithorhynchus anatinus*) CP to scale with elephant's; right: inset with enlarged view of platypus CP. **c,** Tarsier (*Tarsius syrichta*) CP to scale with elephant's; right: inset with enlarged half of tarsier's CP, with foramina outlined in red.

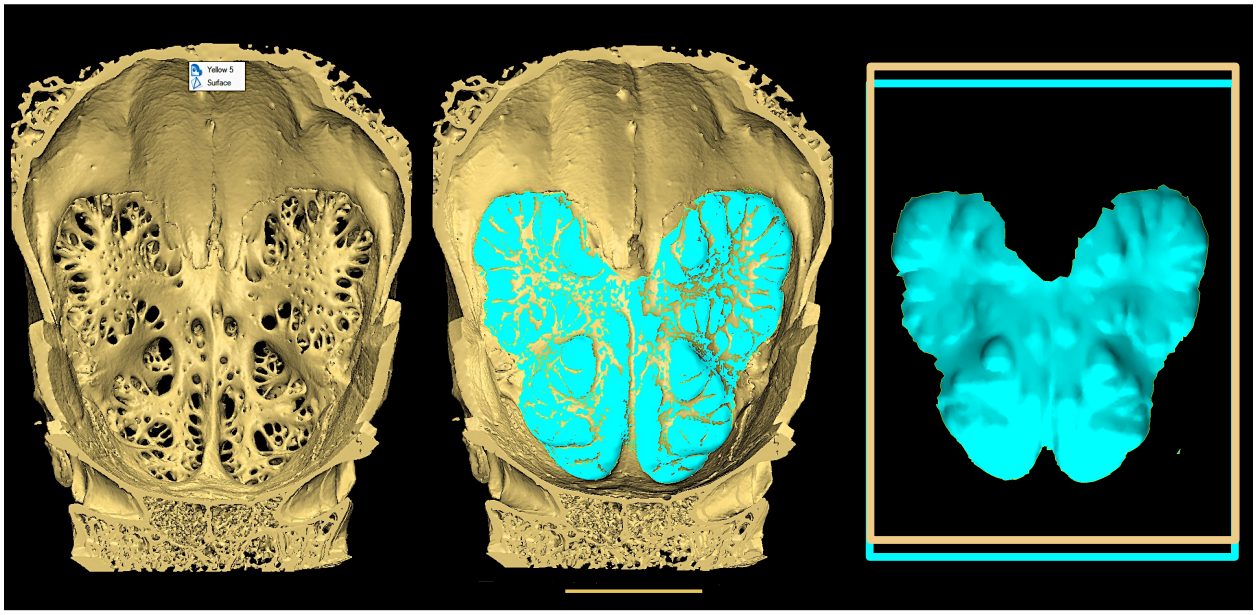

Figure 2-3. Quantifying the CP surface area. Left: 3D model of French bulldog (*Canis familiaris*) CP rendered in Mimics; center, CP foramina are digitally filled to create a continuous surface from the perforate region; right, Perforated area is isolated and surface area is calculated from cumulative pixels with imaging software 3-matics. Scale bar: 10 mm.

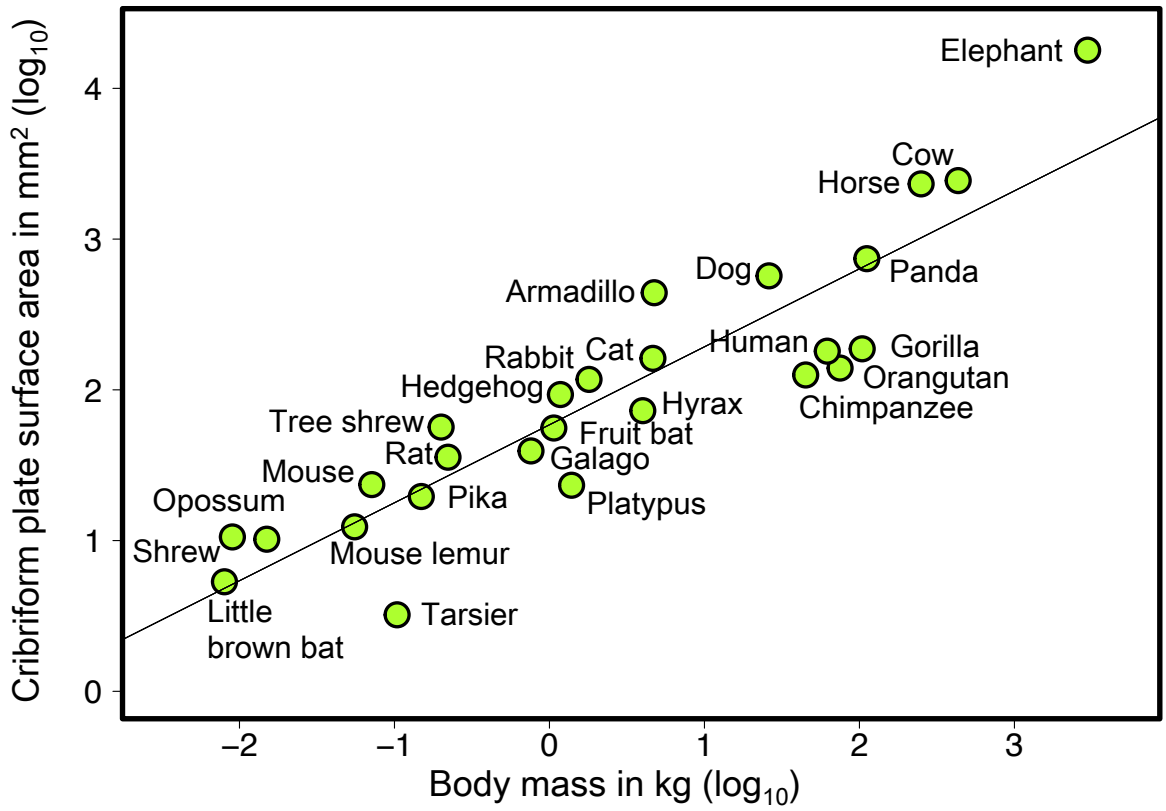

Figure 2-4. Relative CP size. Regression of absolute CP surface area $_{(log10)}$ against body mass $_{(log10)}$ for 26 species ($r^2 = 0.83$, $p < 0.001$; $y = 0.517x + 1.77$). Residuals from regression constitute the relative CP size (RelCP) for each species and are used in subsequent analyses.

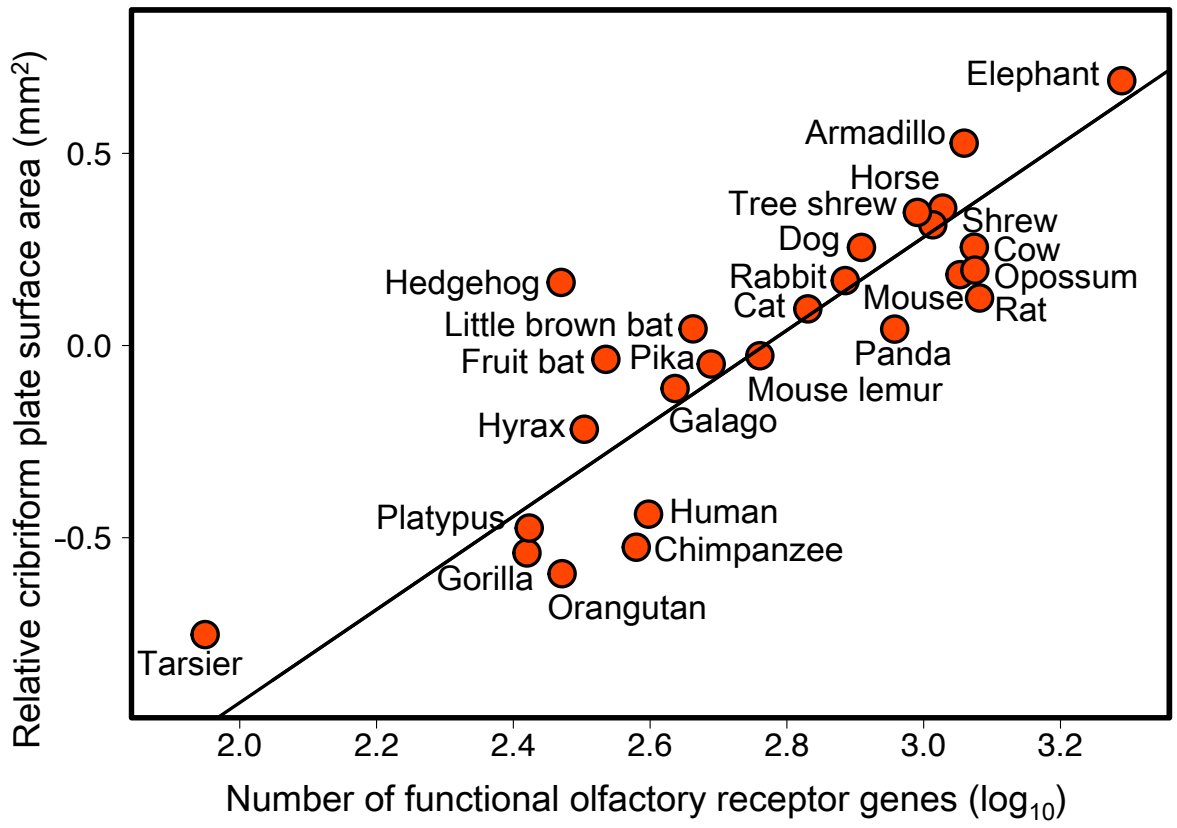

Figure 2-5. Relationship between RelCP and ORG. Reduced major axis regression of RelCP against the number of functioning ORG $_{(\log 10)}$ ($r^2 = 0.76$, $P < 0.001$).

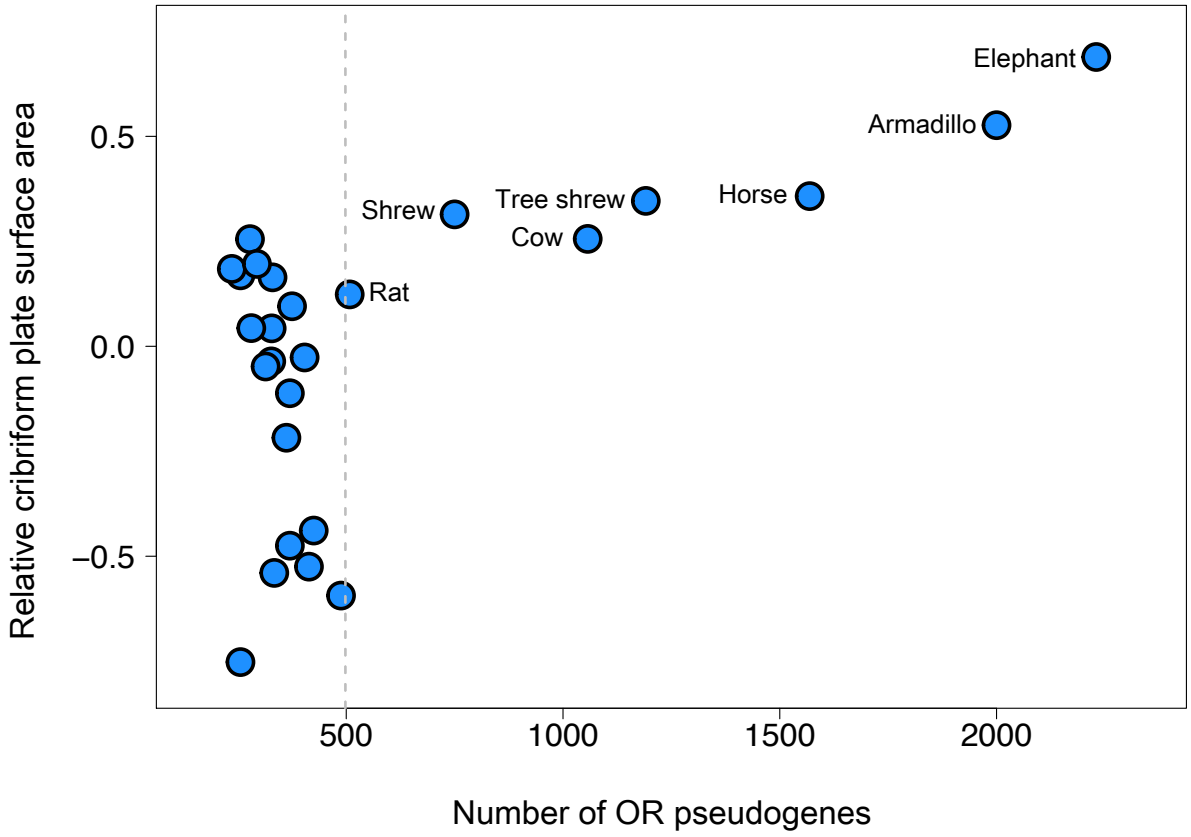

Figure 2-6. Number of pseudogenes and relative CP size. Dual trends in the relationship between RelCP and pseudogenes: in species with <498 pseudogenes, the correlation is nonsignificant when corrected for phylogenetic covariance; in species with >498 pseudogenes, the correlation is robust ($r^2 = 0.83$, $P = 0.004$, PGLS $r^2 = 0.82$, $P = 0.005$).

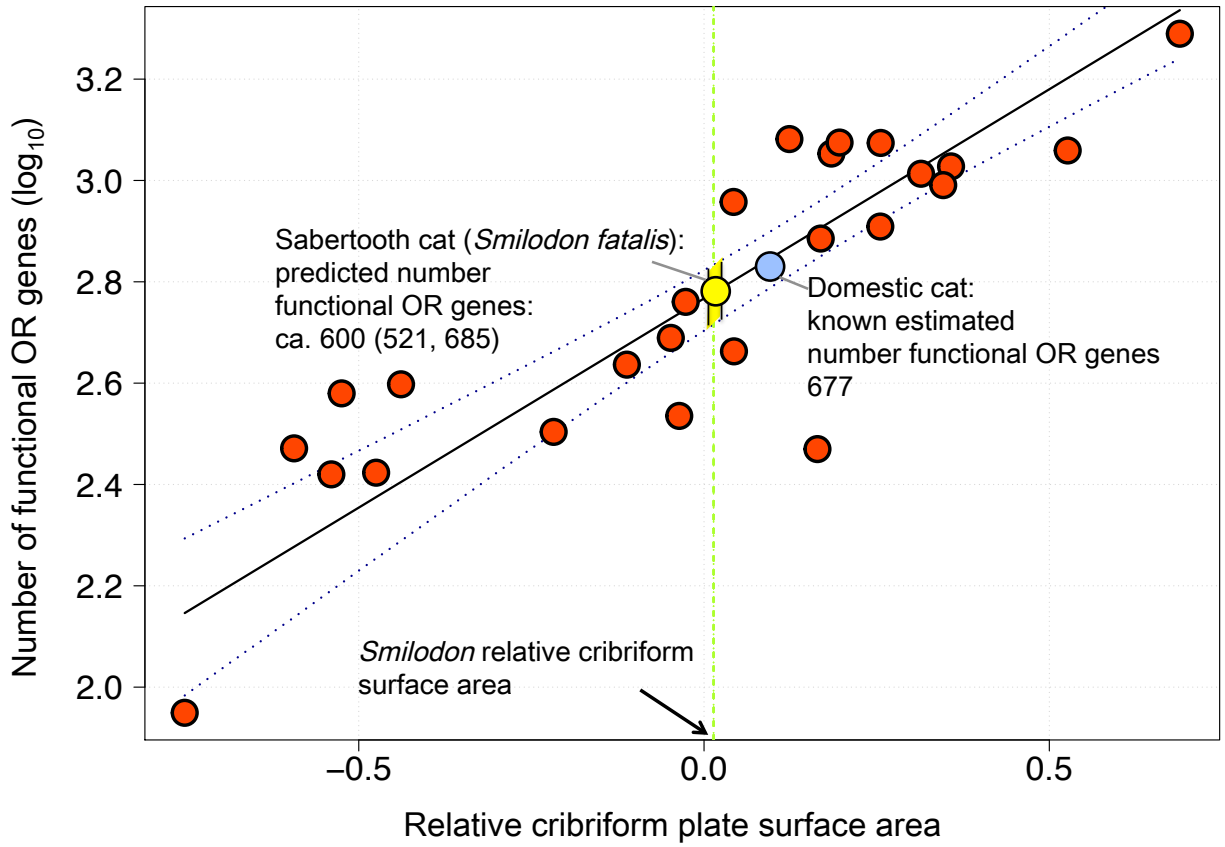

Figure 2-7. Predicting functional ORG repertoire for extinct felid from CP.
To predict an approximate number of ORG from RelCP, axes from the regression in Fig. 2-5 are inverted and the RelCP value (green vertical line) for the sabertooth cat (*Smilodon fatalis*) is applied to the regression equation. This predicts *Smilodon* to have had ca. 600 (521, 685) functional ORG. Dotted lines: 95% confidence intervals around regression line. See Materials and Methods for details.

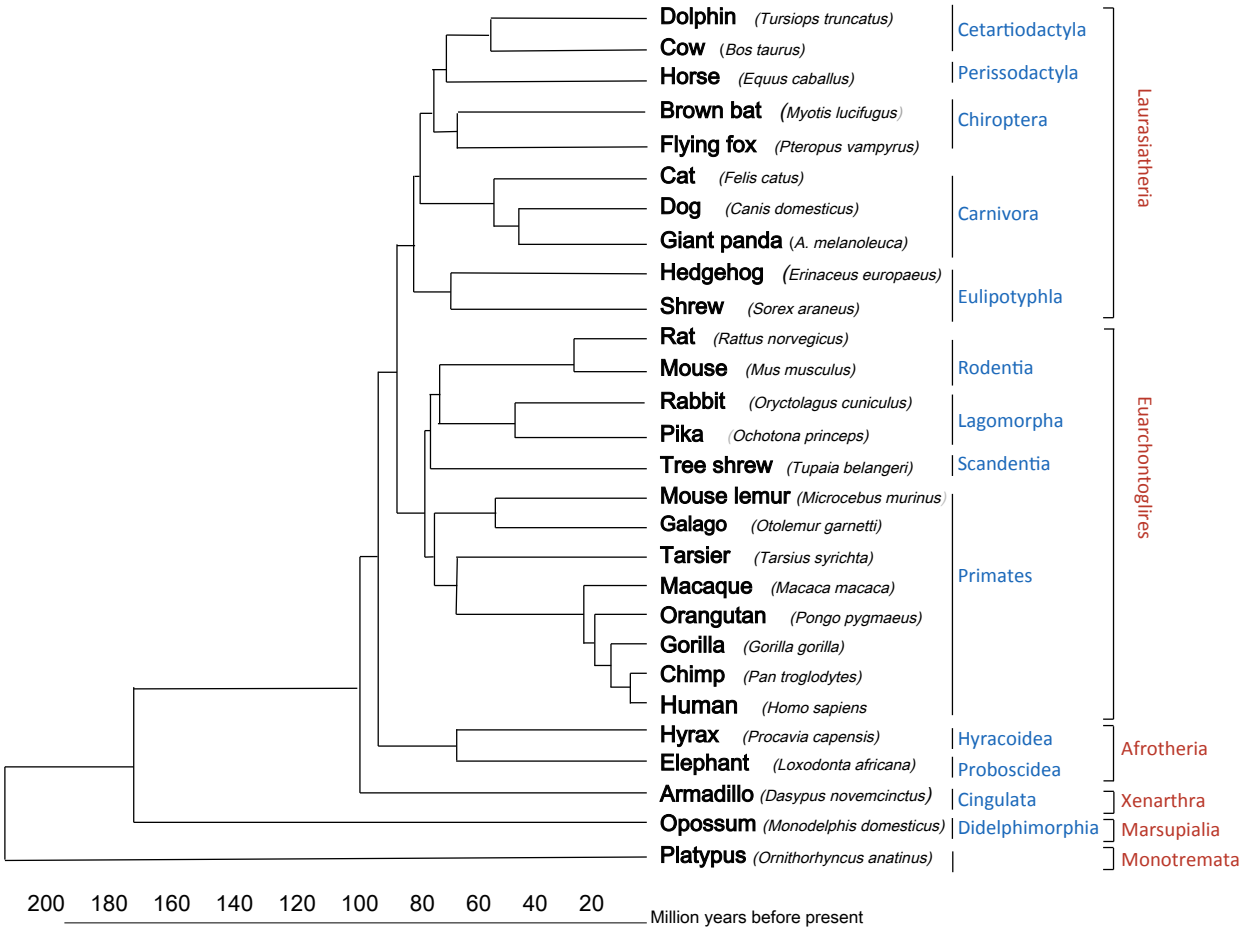

Figure 2-S1. Time-calibrated phylogeny of sample species. Tree compiled from published molecular phylogenies (Meredith et al., 2011; Foley et al., 2016 (see Main References).

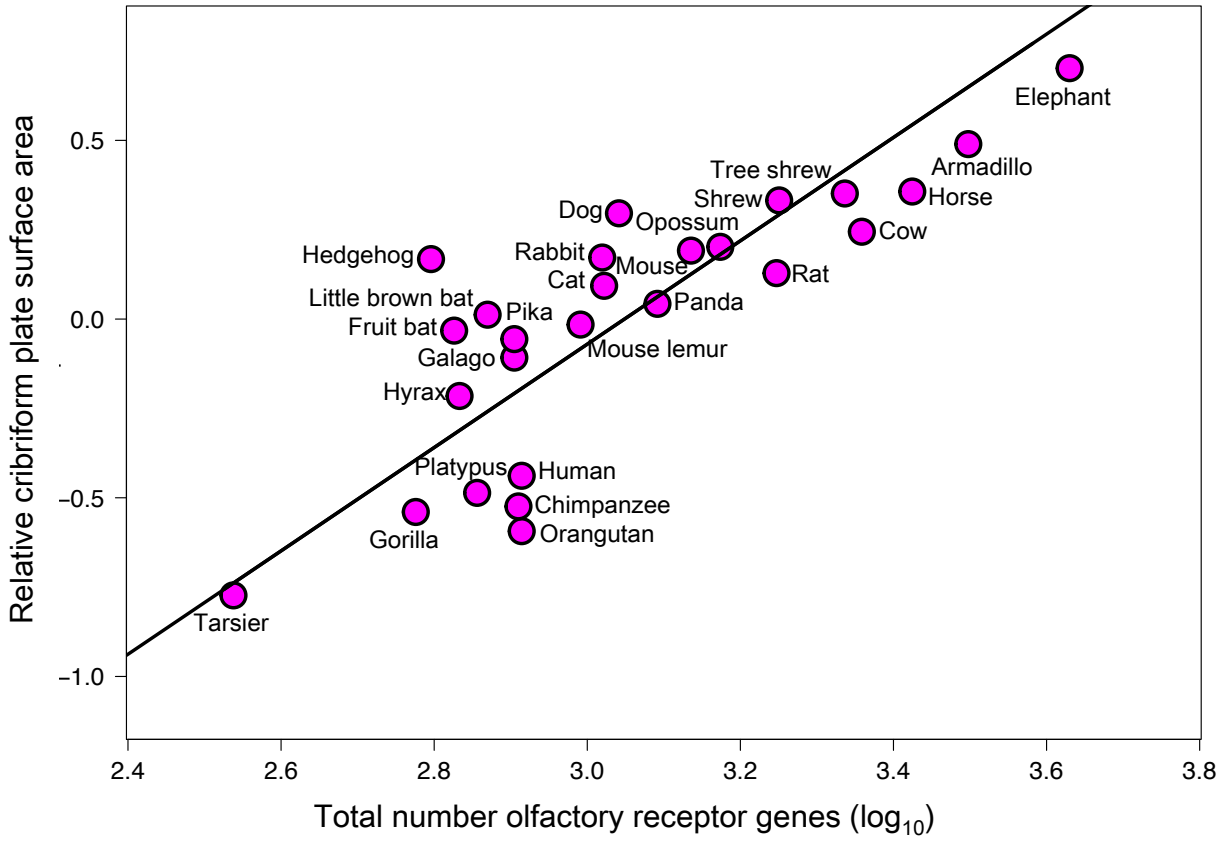

Figure 2-S2. Relationship between RelCP and Total ORGs. There is a strong linear positive correlation between relative CP size (RelCP) and the total number of OR genes (ORGs) (r^2 = 0.69, $P < .0001$; r= 0.83 [0.67, 0.93], $P < 0.0001$). The total number of ORG includes both functional genes as well as pseudogenes.

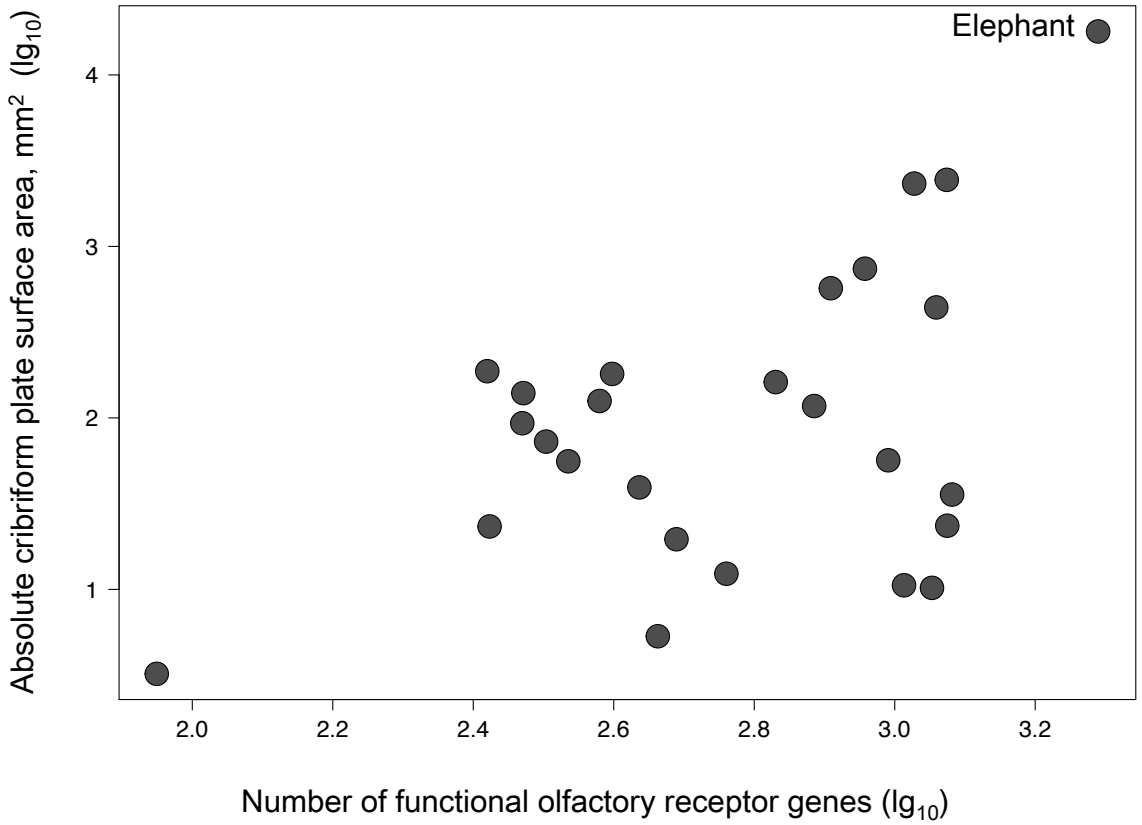

Figure 2-S3. Relationship between absolute CP surface area and functional ORGs. There is a weak but significant linear correlation between absolute cribriform plate (CP) surface area and the number of functional olfactory receptor genes (log-transformed data) ($r^2 = 0.22$, $P = 0.015$, $n = 26$). The African elephant, by far the largest species in our sample, also has an extremely large CP, both in absolute terms and relative to its body size. If we omit just the elephant from the sample, the correlation disappears ($r^2 = 0.13$, $P = 0.79$, $n = 25$). CP surface area is closely coupled to body mass (Fig. 2-4 in the main text, $r^2 = 0.83$, $P < 0.0001$), therefore it needs to be considered to resolve the relationship between CP morphology and ORG repertoires.

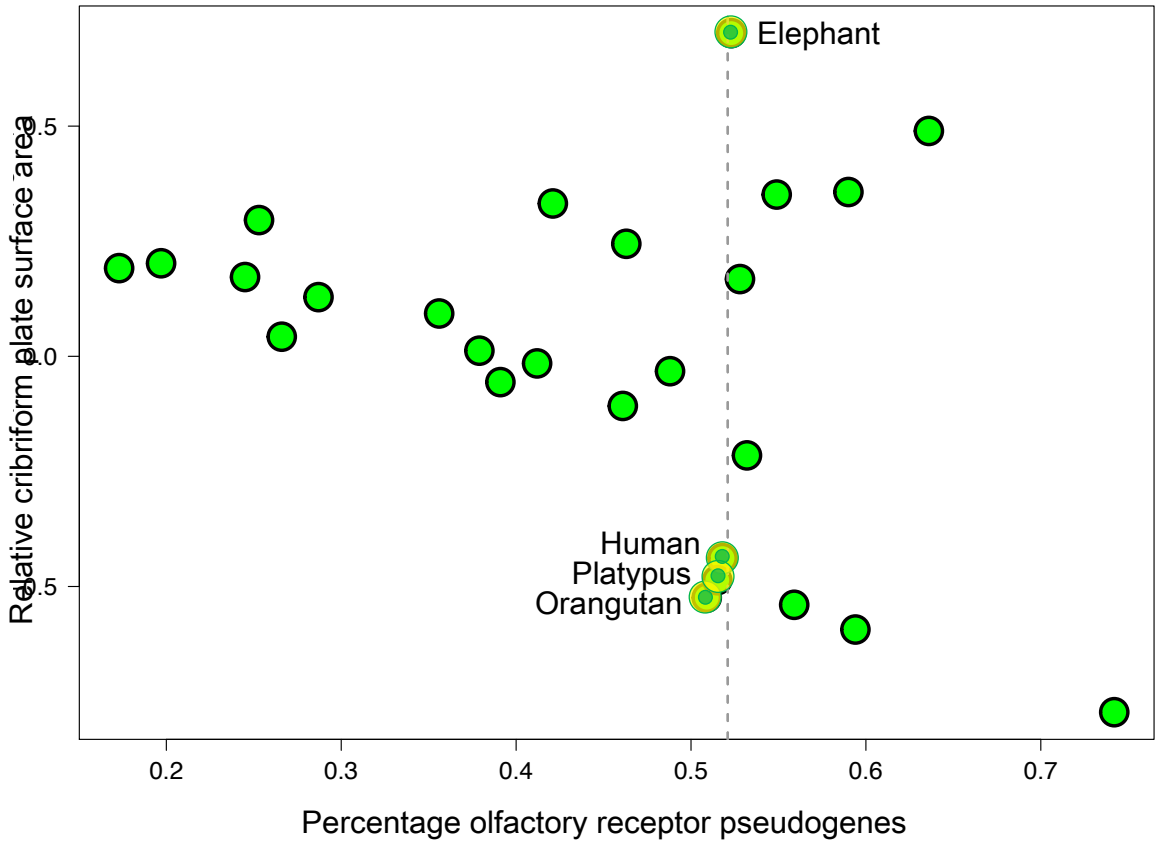

Figure 2-S4. Relationship between RelCP and percentage pseudogenes. No linear correlation was found between relative CP surface area (RelCP) and the percentage pseudogenes present in species' genomes ($r^2 = 0.11$, $P = 0.11$; PGLS $r^2 = 0.08$, $P = 0.17$, $n = 26$). Further analysis with a maximal information-based nonparametric exploration (MINE) statistic, a possible nonlinear relationship emerges [Maximal Information Coefficient (MIC) = 0.67, $P = 0.0008$]. A v-shaped pattern is observed in which species with the largest percentage pseudogenes have either a large or very small RelCP. For example, the elephant, with the largest CP of all species, has a slightly higher fraction of pseudogenes than even the orangutan, human and platypus. For this reason, the percentage of pseudogenes is a poor indicator of olfactory function or olfactory loss.

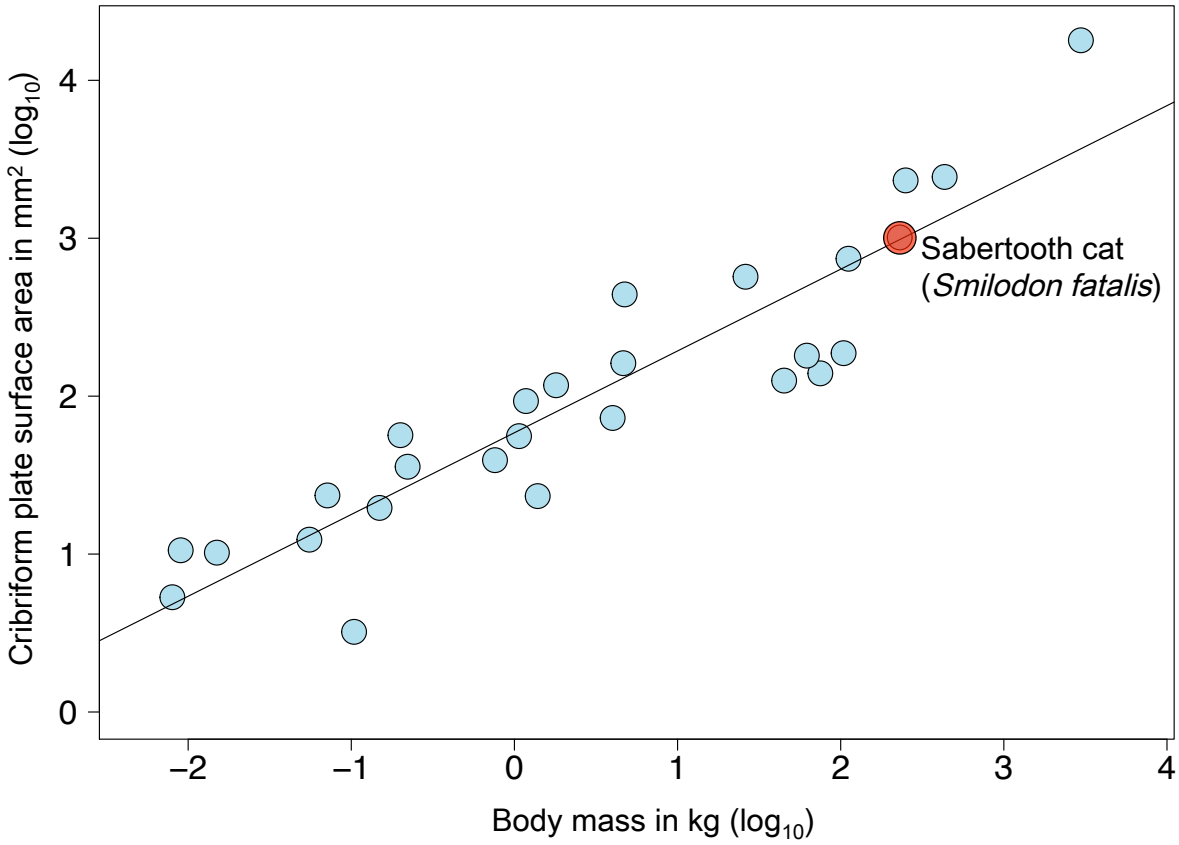

Figure 2-S5. Estimating RelCP of sabertooth cat. Regression plot: CP surface area to body mass (log-transformed data), adding the saber-toothed cat (*Smilodon fatalis*) to our sample (r^2 = 0.833, $P < .0001$, $n = 27$). Residuals constitute relative CP size (RelCP).

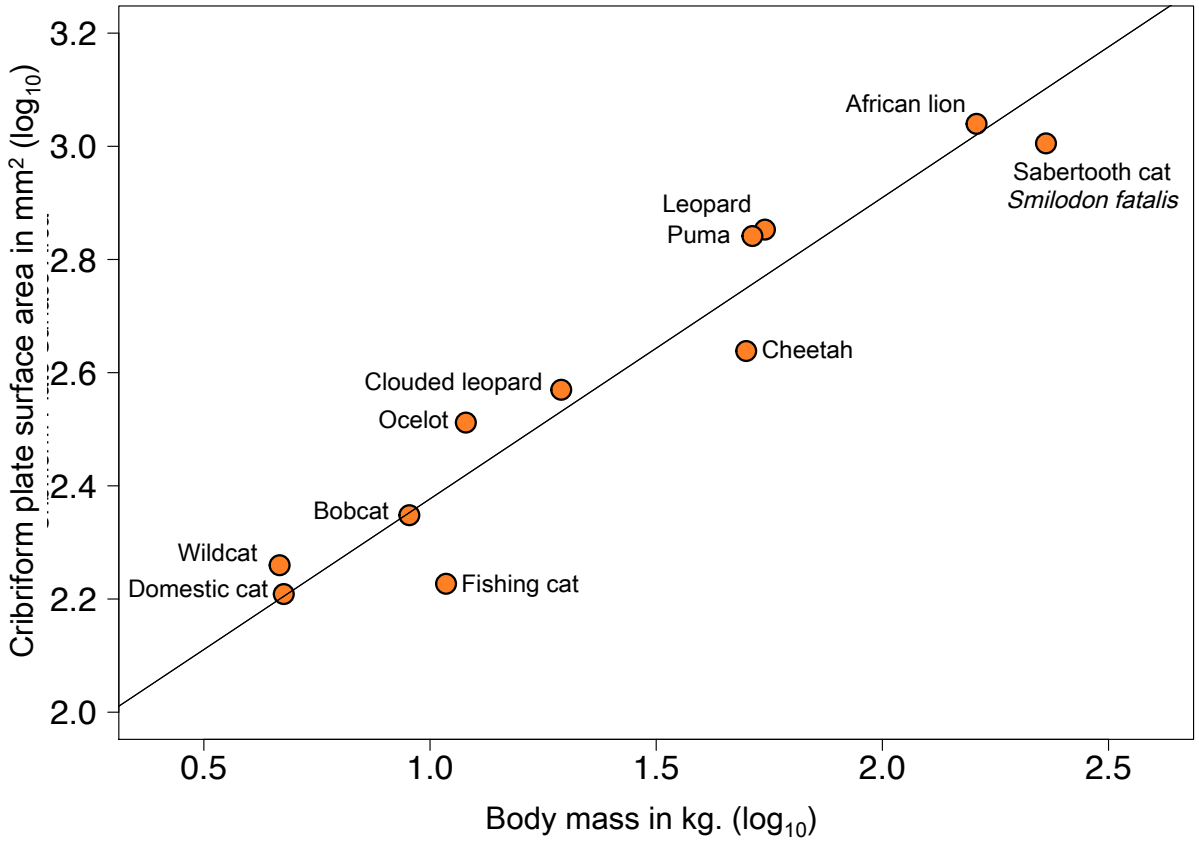

Figure 2-S6. Comparison of felid CP surface areas. Sabertooth cat (*Smilodon fatalis*) CP morphology viewed within a sample of 10 living felids. *Smilodon's* absolute CP surface area is within the range of other large cats, however when its body mass is considered, its relative CP (RelCP) appears to be smaller than all other felid species in the sample expect the fishing cat (*Prionailurus viverrinus*) and perhaps the cheetah (*Acinonyx jubatus*).

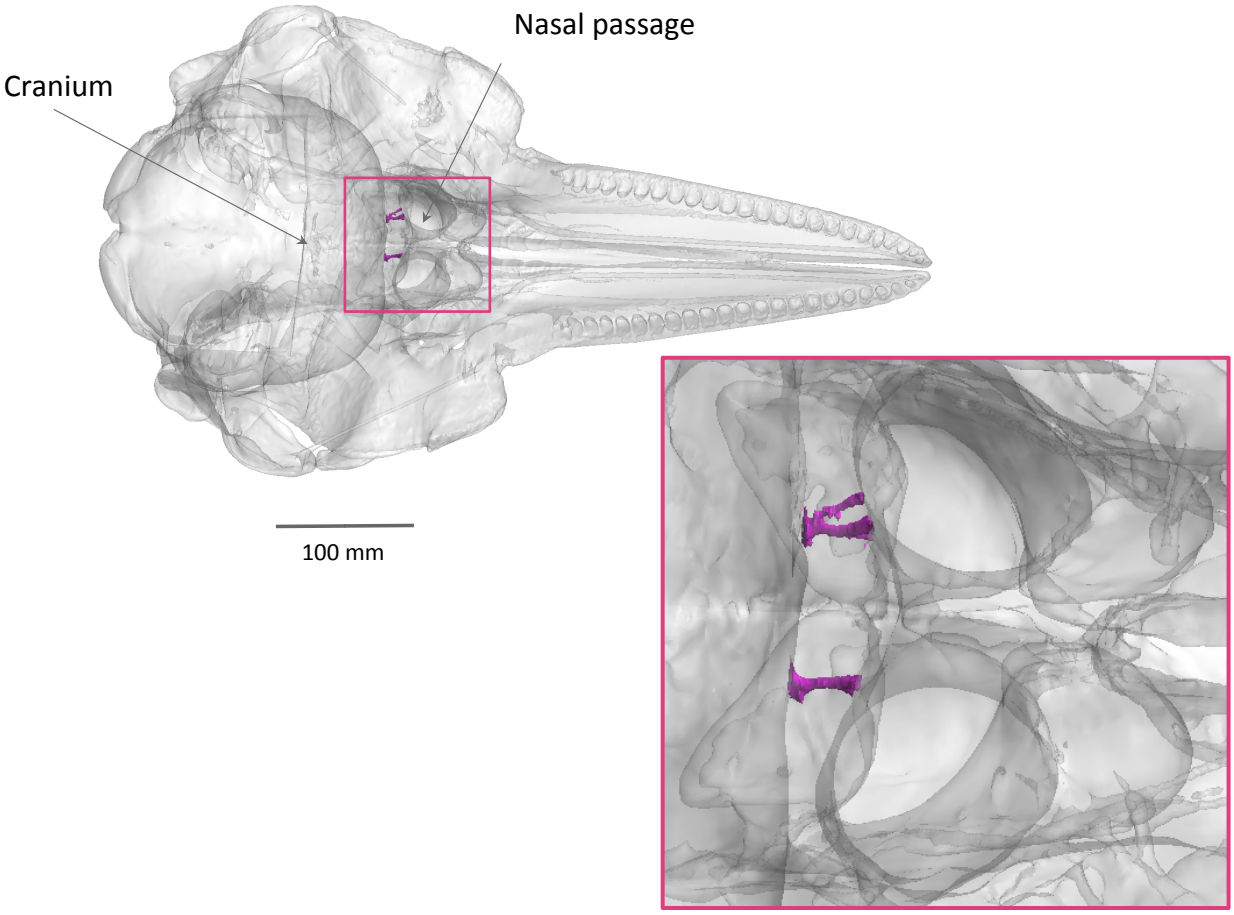

Figure 2-S7. Dolphin nasal morphology. Bottlenose dolphin (*Tursiops truncatus*) skull, dorsal view. Scale bar: 100 mm. Pink: 3D models of the filled foramina connecting ethmoid area of nasal passages to cranium in the **Inset:** Close up of foramina in the ethmoid bone.

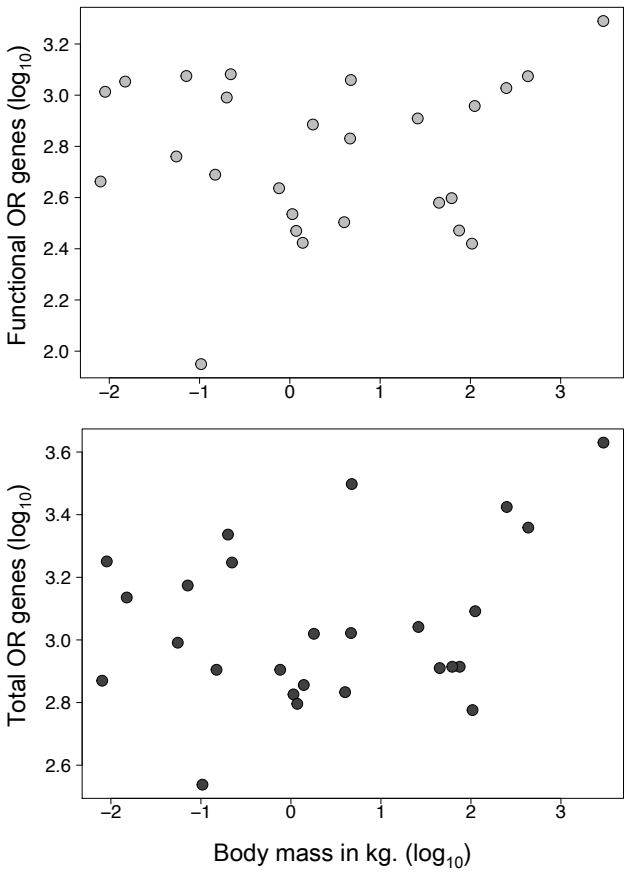

Figure 2-S8. No relationship between Olfactory receptor genes (ORGs) and body size. Because there is no significant relationship between the number of ORGs (functional or total) and body mass for sample species, the number of ORGs is not corrected for body size in further regressions and analyses.

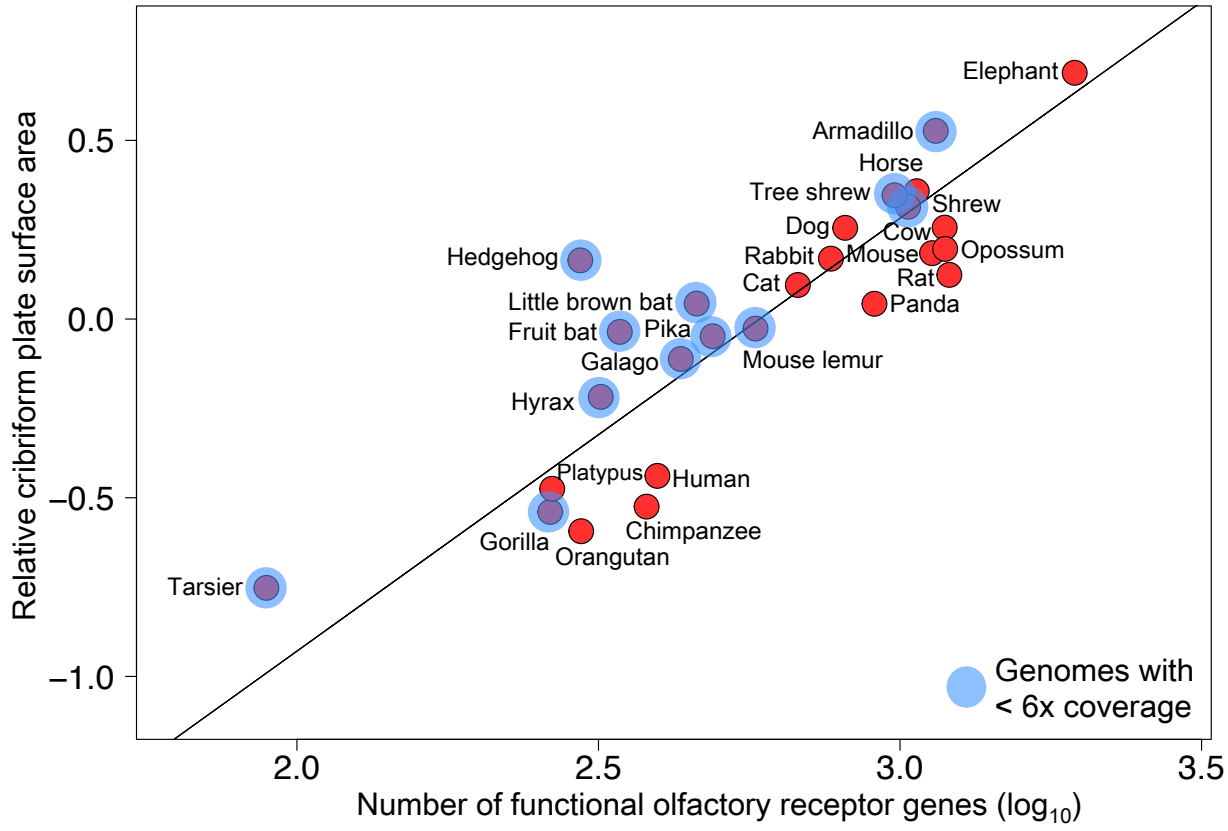

Figure 2-S9. RelCP vs ORGs. Regression plot of relative CP surface area (RelCP) vs. Number of functional ORG $_{(log10),}$ identical to Figure 4 in the main text, except that the twelve species with low coverage (< 6x) draft genomes are featured in blue here ($r^2 = 0.76$, $P < 0.0001$, $n = 26$).

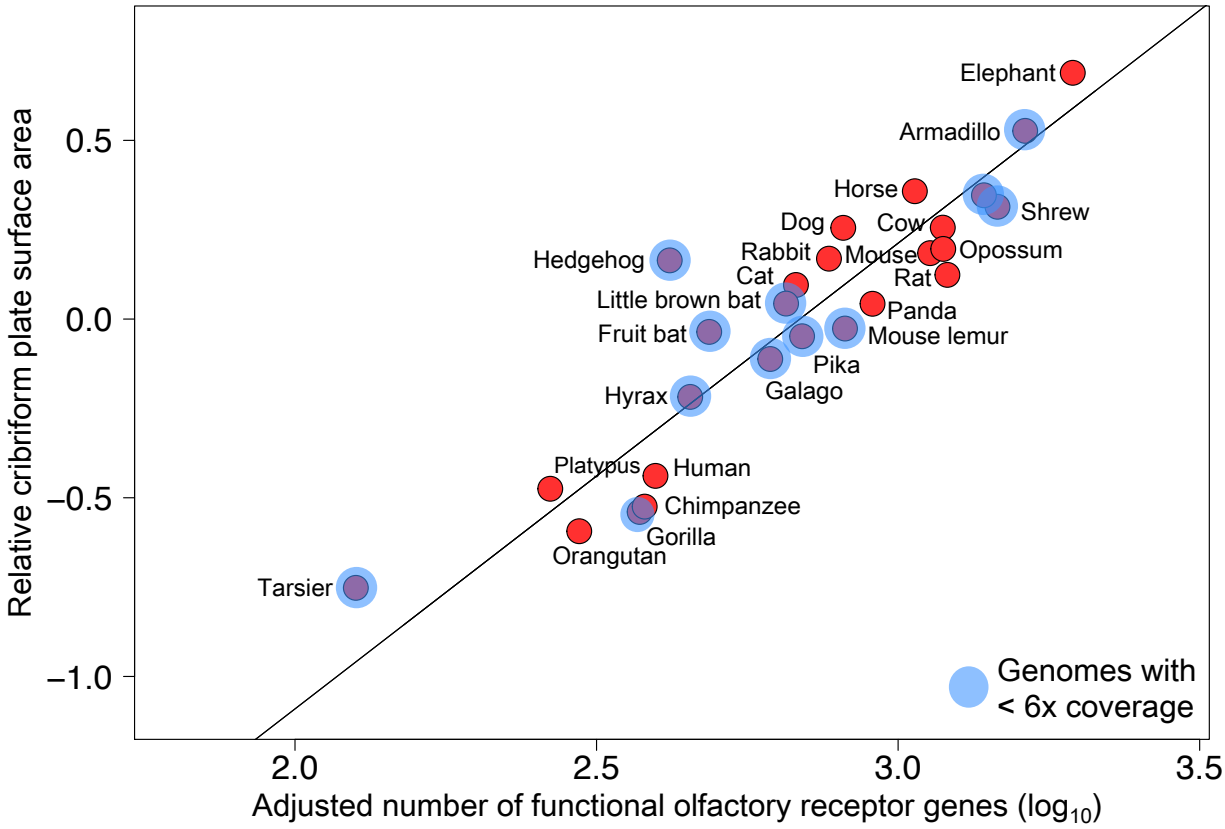

Figure 2-S10. Adjusted RelCP vs ORGs. Hypothetical regression plot of RelCP vs. Number of functional ORGs $_{(\log 10),}$ in which the number of functional ORGs has been increased by 41.5% in all low-coverage genomes (in blue, see Figure 2-S9). The 41.5% increase was derived by comparing the number of ORG extracted from earlier, low-coverage (1.5-2%) draft genomes to the number extracted from current ≥ 6x coverage assemblies, averaged over four available applicable cases (elephant, dog, cat, rabbit). Correlation: $r^2 = 0.84$ (PGLS $r^2 = 0.81$), $P < 0.0001$, $n = 26$. Any increase in the number of OR genes in low-coverage species strengthens the correlation, as all but two of these species have relatively few ORGs for their RelCP size.

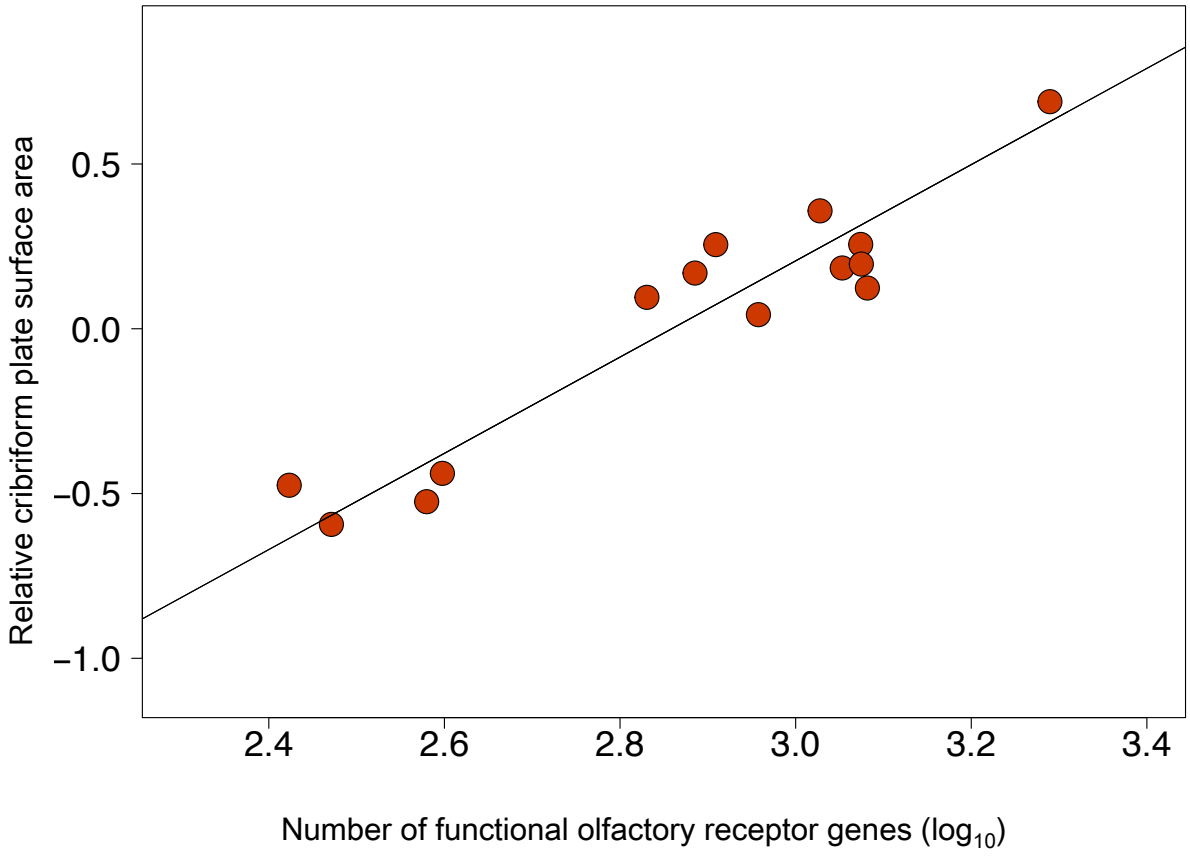

Figure 2-S11. RelCP vs ORGs in ≥ 6x genomes. After omitting species with low-coverage (≤ 6x) genomes, the correlation between RelCPSA and number of functional OR genes strengthens to $r^2 = 0.89$ (PGLS $r^2 = 0.84$), $P < 0.0001$, $n = 14$.

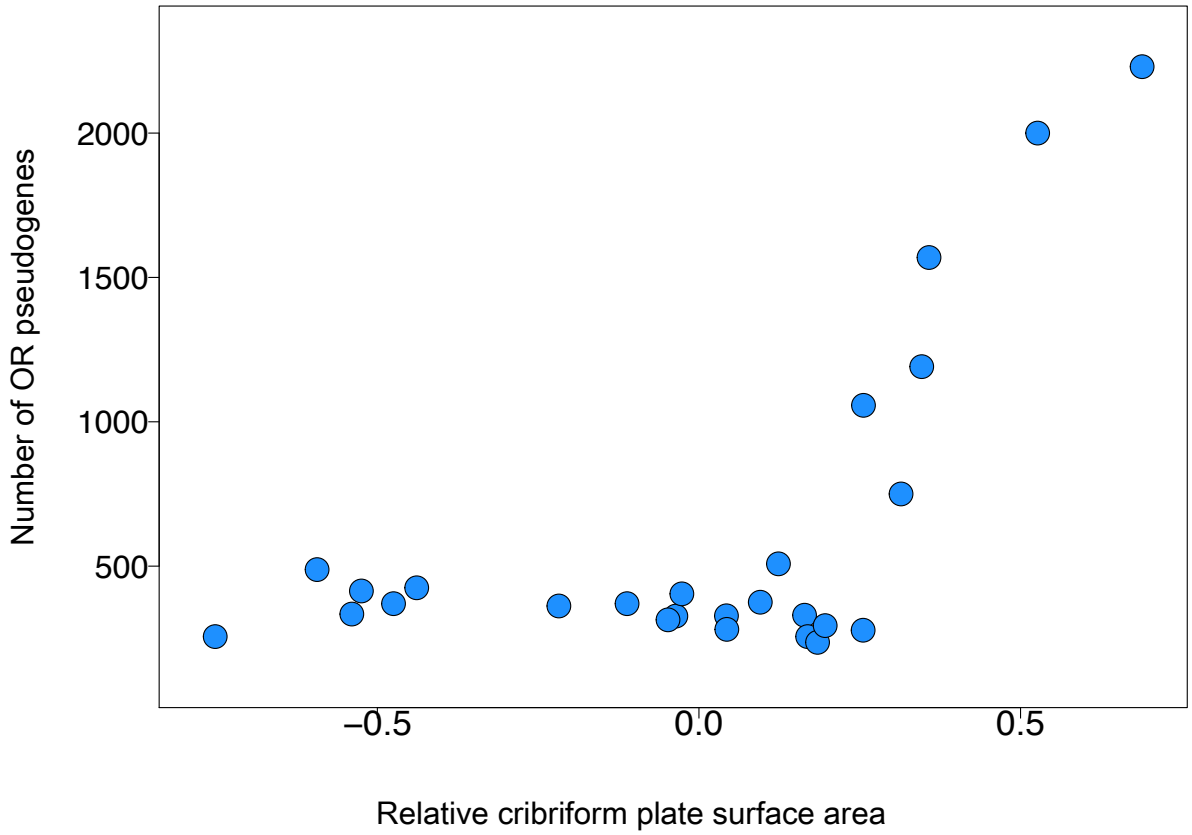

Figure 2-S12. Pseudogenes vs RelCP. Regression of the number of pseudogenes against RelCP. The inversion of the axes from Figure 2-6 in the main text. Species with the largest RelCP tend to have high numbers of pseudogenes.

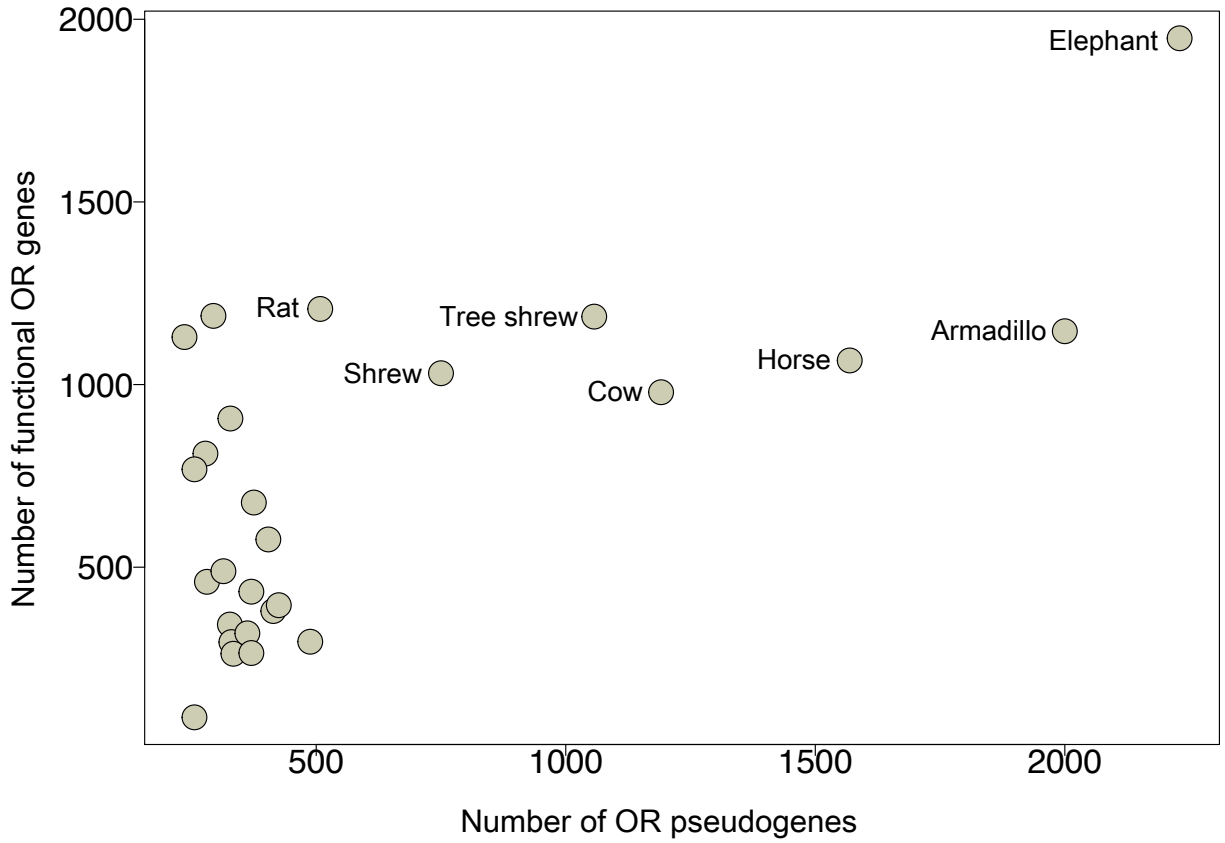

Figure 2S13. Functional ORGs vs Pseudogenes. Regression of the number of functional ORG against number of pseudogenes. Species with the largest number of pseudogenes in their ORG subgenomes tend to possess the largest functional ORG repertoires. This matches the pattern in Figure 2-6 in the main text, in which species with high numbers of pseudogenes tend to have the largest RelCP. However, these two regressions are also different. In this regression, aside from the elephant, large increases in pseudogene counts over ~498 (an inflection point estimated in R package "rpart") are not associated with any significant rise in the number of functional ORG, while the same large increases are accompanied by significant increases in RelCP size (Figure 2-6).

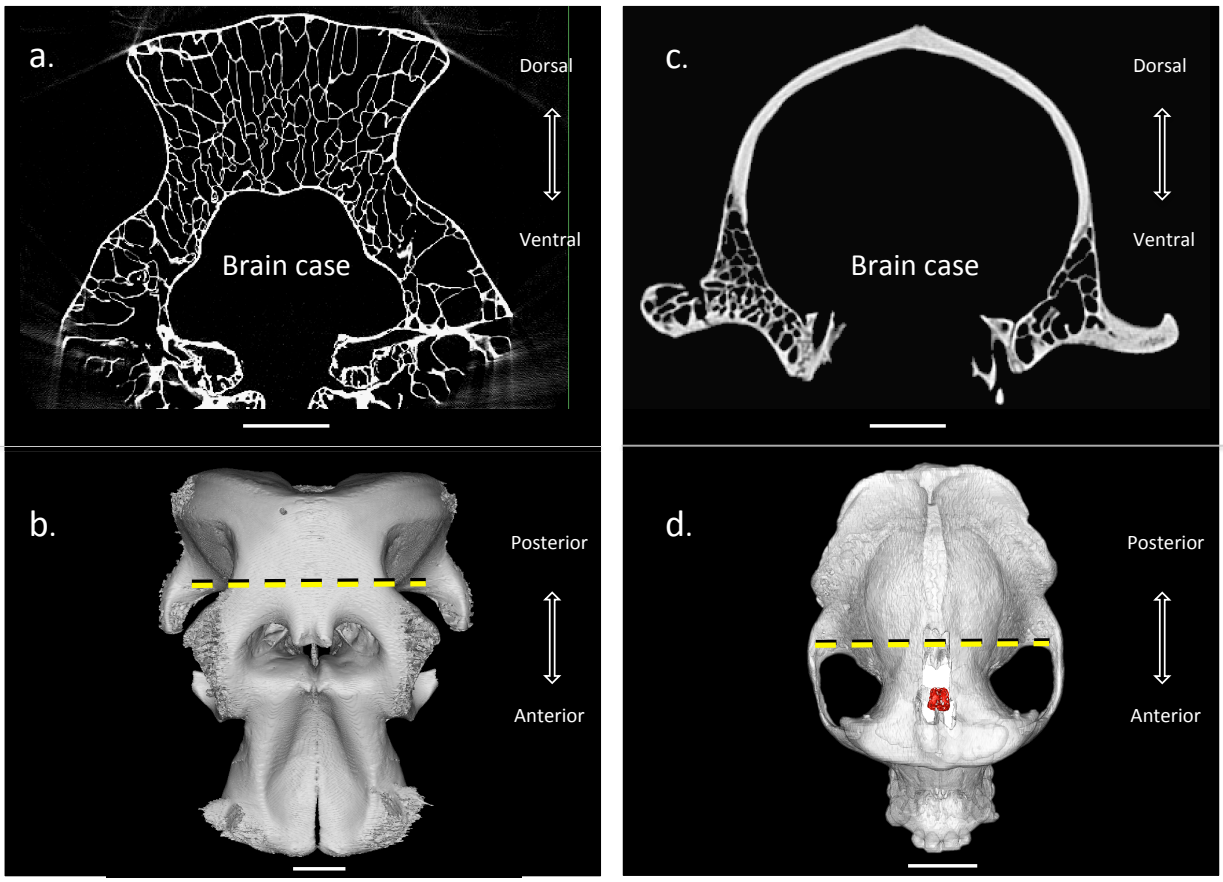

Figure 2-S14. Skull pneumatization surrounding CP. Contrast between pneumatized skull of the African elephant (*Loxodonta africana*) and non-pneumatized skull of the gorilla. **a,** Coronal cross-section slice from high-resolution CT scan of the elephant skull showing the brain case surrounded by a honeycomb of pneumatized bone. Scale bar: 100 mm. **b,** Dorsal view of 3D model of the elephant skull. Yellow dashed line: location of cross-section shown in image **a** above. Scale bar: 100 mm. **c,** Coronal cross-section slice from high-resolution CT scan of the gorilla skull (*Gorilla gorilla*) showing the brain case surrounded by non-pneumatized cortical bone. Scale bar: 40 mm. **d,** Dorsal view of a 3D model of the gorilla skull. Yellow dashed line: location of cross-section shown in the image **b** above. Scale bar: 50 mm.

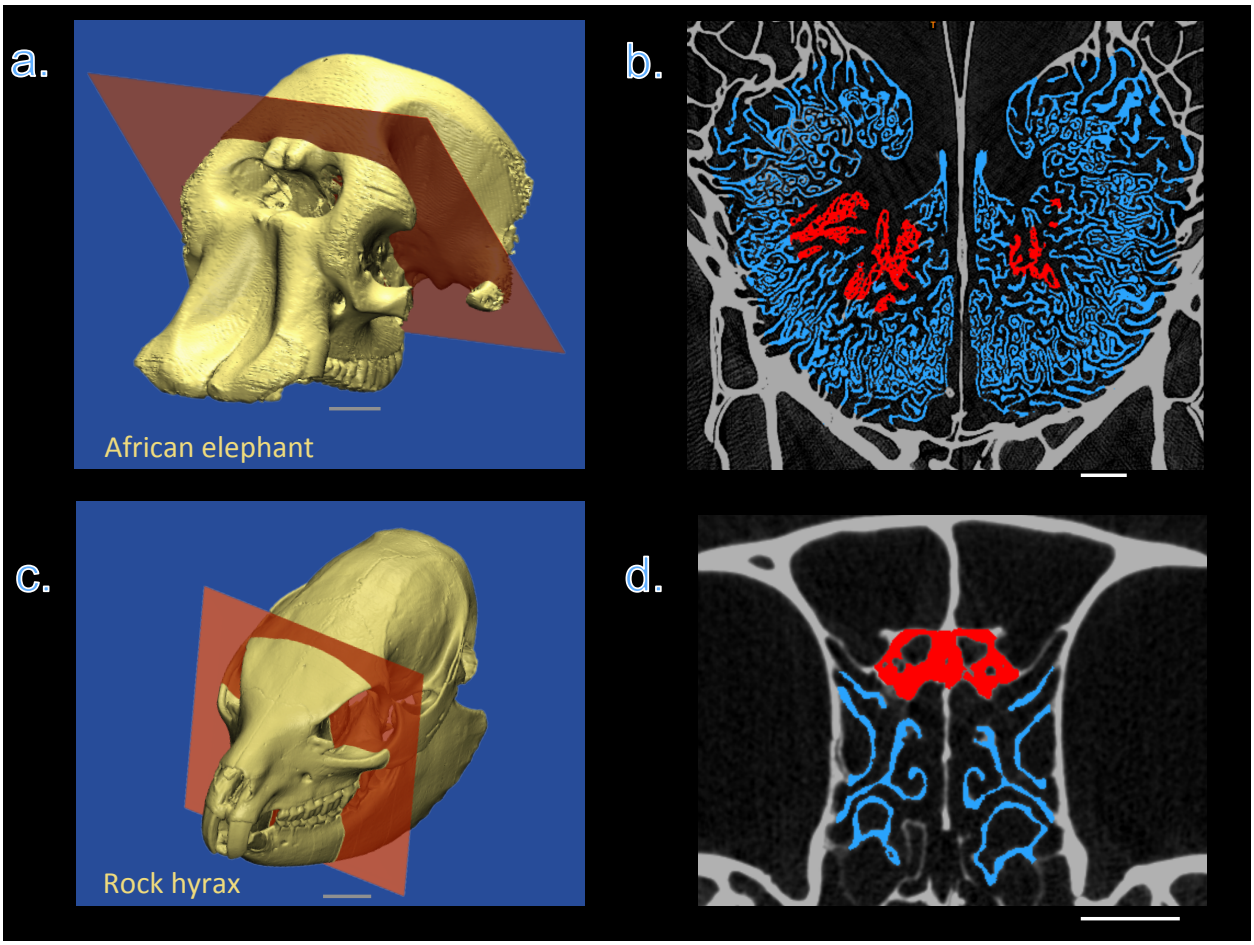

Figure 2-S15. Ethmoturbinals in elephant and hyrax. The ethmoturbinals, nasal bones that carry the olfactory epithelium, are unusually expansive and dense in the African elephant (*Loxodonta africana*). Quantifying turbinal surface area is beyond the scope of this paper, but we contrast here two homologous cross-sections through the nasal chamber at the anterior-most extension of the cribriform plate (CP) in the elephant and its closest living relative, the rock hyrax (*Procavia capensis*). **a,** 3D model of elephant skull seen in anterolateral aspect. Orange plane: location of cross-section shown in next panel. Scale bar: 100 mm. **b,** coronal cross-section of elephant nasal chamber from CT scan. Scale bar: 20 mm. **c,** 3D model of hyrax skull. Scale bar: 10 mm. Orange plane: location of cross-section. **d,** coronal cross-section of hyrax nasal chamber from CT scan. Scale bar: 5 mm. Blue: ethmoturbinal bones. Red: Anterior-most extension of CP.

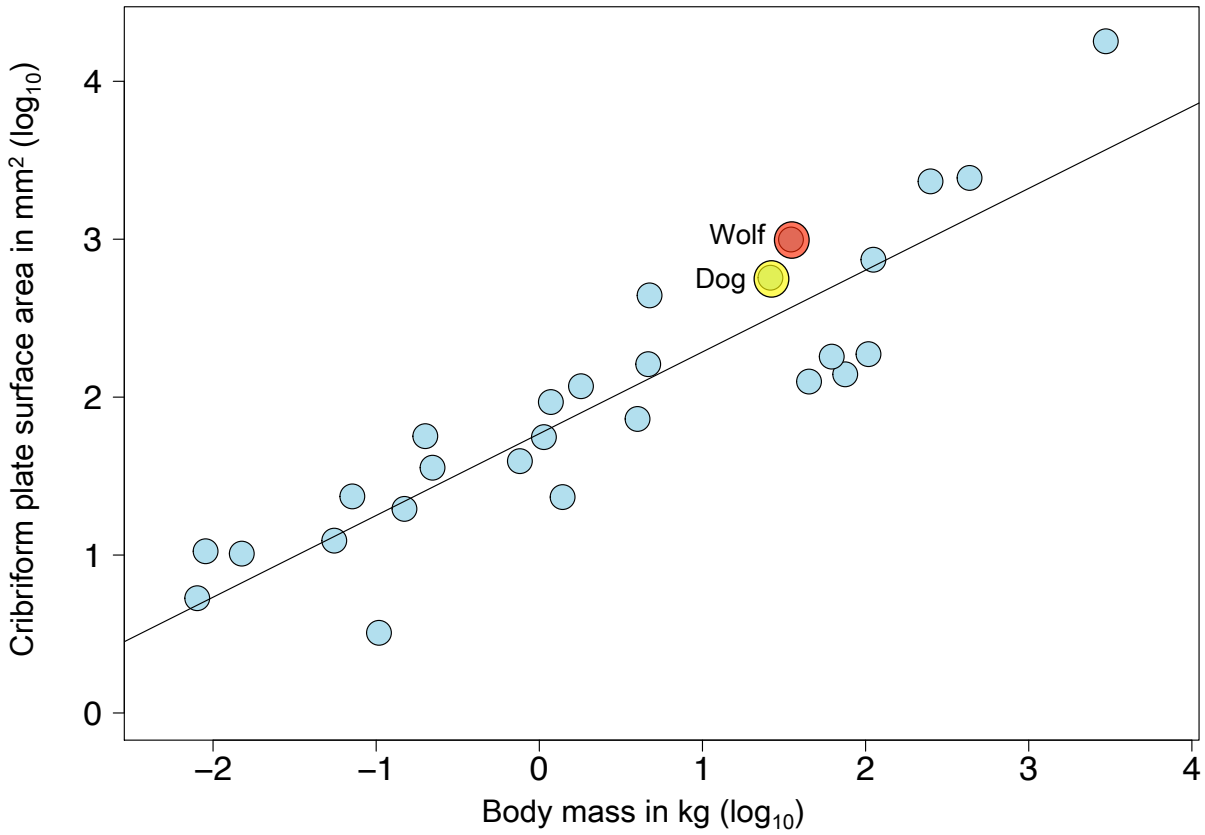

Figure 2-S16. Gray wolf RelCP. The gray wolf (*Canis lupus*) has a larger CP relative to body size within the Log_{10}/Log_{10} plot of CP surface area to body mass when added to the entire sample. The wolf's ORG subgenome has not yet been annotated, but given that the wolf has a larger RelCP, we expect its ORG repertoire to be larger than the dog's.

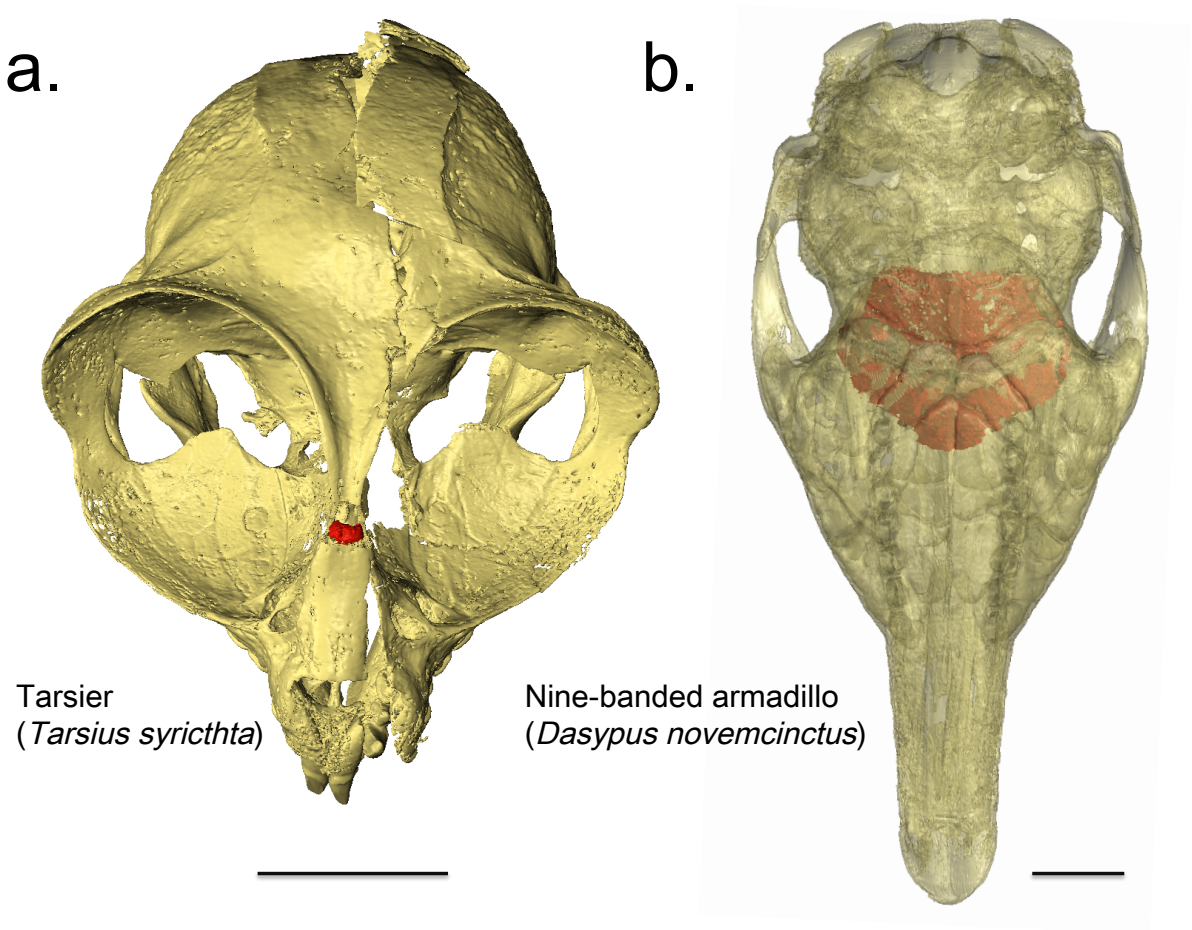

Figure 2-S17. Orbit size and CP size. **a,** The tarsier (*Tarsius syrichta*) is a nocturnal primate with elaborate visual specializations, including enlarged eyes and forward facing orbits. The tarsier's miniscule CP (in red) sits in the posterior nasal chamber squeezed between convergent orbits. Scale bar: 10 mm. **b,** The nine-banded armadillo's (*Dasypus novemcinctus*) orbits are small, laterally oriented, and spaced far apart. Its CP fills the wide space between the orbits. Scale bar: 10 mm.

Table 2-S1: Morphological and genomic data for sample species. Abbreviations: CP, cribriform plate; ORG, olfactory receptor gene. Body mass estimates are listed per species. Where sexual dimorphism was present, we took the sex of individual specimens into consideration when deriving the species body mass. Individual dog breed body size estimates were averaged to calculate the mean body mass of the dog (*Canis familiaris*). For cribriform plate surface area data for individual specimens, see Supplementary Table 3.

Species	Common name	n	CP surface area (mm^2)	Body mass (kg)	Body mass references[a]	Relative CP surface area	Total ORGs	Functional ORGs	Pseudo-genes	Percent pseudo-genes	ORG data references[a]
Ailuropoda melanoleuca	Giant panda	1	741.58	111.600	1	0.016	1235	907	328	0.266	22
Bos taurus	Cow	2	2444.10	453.592	2	0.214	2284	1186	1057	0.463	23
Canis familiaris	Dog: French bulldog, saluki, borzoi, dachshund	4	570.42	21.890	3,4,5,4	0.274	1100	811	278	0.253	23
Canis lupus	Gray wolf	2	995.81	34.875	6	0.410	NA	NA	NA	NA	NA
Dasypus novemcinctus	Nine-banded armadillo	2	440.87	5.647	7	0.472	3146	1146	2000	0.636	24
Equus caballus	Horse	2	2324.24	250.000	4	0.328	2658	1066	1569	0.59	23
Erinaceus europaeus	Hedgehog	3	93.09	1.177	8	0.155	625	295	330	0.528	24
Felis catus	Cat	2	161.72	4.750	9	0.081	1052	677	375	0.356	25
Gorilla gorilla	Gorilla	3	187.17	104.167	10	-0.566	597	263	334	0.559	24
Homo sapiens	Human	3	180.53	62.000	11	-0.463	821	396	425	0.518	26
Loxodonta africana	African elephant	1	17922.00	2766.000	12	0.650	4267	1948	2230	0.523	23
Microcebus murinus	Mouse lemur	3	12.34	0.054	13	-0.018	980	576	404	0.412	24
Monodelphis domestica	Opossum	2	23.52	0.071	4	0.198	1492	1188	294	0.197	27
Mus musculus	Mouse	1	10.21	0.015	4	0.192	1366	1130	236	0.173	24
Myotis lucifugus	Little brown bat	2	5.33	0.010	4	0.015	741	460	281	0.379	22
Ochotona princeps	Pika	2	19.60	0.158	4	-0.062	803	489	314	0.391	24
Ornithorhynchus anatinus	Platypus	2	23.29	1.484	4	-0.500	718	265	370	0.515	27
Oryctolagus cuniculus	Rabbit	2	117.26	1.800	14	0.158	1046	768	256	0.245	23
Otolemur garnettii	Galago	1	39.33	0.760	4	-0.119	803	433	370	0.461	24
Pan troglodytes	Chimpanzee	1	125.47	45.000	4	-0.548	813	380	414	0.509	26
Pongo pygmaeus	Orangutan	2	139.46	75.000	15	-0.619	821	296	488	0.594	26
Procavia capensis	Rock hyrax	2	72.74	4.000	16	-0.231	681	319	362	0.532	24
Pteropus vampyrus	Large flying fox	3	55.82	1.067	17	-0.045	670	343	327	0.488	24
Rattus norvegicus	Rat	2	35.74	0.222	18	0.121	1767	1207	508	0.287	23
Smilodon fatalis	Sabertooth cat	1	1012.00	230.000	19	-0.014	NA	NA	NA	NA	NA
Sorex araneus	Shrew	2	10.57	0.009	20	0.335	1781	1031	750	0.421	24
Tarsius syrichta	Tarsier	1	3.22	0.117	21	-0.778	345	89	256	0.742	24
Tupaia belangeri	Tree shrew	2	56.61	0.200	4	0.344	2170	979	1191	0.549	24
Tursiops truncatus	Bottlenose dolphin	3	NA*	175.000	4	NA	26	12	14	0.538	24

*Presence of cribriform plate in the ethmoid bone of the bottlenose dolphin (*Tursiops truncatus*) cannot be established from this study. [a] For sources of body size and gene counts, see Supplementary References.

Table 2-S2: Summary statistics. Abbreviations: CP, Cribriform plate; RelCP, Relative cribriform plate; ORG, Olfactory receptor genes; MIC, Maximal information coefficient; PGLS, Phylogenetic generalized least squares.

Regression	n	r^2	*P* value	Pearson's r	*P* value	MIC	*P* value	PGLS r^2	*P* value
CP surface area (log_{10}) vs body mass (log_{10})	26	0.823	<0.0001	0.91 (.84,.96)	<0.0001	NA	NA	0.875	<0.0001
RelCP vs functional ORG (log10)	26	0.763	< 0.0001	0.87 (.73, .95)	<0.0001	NA	NA	0.7468	<0.0001
RelCP vs functional ORG (log_{10}) (species with $\geq$ 6x coverage genomes)	14	0.89	<0.0001	0.94 (.85, .98)	<0.0001	NA	NA	0.815	<0.0001
RelCP vs functional ORG (log_{10}) (with $\leq$ 2x species corrected to match predicted count for higher-coverage assemblies)	26	0.841	<0.0001	0.92 (.81, .97)	<0.0001	NA	NA	0.81	<0.0001
RelCP vs total ORG (log_{10})	26	0.68	< 0.0001	0.82 (.66, .92)	<0.0001	NA	NA	0.682	<0.0001
RelCP vs number of pseudogenes (all species)	26	0.358	0.001	0.6 (.3, .77)	0.0013	NA	NA	0.41	0.0004
RelCP vs number of pseudogenes (species with < 500 pseudogenes)	19	0.225	0.04	- 0.47 (-.87, .06)	0.0019	NA	NA	0.029	0.485
RelCP vs number of pseudogenes (species with > 500 pseudogenes)	7	0.825	0.004	0.91 (.59,.995)	0.041	NA	NA	0.82	0.005
RelCP vs percentage of pseudogenes	26	0.114	0.09	-0.84 (-.95, -.63)	0.074	0.673	0.0016	0.09	0.135
Number functional ORG vs pseudogenes	26	0.465	0.0001	0.68 (0.32, .87)	0.0005	NA	NA	0.54	<0.0001
Number functional ORG vs percent pseudogenes	26	0.119	0.084	-0.35 (-.75, .14)	0.084	0.667	0.001	0.066	0.2
Raw CP surface area (log_{10}) vs functional ORG (log_{10})	26	0.22	0.015	0.47 (-.01, 0.74)	0.013	NA	NA	0.27	0.006
Raw CP surface area (log_{10}) vs functional ORG (log_{10}) elephant omitted	25	0.128	0.079	0.36 (-.12, 0.66)	0.078	NA	NA	0.16	0.047

Table 2-S3. Sources and morphological data from felid species. Museums and collections are as follows: FMNH, Field Museum of Natural History; LACM, Museum of Natural History of Los Angeles County; LACMRLP, Rancho La Brea Tar Pits; MMNH, James Ford Bell Museum University of Minnesota, Minneapolis; UCLAEEB, University of California Los Angeles Department of Ecology and Evolutionary Biology

Species	Sex	Specimen	Body mass[a]	Cribriform plate surface area (mm^2)
Acinonyx jubatus	M	FMNH29635	50.00	473.072
Acinonyx jubatus	F	FMNH127834	50.00	396.43
Felis catus	M	UCLAEEB110_4	4.65	188.858
Felis catus	U	UCLAEEB110_3	4.75	134.59
Felis silvestris	M	LACM14480	4.75	206.265
Felis silvestris	F	LACM14474	4.65	157.456
Leopardus pardalis	M	FMNH34339	12.00	296.37
Leopardus pardalis	F	LACM26789	12.00	353.497
Lynx rufus	M	UCLA10115	9.00	225.126
Lynx rufus	F	LACM15254	9.00	220.712
Neofelis nebulosa	M	LACM31155	19.50	371.343
Neofelis nebulosa	M	USNM282124	19.50	429.038
Panthera leo	M	MMNH17537	161.50	1149.921
Panthera leo	F	MMNH17533	161.50	1041.53
Prionailurus viverrinus	U	LACM90838	10.85	184.974
Prionailurus viverrinus	F	LACM56718	10.85	152.295
Puma concolor	M	LACM87430	51.60	701.497
Puma concolor	F	LACM85440	51.60	686.83
Smilodon fatalis	U	LACMRLP_R37376	230.00	820.05

[a]Estimated body masses are from Smith et al. (2003)[4], except for two species, *Felis catus*[5] and *Smilodon fatalis*[19].

Table 2-S4. Sources and cribriform plate surface area for individual specimens of the sample species. AMNH: American Museum of Natural History. CMNH: Cleveland Museum of Natural History. DLC: Duke Lemur Center. DUPC: Duke University Primate Center. IZCAS: Institute of Zoology of the Chinese Academy of Sciences. LACM: Natural History Museum of Los Angeles County. LACMRLP: Rancho La Brea Tar Pits. MVZ: Museum of Vertebrate Zoology. SDSMH: San Diego Society of Natural History. UCLA: Donald R. Dickey Collection at the University of California Los Angeles. UCLAEEB: UCLA Department of Ecology and Evolutionary Biology. USNM: National Museum of Natural History. UTO: University of Texas Austin.

Species	Specimen	Sex	Cribriform plate surface area (mm^2)
Ailuropoda melanoleuca	IZCAS6072	U	741.58
Bos taurus	MVZ114370	F	2482.09
Bos taurus	UCLAEEB110_1	U	2406.12
Canis familiaris	LACM031106	M	382.21
Canis familiaris	LACM022825	U	601.60
Canis familiaris	LACM30539	M	851.57
Canis familiaris	UCLA3054	U	446.28
Canis lupus	USNM291011	M	1045.53
Canis lupus	USNM507338	F	946.09
Dasypus novemcinctus	LACM46145	M	425.00
Dasypus novemcinctus	UCLA1697	M	456.73
Equus cabalus	MVZ223018	M	2321.06
Equus cabalus	UCLAEEB110_2	U	2327.43
Erinaceus europea	LACM58376	M	93.44
Erinaceus europea	LACM58375	F	81.04
Erinaceus europea	MVZ183386	M	104.79
Felis catus	UCLAEEB110_3	M	188.86
Felis catus	UCLAEEB110_4	U	134.59
Gorilla gorilla	MVZ174521	F	165.18
Gorilla gorilla	UCLA1788	M	261.12
Gorilla gorilla	UCLA2367	F	135.21
Homo sapiens	MVZ106555	F	208.91
Homo sapiens	UTO_HS01	M	171.03
Homo sapiens	UCLAEEB110_5	F	161.65
Loxodonta africana	LACM52471	F	17922.00
Microcebus murinus	MVZ132535	F	12.82
Microcebus murinus	DLC7006	M	11.02
Microcebus murinus	DUPC098	U	13.18
Monodelphis domestica	MVZ144306	F	24.01
Monodelphis domestica	MVZ144307	M	23.03
Mus musculus	TMM3196	M	10.21

Species	Specimen	Sex	Cribriform plate surface area (mm^2)
Myotis lucifugus	AMNH232239	U	5.83
Myotis lucifugus	AMNH232244	U	4.83
Ochotona princeps	UCLA17230	M	19.29
Ochotona princeps	MVZ42613	M	19.29
Ornithorrynchus anatinus	MVZ126977	M	22.42
Ornithorrynchus anatinus	MVZ126978	M	24.16
Orychtolagus cuniculus	LACM7601	M	124.79
Orychtolagus cuniculus	LACM7603	M	109.74
Otolemur garnetti	CMNH_B0748	U	39.33
Pan troglodyes	USNM395820	U	125.47
Pongo pygmaeus	MVZ65532	M	129.65
Pongo pygmaeus	UT49859	M	149.27
Procavia capensis	LACM90782	M	77.33
Procavia capensis	UCLATMM4351	M	68.16
Pteropus vampyrus	LACM91185	U	44.92
Pteropus vampyrus	LACM91183	U	47.67
Pteropus vampyrus	MVZ116834	M	74.87
Rattus norvegicus	UCLA6994	F	35.61
Rattus norvegicus	UCLA9452	M	35.86
Smilodon fatalis	LACMRLP_R37376	U	1012.00
Sorex araneus	MVZ179796	F	10.57
Tarsius syrichtus	DLC1406_82	F	3.22
Tupaia belangeri	LACM008157	M	57.93
Tupaia belangeri	MVZ119721	M	55.30
Tursiops truncatus	SDSNH 21212	U	NA*
Tursiops truncatus	LACM84269	M	NA*
Tursiops truncatus	LACM95828	U	NA*

*The presence of a cribriform plate in the ethmoid bone of the bottlenose dolphin (*Tursiops truncatus*) could not be established in this study.

References

Albanese, D. *et al.* Minerva and minepy: A C engine for the MINE suite and its R, Python and MATLAB wrappers. *Bioinformatics* **29,** 407–408 (2013).

Bates, L. A. *et al.* African elephants have expectations about the locations of out-of-sight family members. *Biol Lett* **4,** 34–36 (2008).

Bates, L. A. *et al.* Elephants Classify Human Ethnic Groups by Odor and Garment Color. *Curr. Biol.* **17,** 1938–1942 (2007).

Bhatnagar, K. P. & Kallen, F. C. Cribiform plate of ethmoid, olfactory bulb and olfactory acuity in forty species of bats. *J. Morphol.* **142,** 71–90 (1974).

Bird, D. J., Amirkhanian, A., Pang, B. & Van Valkenburgh, B. Quantifying the cribriform plate: influences of allometry, function, and phylogeny in Carnivora. *Anat. Rec. (Hoboken).* **297,** 2080–2092 (2014).

Bressel, O. C., Khan, M. & Mombaerts, P. Linear correlation between the number of olfactory sensory neurons expressing a given mouse odorant receptor gene and the total volume of the corresponding glomeruli in the olfactory bulb. *J. Comp. Neurol.* **524,** 199–209 (2015).

Browne, C., Stafford, K. & Fordham, R. The use of scent-detection dogs. **59,** (2006).

Buck, L. & Axel, R. A novel multigene family may encode odorant receptors: a molecular basis for odor recognition. *Cell* **65,** 175–187 (1991).

Chen, I. H. *et al.* Armadillo armor: Mechanical testing and micro-structural evaluation. *J. Mech. Behav. Biomed. Mater.* **4,** 713–722 (2011).

Chess, A., Simon, I., Cedar, H. & Axel, R. Allelic inactivation regulates olfactory receptor gene expression. *Cell* **78,** 823–834 (1994).

Collins, C. E., Hendrickson, A. & Kaas, J. H. Overview of the visual system oftarsius. *Anat. Rec. Part A Discov. Mol. Cell. Evol. Biol.* **287A,** 1013–1025 (2005).

Fan, Z. *et al.* Worldwide patterns of genomic variation and admixture in gray wolves. *Genome Res.* **26,** 163–173 (2016).

Farbman, A. I. *Cell biology of olfaction*. **27,** (Cambridge University Press, 1992).

Foley, N. M., Springer, M. S. & Teeling, E. C. Mammal madness: is the mammal tree of life not yet resolved? *Philos. Trans. R. Soc. Lond. B. Biol. Sci.* **371,** 3667–3679 (2016).

Foley, N. M., Springer, M. S. & Teeling, E. C. Mammal madness: is the mammal tree of life not yet resolved? *Philos. Trans. R. Soc. B Biol. Sci.* **371,** 20150140 (2016).

Fritz, S. A., Bininda-Emonds, O. R. P. & Purvis, A. Geographical variation in predictors of mammalian extinction risk: Big is bad, but only in the tropics. *Ecol. Lett.* **12,** 538–549 (2009).

Garrett, E. C. & Steiper, M. E. Strong links between genomic and anatomical diversity in both mammalian olfactory chemosensory systems. *Proc Biol Sci* **281,** 20132828 (2014).

Gilad, Y., Wiebe, V., Przeworski, M., Lancet, D. & Pääbo, S. Correction : Loss of Olfactory Receptor Genes Coincides with the Acquisition of Full Trichromatic Vision in Primates Correction : Structural and Chemical Profiling of the Human Cytosolic Sulfotransferases. *PLoS Biol.* **2,** 50165 (2007).

Hayden, S. *et al.* Ecological adaptation determines functional mammalian olfactory subgenomes. *Genome Res.* **20,** 1–9 (2010).

Hughes, G. & Mur. Myotis_lucifugus_genomicORs.

Lindblad-Toh, K. *et al.* Genome sequence, comparative analysis and haplotype structure of the domestic dog. *Nature* **438,** 803–819 (2005).

Ma, L. *et al.* A developmental switch of axon targeting in the continuously regenerating mouse olfactory system. *Science (80-.).* **344,** 194–197 (2014).

Matsui, A., Go, Y. & Niimura, Y. Degeneration of olfactory receptor gene repertories in primates: No direct link to full trichromatic vision. *Mol. Biol. Evol.* **27,** 1192–1200 (2010).

McDonough, C. M. & Loughry, W. J. *The nine-banded armadillo: a natural history*. **11,** (University of Oklahoma Press, 2013).

Meredith, R. W. *et al.* Impacts of the Cretaceous Terrestrial Revolution and KPg extinction on mammal diversification. *Science* **334,** 521–4 (2011).

Miller, A. M., Maurer, L. R., Zou, D.-J., Firestein, S. & Greer, C. A. Axon fasciculation in the developing olfactory nerve. *Neural Dev.* **5,** 20 (2010).

Miyamichi, K. Continuous and Overlapping Expression Domains of Odorant Receptor Genes in the Olfactory Epithelium Determine the Dorsal/Ventral Positioning of Glomeruli in the Olfactory Bulb. *J. Neurosci.* **25,** 3586–3592 (2005).

Mombaerts, P. *et al.* Visualizing an olfactory sensory map. *Cell* **87,** 675–686 (1996).

Montague, M. J. *et al.* Comparative analysis of the domestic cat genome reveals genetic signatures underlying feline biology and domestication. *Proc. Natl. Acad. Sci. U. S. A.* **111,** 17230–5 (2014).

Negus, V. The Comparative Anatomy of the Nose and Paranasal sinuses Livingstons. (1958).

Nei, M., Niimura, Y. & Nozawa, M. The evolution of animal chemosensory receptor gene repertoires: roles of chance and necessity. *Nat Rev Genet* **9,** 951–963 (2008).

Ngwenya, A., Patzke, N., Ihunwo, A. & Manger, P. R. Organisation and chemical neuroanatomy of the African elephant (Loxodonta africana) olfactory bulb. *Brain Struct. Funct.* **216,** 403–416 (2011).

Niimura, Y. Identification of olfactory receptor genes from mammalian genome sequences. *Methods Mol. Biol. (Clifton, NJ)* **1003,** 39–49 (2012).

Niimura, Y., Matsui, A. & Touhara, K. Extreme expansion of the olfactory receptor gene repertoire in African elephants and evolutionary dynamics of orthologous gene groups in 13 placental mammals. *Genome Res.* **24,** 1485–1496 (2014).

Niimura, Y. & Nei, M. Extensive gains and losses of olfactory receptor genes in mammalian evolution. *PLoS One* **2,** e708 (2007).

Oelschläger, H. H. a & Buhl, E. H. Development and rudimentation of the peripheral olfactory system in the harbor porpoise *Phocoena phocoena* (Mammalia: Cetacea). *J. Morphol.* **184,** 351–360 (1985).

Orme, D. *et al.* caper: Comparative Analyses of Phylogenetics and Evolution in R. R package version 0.5.2. http://CRAN.R-project.org/package=caper. (2013).

Pease, M., Marquez, Y., Tuchman, A., Markarian, A. & Zada, G. Diagnosis and surgical management of traumatic cerebrospinal fluid oculorrhea: case report and systematic review of the literature. *J. Neurol. Surg. reports* **74,** 57–66 (2013).

Pettigrew, J. D. Electroreception in monotremes. *J. Exp. Biol.* **202,** 1447–1454 (1999).

Pihlström, H., Fortelius, M., Hemilä, S., Forsman, R. & Reuter, T. Scaling of mammalian ethmoid bones can predict olfactory organ size and performance. *Proc. Biol. Sci.* **272,** 957–962 (2005).

Poliseno, L. *et al.* A coding-independent function of gene and pseudogene mRNAs regulates tumour biology. *Nature* **465,** 1033–8 (2010).

R Core Team. R: A language and environment for statistical computing (Version 3.0. 2). *R Found. Stat. Comput. Vienna, Austria* (2014).

Reshef, D. *et al.* in Large Data Sets. *Sci. Transl. Med.* **334,** 1518–1524 (2011).

Ridgeway, S. The Terminal Nerve in Odontocete Cetaceans. *Ann. N. Y. Acad. Sci.* 1–5 (1987).

Rouquier, S., Blancher, a & Giorgi, D. The olfactory receptor gene repertoire in primates and mouse: evidence for reduction of the functional fraction in primates. *Proc. Natl. Acad. Sci. U. S. A.* **97,** 2870–2874 (2000).

Rowe, Timothy; Macrini, Thomas E; Luo, Z.-X. Fossil Evidence on Origin of the Mammalian Brain. *Science (80-.).* **332,** 955–957 (2011).

Shoshani, J., Kupsky, W. J. & Marchant, G. H. Elephant brain. Part I: Gross morphology, functions, comparative anatomy, and evolution. *Brain Res. Bull.* **70,** 124–157 (2006).

Shum, E. Y., Espinoza, J. L., Ramaiah, M. & Wilkinson, M. F. Identification of novel post-transcriptional features in olfactory receptor family mRNAs. *Nucleic Acids Res.* **43,** 9314–9326 (2015).

Stock, C. & Harris, J. M. *Rancho La Brea: a record of Pleistocene life in California*. (Natural History Museum of Los, 1992).

Team, R. C. R: A language and environment for statistical computing. R Foundation for Statistical Computing, Vienna, Austria. 2013. (2014).

Therneau, T. M., Atkinson, B. & Ripley, B. rpart: Recursive partitioning. *R Packag. version* **3,** 1–46 (2010).

Turcsán, B., Kubinyi, E. & Miklósi, Á. Trainability and boldness traits differ between dog breed clusters based on conventional breed categories and genetic relatedness. *Appl. Anim. Behav. Sci.* **132,** 61–70 (2011).

Supplementary References

1. Smith, F. A. *et al.* Body mass of late Quaternary mammals. *Ecology* **84,** 3403 (2003).

2. Oklahoma Dept. Agriculture, Food, Forestry. How much meat? http://www.oda.state.ok.us/, (2015)

3. French bulldog breed standard. French Bulldog Club of America. http://fbdca.org/, (2014)

4. Crowley, J. & Adelman, B. The complete dog book: official publication of the American Kennel Club. *New York Howell House* (1998).

5. Shiel, R. E., Sist, M., Nachreiner, R. F., Ehrlich, C. P. & Mooney, C. T. Assessment of criteria used by veterinary practitioners to diagnose hypothyroidism in sighthounds and

investigation of serum thyroid hormone concentrations in healthy Salukis. *J. Am. Vet. Med. Assoc.* **236,** 302–308 (2010).

6. Ernest, S. K. M. Life history characteristics of placental nonvolant mammals. *Ecology* **84,** 3402 (2003).

7. Wetzel, R. M. & Mondolfi, E. *The subgenera and species of long-nosed armadillos, genus Dasypus L*. (Smithsonian Inst. Press, Washington, 1979).

8. Rautio, A., Valtonen, A. & Kunnasranta, M. The Effects of Sex and Season on Home Range in European Hedgehogs at the Northern Edge of the Species Range. *Ann. Zool. Fennici* **50,** 107–123 (2013).

9. Myers, P. *et al.* The animal diversity web. *Accessed Oct.* **12,** 2 (2006).

10. Jungers, W. L. in *Size and scaling in primate biology* 345–381 (Springer, 1985).

11. Walpole, S. C. *et al.* The weight of nations: an estimation of adult human biomass. *BMC Public Health* **12,** 439 (2012).

12. Laws, R. M. (1970). Elephants and habitats in north Bunyoro, Uganda. *African Journal of Ecology*, *8*(1), 163–180.

13. Fietz, J. Body Mass in Wild Microcebus murinus over the Dry Season. *Folia Primatol.* **69,** 183–190 (1998).

14. Nowak, R. M. *Walker's Mammals of the World*. **1,** (JHU Press, 1999).

15. Groves, C. P. Pongo pygmaeus. *Mamm. Species* 1–6 (1971).

16. Olds, N. & Shoshani, J. Procavia capensis. *Mamm. Species* 1–7 (1982).

17. McNab, B. K. & Armstrong, M. I. Sexual dimorphism and scaling of energetics in flying foxes of the genus Pteropus. *J. Mammal.* **82,** 709–720 (2001).

18. Glass, G. E., Korch, G. W. & Childs, J. E. Seasonal and habitat differences in growth rates of wild Rattus norvegicus. *J. Mammal.* **69,** 587–592 (1988).

19. Van Valkenburgh, B., Hayward, M. W., Ripple, W. J., Meloro, C. & Roth, V. L. The impact of large terrestrial carnivores on Pleistocene ecosystems. *Proc. Natl. Acad. Sci.* **113,** 1–6 (2015).

20. Gębczyński, M. Seasonal and age changes in the metabolism and activity of Sorex araneus Linnaeus 1758. *Acta Theriol. (Warsz).* **10,** 303–331 (1965).

21. Kappeler, P. M. Patterns of Sexual Dimorphism in Body Weight among Prosimian Primates. *Folia Primatol.* **57,** 132–146 (1991).

22. Hughes, G. M., Gang, L., Murphy, W. J., Higgins, D. G. & Teeling, E. C. Using Illumina next generation sequencing technologies to sequence multigene families in de novo species. *Mol. Ecol. Resour.* **13,** 510–521 (2013).

23. Niimura, Y., Matsui, A. & Touhara, K. Extreme expansion of the olfactory receptor gene repertoire in African elephants and evolutionary dynamics of orthologous gene groups in 13 placental mammals. *Genome Res.* **24,** 1485–1496 (2014).

24. Hayden, S. *et al.* Ecological adaptation determines functional mammalian olfactory subgenomes. *Genome Res.* **20,** 1–9 (2010).

25. Montague, M. J. *et al.* Comparative analysis of the domestic cat genome reveals genetic signatures underlying feline biology and domestication. *Proc. Natl. Acad. Sci. U. S. A.* **111,** 17230–5 (2014).

26. Matsui, A., Go, Y. & Niimura, Y. Degeneration of olfactory receptor gene repertories in primates: No direct link to full trichromatic vision. *Mol. Biol. Evol.* **27,** 1192–1200 (2010).

27. Niimura, Y. & Nei, M. Extensive gains and losses of olfactory receptor genes in mammalian evolution. *PLoS One* **2,** e708 (2007).

CHAPTER 3

Olfaction at the interface of aquatic and terrestrial habitats: cribriform plate morphology in arctoid carnivorans

Introduction

Mammals rely to varying degrees on the sense of smell for their existence. Olfactory systems have evolved to operate in distinct ecological contexts; as lineages, foraging landscapes and chemical stimuli change over evolutionary time, species acquire and lose olfactory capacities (Hayden et al., 2010; Van Valkenburgh et al., 2011; Gittleman, 2013). For example, it is widely accepted that cetaceans, obligate aquatic mammals with almost no chemosensory input, rely little on olfaction and have lost the adaptive olfactory anatomy and behaviors present in their terrestrial ancestors. (Buhl et al., 1988; Oelschläger, 1992). There is less agreement on the relative role smell plays in the life of aquatic mammals with residual ties to the land, such as the arctoid carnivoran pinnipeds and sea otter (*Enhydra lutris*). An early report from Harrison and Kooyman (1968) suggested that the olfactory apparatus of pinnipeds is generally and variably reduced, while a more recent study claims that pinniped olfactory anatomy is not significantly different from that of their terrestrial relatives (Pihlström, 2008). The idea that pinnipeds and the sea otter retain a keen sense of smell is reinforced by reported field observations of scent-driven interactions, such as nose-to-nose nuzzling, genital sniffing, alarm responses to upwind biologists, and aversive reaction to con-specific carcass odors (Ross, 1970; Riedman et al., 1990; Lowell et al., 1980; Peterson and Bartholomew, 1967). While these examples describe numerous facets of an aquatic carnivoran's chemosensory ecology on land, there is one olfactory dimension that is overlooked here. For carnivorans that forage underwater, critical odor cues typically used by terrestrial species (Ewer, 1973; Nowak, 1999) are completely absent. Diving mammals forage with their nares closed (Riedman, 1990; Reidenberg, 2007). While underwater, an aquatic mammal is shut off from all chemical cues and forages "noseblind". For this reason we hypothesize that aquatic carnivorans rely less on olfaction than closely related terrestrial

species and predict that this will be reflected in reduced olfactory anatomy. To test this hypothesis, we look to the cribriform plate (CP), a bone in the posterior nasal cavity that is perforated by passageways for olfactory nerve bundles crossing from the periphery to the olfactory bulb of the brain. Because CP size varies with the amount of peripheral innervation found in a mammal's snout (Pihlström et al., 2005), quantifying the CP provides an opportunity to gauge and compare relative olfactory investment within aquatic and terrestrial species (Bird et al., 2014). Here we perform the first extensive comparative and quantitative study of the CP morphology of arctoid carnivorans, a clade that has seen multiple independent invasions into the marine habitat and includes species at the intersection of terrestrial and aquatic life.

The CP is an informative and easily quantifiable feature of olfactory anatomy. It separates the nasal cavity from the brain case and sits at the center of the olfactory sensory pathway. Every axon projecting from an olfactory sensory neuron on the epithelium lining the ethmoturbinals and nasal septum must traverse the CP to deliver its odor signal to the brain (Farbman, 1992). As axons exit the nasal cavity in fasciculated bundles, they leave their imprint in myriad foramina in the CP bone (Negus, 1958) (Fig. 3-1). The CP is developmentally and functionally closely associated with the olfactory-related ethmoturbinals. In fetal mammals, the CP arises as an outgrowth of developing ethmoidal turbinal bones (Rowe et al., 2005). The CP and ethmoturbinals are tightly correlated in size (Bird et al., 2014, Van Valkenburgh et al., 2011) and share space in the posterior-most extent of the nasal cavity.

Using high-resolution CT scans and 3D imaging software and methods developed in Chapter One (Bird et al., 2014), we measured the surface area of the perforated region of the CP as well as the cumulative cross-sectional area of the CP foramina as metrics of relative olfactory innervation found in individual arctoid species.

Our sample group, the arctoid carnivorans, is an ecologically rich clade that includes ursids (bears), mustelids (weasels otters, and related), procyonids (raccoons and related), mephitids (skunks) and pinnipeds, among others (Fig. 3-2) (Meredith et al., 2011; Slater et al., 2012). Within the arctoids across evolutionary time, there were at least three independent, secondary entries into aquatic habitats (Berta et al., 2015), resulting in a diversity of closely related species from disparate ecologies (aquatic, semi-aquatic, terrestrial) along a spectrum of olfactory demands. For example, otters diverged from terrestrial mustelids only ~ 8-9 million years ago (Koepfli et al., 2008). A second aquatic group, the pinnipeds, are nested within the arctoids in a lineage that diverged from the terrestrial ursids an estimated 25-35 ma. (Berta et al., 2015, Meredith et al., 2011). Studying Carnivora is also advantageous because the group has a fairly well resolved phylogeny, allowing the application of comparative methods that account for phylogenetic relatedness in our study of ecological influences on olfaction.

We grouped the arctoids into three behavioral ecologies, terrestrial, aquatic and semi-aquatic. We defined terrestrial species as those that live and forage exclusively on land. These include members of the ursids, mustelids, procyonids and mephitids. Those in the aquatic grouping forage exclusively underwater but also spend some time hauled out on land or pack-ice. The semi-aquatics forage both underwater and on land and include two mustelid species, the American mink (*Neovison vison*) and the North American river otter (*Lontra canadensis*).

As mammals transitioned to foraging in an aquatic habitat without the guidance of odor cues, we expect that the selective pressure on olfactory performance eased, resulting in the partial loss of olfactory function as manifested in smaller CPs. There may also be specific costs that result in a smaller CP in aquatic carnivorans as well. The transition to an aquatic lifestyle requires anatomical specializations that could impose structural constraints on olfactory systems.

Pinnipeds and sea otters pursue their prey while holding their breath in a medium that is bereft of all airborne odor cues, dimly lit and a source of potentially damaging hydrostatic pressure. They have evolved visual and mechanosensory adaptations, such as enlarged eyes and densely innervated vibrissae, to facilitate prey detection under such conditions (Berta et al., 2015; Stephens et al., 1973). Eye orbit size appears to correlate with diving depth suggesting an adaptation to foraging in nearly total darkness (Debey et al., 2012). Additionally, in response to increased pressure on the skull when diving and potential tissue trauma (Kooyman et al., 1998), aquatic carnivorans have lost all pneumatized cranial sinuses (King, 1983; Curtis et al., 2015) and have evolved a plexus of distensible venous tissue postulated to expand at depth and reduce the volume of the air-filled middle ear cavity (Welsch et al., 1997). Because the CP and ethmoturbinals are situated between the orbits and within the posterior nasal cavity, an air-filled space, it is reasonable to hypothesize that evolutionary changes to the latter structures driven by selection for enhanced vision and mitigation of diving pressures might reduce the amount of space available for the olfactory skeleton. For these reasons, we investigate a possible relationship between CP size and dive depth, as well as dive duration, within the group of aquatic carnivorans. We predict that relative CP size will covary inversely with dive depth and duration.

Materials and methods

Specimen collection

We sampled 56 skulls from 28 species representing eight families of arctoid carnivorans (Fig. 3-1). Specimens and their source museums are listed in Table 3-3. All species were extant with the exception of the tropical monk seal (*Monachus tropicalis*). Body sizes span three orders of magnitude from <1 kg (long-tailed weasel, *Mustela* frenata) to ~750 kg (Northern elephant

seal, *Mirounga angustirostris*). Where possible, we sampled two wild-caught adult specimens, one male and one female, for each species.

Morphological data

Thirty-five of the 56 skulls were scanned at the University of Texas High Resolution CT Scanning Facility (http://www.ctlab.geo.utexas.edu). The remaining 21 skulls were scanned on Phoenix nanotom s™ machines at the Molecular Imaging Center of the Keck School of Medicine of USC in Los Angeles, on Phoenix v|tomex™ machines at General Electric's Inspections Technologies Facility in San Carlos, California, or on a Siemens Definition AS64™ scanner at Ronald Reagan Medical Center at UCLA. In order to maximize resolution, the field of view was restricted to the CP area of the skull in most cases, although a number of skulls were scanned in their entirety. Voxel size ranged from 0.044 to 0.5 mm. All scans are available upon request from either Digimorph (http://www.digimorph.org) or MorphoSource (http://www.morphosource.org/). Scans were imported into the 3D imaging software Mimics (v. 15.0-18.0, Materialise, Leuven, Belgium), segmented into two dimensional masks, and reconstructed as volumetric renderings. Edited 3D models of the CP that were constructed for each specimen could be rotated and magnified for closer inspection and quantification. When needed, multiple areas of interest in the skull were segmented and rendered as separate 3D models to better visualize the CP in the context of its surrounding nasal anatomy (Fig. 3-3). Two morphological metrics, CP surface area and cross-sectional area of CP foramina (FXSA), were quantified for all arctoid skulls using Mimics and 3-Matic imaging. For a thorough description of methods involving morphological quantification, see the Materials and Methods sections of Chapters One and Two and Figure 4 in Chapter One. Collecting FXSA data presents multiple challenges. It requires CP specimens with no damage to the foramina, high quality high-

resolution CT scans and involves many hours (up to 12 hours) of concentrated labor per specimen. For this reason we have FXSA data for only one specimen per species for 27 of the 28 species. The CP's cumulative foramina area is the direct imprint of olfactory neural tissue in the bone, and as such may be regarded as a more precise or informative metric of CP size, however, because our FXSA data are limited and FXSA correlates closely with CP surface area (Fig. 3-4) we focus here on CP surface area.

We used skull length as a body size proxy, defined as the distance between the anterior most extent of the orbit and the posterior extent of the occipital condyle (orbit to occipital length, or OOL). Using skull length instead of body mass reduces the excessive influence of large fat stores among pinnipeds on estimates of body size. Furthermore, the skull metric OOL excludes the confounding influence of snout length, a feature that varies widely among arctoids independent of body size (Van Valkenburgh, 1990). OOL was measured from 3D skull reconstructions using Mimics or from skulls directly using digital calipers.

Habitat groupings

We divided the sample species into three habitat groupings, terrestrial, aquatic and semi-aquatic as defined above. Terrestrial species in our sample include four ursids (grizzly bear, *Ursus arctos;* American black bear, *Ursus americanus;* polar bear, *Ursus maritimus;* giant panda, *Ailuropoda melanoleuca*), three mustelids (American badger, *Taxidea taxus;* wolverine, *Gulo gulo;* long-tailed weasel, *Mustela frenata*), two procyonids (raccoon, *Procyon lotor;* kinkajou, *Potos flavus*), and one mephitid (striped skunk, *Mephitis mephitis*). Aquatic carnivoran species include one mustelid (sea otter, *Enhydra lutris*) and 15 pinnipeds from the otariids (Stellar sea lion, *Eumatopias jubatus*; California sea lion, *Zalophus californianus*; South American sea lion, *Otaria byroni*; Northern fur seal, *Callorhinus ursinus*; Galapagos fur seal,

Arctocephalus galapagoensis; Cape fur seal, *Arctocephalus pusillus*), phocids (bearded seal, *Erignathus barbatus*; leopard seal, *Hydrurga leptonyx*; tropical monk seal, *Monachus tropicalis*; Northern elephant seal, *Mirounga angustirostris*; ringed seal, *Phoca hispida*; Baikal seal, *Phoca sibirica*; harbor seal, *Phoca vitulina*) and one odobenid (walrus, *Odobenus rosmarus*). The semi-aquatic species in our sample include two mustelids (North American river otter, *Lontra canadensis;* American mink, *Neovison vison*).

Diving Data

Four diving variables were chosen for this study, maximum dive depth, mean dive depth, maximum dive duration, and mean dive duration. All dive data were compiled from individual behavioral field studies published in the primary literature (Table 3-2). Where possible, we used reported estimates of mean dive depth and duration. Where data from individual dives were published without estimated averages, we used these raw data to calculate the best estimate of average dive depth and duration. Other potentially informative variables describing overall "aquatic-ness" of the aquatic species, such as at-sea duration, migration distances, and haul-out duration, exist for some but not all species, and so could not be used for this study. Because no reliable diving data exist for the extinct tropical monk seal (*Monachus tropicalis*) we substituted available data for its living sister species, the Hawaiian monk seal.

Statistical Analysis

Species means of all morphological and ecological variables were used for data analysis. All species means were log transformed to normalize the data. To view scaling relationships between CP and body size and to derive values for relative CP size, we plotted absolute CP

surface area against OOL using generalized least squares regression. Resulting residuals from this regression were used as relative CP size (RelCP) in all subsequent analyses. To test the influence of habitat on RelCP values, we performed one-way ANOVA and Tukey HSD post-hoc tests. To account for phylogenetic relatedness and covariance among taxa, we performed phylogenetic least squares regressions (PGLS) using the Caper package in R (Orme et al., 2013) and a time-calibrated mammal phylogeny that we trimmed to include only the species in our study (Fitz et al., 2005. For visualization purposes, GLS plots are shown in the figures. All analyses were done in R (R Development Core Team, 2016)

Results

Correlations between cribriform plate (CP) surface area and CP foramina cross-sectional area

Absolute CP surface area, defined as the area encompassing only the perforated CP bone, correlates strongly with the cumulative cross-sectional area of CP foramina (FXSA) across our 28 arctoid carnivorans ($r^2 = 0.91$, $P < 0.0001$) (Fig. 3-4). These two CP metrics scale with isometry (slope = 1.04). Therefore, because of the strong correlation between the two metrics, and because our sample size is larger for CP area, we focus here on the latter metric.

Relative cribriform plate size.

Absolute CP surface area is coupled to the body size proxy, orbit to occipital condyle (OOL) ($r^2 = 0.58$, $P < 0.0001$), and scales with negative allometry (Fig. 3-5). The positive correlation indicates that CP size increases with body size, while the slope of the regression (1.18), significantly lower than expected under geometric similarity (slope =2), indicates that larger animals have relatively smaller CP for their size. The scatter appears to be due to the spread between terrestrial species (Fig. 3-5, green) and the aquatics (Fig. 3-5, dark blue,

turquoise). Among the aquatic species the correlation between CP surface area and OOL is somewhat stronger ($r^2 = 0.76$, $P < 0.0001$, $n = 16$) and among terrestrials alone it is stronger still ($r^2 = 0.9$, $P < 0.0001$, $n = 10$) (Fig. 3-6). CP surface area scales with negative allometry in both aquatic and terrestrial samples with slopes of 1.48 and 1.71, respectively (Fig. 3-6, Table 3-1).

Cribriform plate in terrestrial, aquatic and semi-aquatic species

To test the hypothesis that aquatic species have reduced olfactory morphology relative to terrestrial and semi-aquatic species, we performed a one-way ANOVA on relative CP size (RelCP, see methods) values from the three habitat groups. Terrestrial species appear to have significantly larger RelCP than both aquatic and semi-aquatic species (Tukey HSD post-hoc test, $P < 0.05$) (Fig. 3-7), but when phylogeny is accounted for, only the difference between terrestrial and aquatic species remains significant ($P < 0.0001$). There is no difference between the RelCP of the aquatic and semi-aquatics groups ($P = 0.99$).

RelCP and diving ecology of aquatic carnivorans: dive depth and duration

To derive RelCP values useful in testing phylogenetic and ecological influences on CP morphology within the aquatic group, we used residuals from a linear regression of absolute CP surface area against OOL across the 16 aquatic species (Fig. 3-8). Within the pinnipeds, the clade comprised of otariids and the one odobenid has significantly larger RelCPs than the phocids (Tukey HSD post hoc test, $P < 0.009$), and otariids alone have significantly larger RelCP than phocids (Tukey HSD post hoc test, $P < 0.03$) (Fig. 3-9, Table 3-2).

We tested for correlations between RelCP and mean dive depth, maximum dive depth, mean dive duration, and maximum dive duration, respectively. We found no significant relationship between RelCP and maximum recorded dive depth (Table 3-2), but there was a significant negative correlation between RelCP and mean dive depth for our sample's 16 aquatic species (r^2 = 0.67, $P < 0.0001$) (Table 3-2, Fig. 3-10). After accounting for relatedness by performing a phylogenetic generalized least squares regression (PGLS), the correlation weakened but remained significant ($r^2 = 0.29$, $P = 0.03$). Phocids display a far wider range of mean dive depths (17.2 – 504 m) than their sister clade of otariids and odobenids (17.5 – 58.2 m) (Table 3-1), suggesting wider ecological diversity, and so we examined them separately from other aquatics. To estimate RelCP within phocids alone, we used residuals from the regression of CP surface area against OOL in the eight phocid species. A generalized least squares (GLS) regression revealed a negative correlation between RelCP and mean dive depth in phocids ($r^2 = 0.64$, P = 0.016, $n = 8$) and while the trend persists under PGLS, it was not statistically significant (r^2 = 0.37, $P = 0.12$, $n = 8$) (Fig. 3-11).

Maximum dive duration was also negatively correlated with RelCP across all aquatics (r^2 = 0.56, $P = 0.0009$) but this disappeared when phylogenetic relatedness was considered (Fig. 3-12). As was the case for dive depth, phocid species cover a wider range of maximum dive durations (18.7 – 82 min.) than do otariids and the odobenid (6 – 20.1 min.). Within the phocids alone, there was a strong negative correlation between RelCP and maximum dive duration (r^2 = 0.67, $P = 0.013$, $n = 8$) (Fig. 3-13) that persists after accounting for phylogeny (PGLS $r^2 = 0.6$, $P = 0.02$).

The most robust relationship between CP morphology and diving ecology is found between RelCP and mean dive duration. Among all pinnipeds plus the sea otter, there is a

significant negative correlation ($r^2 = 0.58$, $P = 0.0006$; PGLS $r^2 = 0.42$, $P = 0.006$, $n = 16$) (Fig. 3-14). Again, phocids represent a wider range of mean dive duration values than the otariids and odobenids (2 – 22.5 min., 1.1 – 3.4 min., respectively). There is a significant negative correlation between RelCP and mean dive duration among phocids alone, initially revealed in a GLS regression ($r^2 = 0.59$, $P = 0.027$) (Fig. 3-15) and strengthened with PGLS ($r^2 = 0.67$, $P = 0.012$, $n = 8$).

Discussion

Our analysis of variation in relative CP size and habitat (terrestrial, semi-aquatic and aquatic) in arctoid carnivorans was conducted at two levels, first across our entire sample of arctoids, and then in more depth within the aquatic species alone. For the latter, we compared relative CP size among aquatic species with different diving behaviors. At both levels, results suggest that reduction in CP size among aquatic mammals is a secondary adaptation to an aquatic lifestyle that reflects reduced reliance on olfaction.

As a group, pinnipeds and the sea otter have smaller RelCPs than terrestrial arctoid carnivorans. These findings contradict an earlier study that concluded that otariids and phocids CPs are not significantly different from those of terrestrial carnivorans (Pihlstrom, 2005, 2008). There are several likely reasons for differences in our findings. First, Pihlström et al. used linear CP measurements fitted to a generalized ellipsoid semi-sphere to calculate CP surface area. As CP shape varies widely and is generally irregular (Bird et al., 2014), such an approach may produce less accurate estimates of CP surface area than digital quantification. Secondly, their body size proxy, skull area, includes snout length within its skull length metric, which tends to underestimate body size in the generally shorter-snouted aquatic pinnipeds and sea otter

compared to the long-snouted ursids. This results in the pinnipeds appearing to have a relatively larger CP for their skull size. Finally, our sample included additional phocid species with some of the smaller RelCPs among carnivorans, such as the Northern elephant seal, the Weddell seal, Baikal seal, harbor seal and tropical monk seal (Bird et al., 2014)

Our results are consistent with earlier evidence that the surface area of olfactory-related ethmo- and nasoturbinals are reduced in aquatic carnivorans when compared with terrestrial species (Van Valkenburgh et al., 2011). We might expect that CP and olfactory turbinals share a similar reduction in aquatics, given that CP and ethmoturbinals share a developmental origin (Rowe, 2005) and are strongly correlated in size across all carnivorans (Bird et al., 2014).

There are at least two possible evolutionary interpretations for our finding that aquatic arctoids have relatively reduced CPs. First, although odor cues play an important role in social interactions among aquatic carnivorans above water, below water, where pinnipeds and sea otters do all their foraging, odor cues are completely absent. Because aquatics dive with shut nostrils, prey detection is accomplished without scent cues except those detected above water upon surfacing. This last point is not trivial, as harbor seals have shown a fine sensitivity to dimethyl sulphide (DMS), a volatile phytoplankton odorant and indicator of local marine productivity that is detected by sea birds as well (Kowalesky et al., 2006; Nevitt et al., 1995). However, for the most part, aquatic mammals forage "noseblind." Olfactory anatomy is a costly sensory system made up of millions of continually self-replacing olfactory sensory neurons (Graziadei et al., 1985). As selective pressure for sensing prey via odors was relaxed, olfactory systems among carnivorans transitioning to a life in water likely decreased in size over time.

A second and related explanation for the reduction of olfactory anatomy in aquatic mammals focuses on sensory trade-offs. Aquatic carnivorans have evolved keen alternative

sensory systems that are well adapted to underwater foraging. For example, they possess a tactile acuity exhibited in dense arrays of highly innervated vibrissae, the most prominent of which are the mystacial (mustache) whiskers (Berta et al., 2015). Such compact arrangements of whiskers in the phocid bearded seal (*Erignathus barbatus*) and the walrus (*Odobenus rosmarus*) are thought to assist in locating mollusks in the shallow benthic substrate (Marshall et al., 2006). Experiments using blindfolded animals revealed that harbor seals (*Phoca vitulina*) use their vibrissae to track the hydrodynamic trails of swimming fish (Denhardt et al., 2001). Even the sea otter, the most recent carnivoran to return to an aquatic existence, has evolved a thick matt of large vibrissae with levels of innervation comparable to that of phocids (Marshall et al., 2014). In addition to the enhanced vibrissae, aquatic carnivorans rely on a visual system adapted for hunting in dark waters. With the possible exception of the walrus and sea otter, aquatic carnivorans possess proportionally large eye orbits (Debey et al., 2012). Additional features that enhance visual acuity under low light include nearly spherical lenses (Berta et al., 2015), wide pupil size range and highly efficient dark adaptation (Levenson and Schusterman, 1999) as well as a tapetum lucidum (Kröger et al., 2008). The reduction of olfactory anatomy in aquatic mammals over time likely stems from a relaxation of selective pressures that follows a loss of chemosensory input as well as an increased reliance on alternative sensory systems in underwater foraging.

Although aquatic arctoid carnivorans have on average smaller RelCP values than their terrestrial relatives, there is substantial morphological variation within this group, much of which appears to reflect phylogeny. Phocids tend to have relatively smaller CPs than the otariids. However, there are exceptions. Two phocid species, the bearded seal (*Erignathus barbatus*) and the leopard seal (*Hydrurga leptonyx*), have relatively large CPs, more similar to those of otariids

or walrus than to other phocids (Figs. 3-8, 3-16). Notably, relative to others phocids, these two species are shallow divers. The bearded seal retrieves mollusks and fish from the benthic substrate (Krafft et al., 2000) and the leopard seal feeds primarily in the shallows on krill colonies, penguins and occasional pinniped pups (Nordøy et al., 2008). This suggests that shallow diving pinnipeds may rely more on olfactory cues than deeper diving pinnipeds.

The correlation between diving behavior and CP size was confirmed in our examination of CP among species that differed is aspects of dive depth and duration. Although there was no significant association between maximum dive depth and RelCP that held up after phylogenetic accounting, there were significant negative correlations between RelCP and each of the other dive variables: mean dive depth, mean dive duration and maximum dive duration. Initially, the absence of a relationship between maximum dive depth and RelCP was surprising because maximum dive depth values exhibit the widest range of all the variables and because the smallest RelCP value by far in our sample belongs to the most extreme diver, the Northern elephant seal, which has been recorded diving to 1529 meters (DeLong et al., 1991). However, upon closer consideration of the published literature, it becomes apparent that maximum depth values are in many cases not representative of a species' overall diving patterns, as indicated by a number of extreme maxima recorded and published for otherwise relatively shallow divers. For example, the California sea lion has been recorded at an impressive depth of 575 meters (Costa et al., 2007), yet this otariid is generally considered a moderately shallow diver (Berta et al., 2015).

Why does selection favor reduced RelCP in aquatic carnivorans exhibiting longer and deeper average dives? There are a number of alternative hypotheses, all of which require further testing. First, it is possible that shallow, short dive patterns reflect a relatively closer tie to the

land/ice, while deeper and longer dive patterns represent a more pronounced separation from a terrestrial habitat. Longer separation from land, that is, a more aquatic life, may mean an increased separation from airborne odor cues that terrestrial animals rely on for food, predator protection, social communication and reproduction. To test whether longer, deeper diving reflects a more fully aquatic lifestyle, all diving variables need to be viewed in relationship to other ecological factors that describe relative proximity to land/ice and relative duration at sea for all the aquatic carnivoran species. These factors could include foraging trip duration (Kooyman et al., 1986), long-distance migration patterns (Burton et al., 2012), pupping season duration (Stirling, 1991), haul-out patterns (Cunningham el al., 2009), and overall at-sea duration (Costa et al., 2010), among others. Data exist for each of these variables for some but not many species, prohibiting a comprehensive comparison with diving behavior.

An alternative, or complementary, interpretation for the negative relationship between diving depth/duration and RelCP relates to odorants at the water's surface that are emitted by underwater prey. Shallower diving mammals may retain a larger RelCP if their prey species produce volatile chemicals that readily reach the water's surface and can be used as odor cues. One such volatile, mentioned above, is DMS, an odorant emitted by phytoplankton, particularly when grazed upon by krill and other zooplankton (Dacey et al., 1986). The presence of DMS, especially in higher concentrations, signals an underlying trophic web based on krill and including krill-feeding animals, such as fish or penguins. A number of procellariiform seabirds, as well as penguins, are able to detect DMS and are thought to use its presence to locate krill (Nevitt et al., 1995; Amo et al., 2013). Recent evidence that harbor seals (*Phoca vitulina*) also detect DMS (Kowalewsky et al., 2006) introduces the possibility that other pinniped species may do so as well. This may explain why the leopard seal (*Hydrurga leptonyx*), a shallow and short

diver that feeds primarily on krill, penguins and crabeater seal pups (Pauly et al., 1998), has the largest RelCP among the phocids. If the leopard seal navigates a rich landscape of scent cues at the surface of the water, as well as on the ice sheet, a larger olfactory system would be adaptive. The functional significance of the relatively large CP in the leopard seal is reinforced by the fact that their close relative, the elephant seal, is the deepest and longest diving pinniped with the smallest RelCP (Fig. 3-12). However, our other species with a large RelCP, the shallow, short diving bearded seal, appears to rely more on its vibrissae than surface scent cues in detecting invertebrates buried in the soft substrate (Marshall et al., 2006). To strengthen the argument that shallower divers rely on surface odor cues emitted by prey, it would be useful to look at the CP of a crabeater seal, a short diving phocid (11 min. maximum dive duration) (Schreer et al., 1997) that depends on up to 90% krill for its diet (Pauly et al., 1998.

As important as surface odor cues could be for shallow divers, they are likely far less significant for deep divers. For example, the Northern elephant seal dives in a staggered stair-step pattern, reaching its prey of pelagic squid and mesopelagic fish (Pauly et al., 1998) at depths between ~300-1500 meters and far displaced horizontally, sometimes by several hundreds of meters, from the dive initiation location (Davis et al., 2007). The combined depth and horizontal displacement likely obscures any odor signals that may be given off by the elephant seal's prey.

The inverse relationship between RelCP and diving depth and duration may also indicate a structural constraint on CP size imposed by the stresses of diving. The adverse effects of diving to depth are well cited in the literature. Two notable effects are 1) the potential deformation of tissue surrounding compressed gas-filled cavities and 2) the risk of increased nitrogen diffusion into the blood stream as gas tensions rise (Kooyman and Ponganis, 1998). Adaptations to these challenges are many and varied. First, under ambient pressure during a

descent, lung bronchioles and alveoli collapse, shunting the air from the lungs into reinforced bronchi and trachea thereby avoiding gas exchange (Scholander, 1940). Additionally, they have evolved skulls with fewer, smaller air-filled chambers as well as mechanisms for reducing the volume of empty skull cavities under diving pressures. For example, the middle ear and external auditory meatus of in the pinniped are partially lined in modified respiratory tissue with a basal layer of cavernous venous tissues that are postulated to swell with venous blood in response to increasing hydrostatic pressure, thereby reducing the volume of necessary air cavities, equilibrating pressure and avoiding damage to the tympanic membrane (Odend'hal and Poulter, 1966, Repenning, 1972). The elephant seal displays an additional reduction of air spaces in the ear with pronounced narrowing of the external auditory meatus (Kastak and Schusterman, 1999).

How might the adaptive reduction of compressible airways in the skull, and particularly the nasal cavity, of aquatic carnivorans constrain olfactory morphology? First, pinnipeds and the sea otter lack pneumatized frontal sinuses (Curtis et al., 2015). In terrestrial carnivorans, ethmoturbinals extend from the nasal cavity into the frontal sinuses (Negus, 1958) (Fig. 3-17a). Without the doming of the skull afforded by large frontal sinuses, the space available for ethmoturbinals and the CP in pinnipeds and the sea otter is limited dorsally (Fig. 3-17c). A survey of snout lengths in our sample reveals that the aquatic carnivorans have significantly shorter snouts than terrestrials, further reducing the nasal air space, and perhaps constraining available anterior space for ethmoturbinals as well (Tukey, $P = 0.006$). Two clear exceptions to this are the California sea lion (*Zalophus californianus*) and the leopard seal (*Hydrurga leptonyx*), each of which has ethmoturbinals that extend from the CP into a relatively long anterior nasal cavity, as well as a large RelCP, compared with species within their respective otariid and phocid clades (Fig. 3-8). Additionally, the posterior nasal cavity, squeezed between

large orbits, is relatively narrow in aquatic carnivorans (Berta et al., 2015), further limiting space for ethmoturbinals laterally as well as ventrally (Fig. 3-18a top and center rows). Finally, it has been postulated the volume of skull cavities in a diving mammal can be reduced by the engorging of cavernous tissue by venous blood (Repenning, 1972). In the anterior nasal cavity, respiratory tissue lining the turbinals and nasal septum contains a basal lamina propria that includes a rich network of distensible venous sinuses that can dilate and expand into the surrounding air spaces (Negus, 1958; Folkow et al., 1988). Unlike the respiratory tissue, however, the lamina propria below the olfactory epithelium lining the ethmoturbinals lacks the cavernous tissue and cannot expand to fill the air spaces (Craven et al., 2009). It may therefore be adaptively advantageous for deep diving mammals to have a relatively small cavity for the ethmoturbinals. Because the surface area of ethmoturbinals and CP are tightly correlated (Bird et al., 2014), we expect any structural constraints on ethmoturbinal development to be reflected in smaller CPs as well.

The effects of diving on nasal anatomy appear to be understudied. Our results linking CP morphology to diving behavior point to a need for future work investigating specific selective pressures of diving that may have driven the morphological and functional changes to the olfactory system of marine carnivorans. A first step would be the expansion of our sample of species to include other ecological exceptions and extremes, such as the unusually deep diving otariid, the New Zealand sea lion (*Phocarctos hookeri*), and additional shallow phocids, such as the crabeater seal (*Lobodon carcinophagus*). Second, our phylogenetic comparative methods need to be expanded to test our aquatic-specific data against multiple Arctoidea trees, as there is no single consensus on the relationships within Pinnipedia. Morphological analysis places the Odobenidae as sister clade to Phocidae (Demeré et. al., 2003). Multiple molecular analyses

group Odobenidae with Otariidae but differ to some degree in their groupings within Phocidae, so additional trees could be considered when accounting for phylogeny. Additionally, the question of whether diving pressures have imposed adaptive structural constraints on the ethmoturbinal anatomy and its surrounding cavity could be explored with Finite Element Analysis (FEA). For example, the effects of deep diving on empty cranial cavities, ethmoturbinal bone and the CP itself might be simulated with FEA by applying appropriate compressive forces and assigning variable material properties to the 3D skull models. With advances in portable CT scanning, it might be possible to test the effects of static pressure on posterior nasal cavity volume using fresh heads and a small custom hyperbaric chamber. Furthermore, controlled behavioral experiments are needed to address the relative importance of surface odor cues to foraging aquatic animals. Working with captive animals, it should be possible to apply odorants such as DMS, fish oil, squid and bivalve rinses, as well as neutral rinses as controls, on the water's surface to test if and how animals alter their diving patterns in relationship to surface odor cues.

Convergent evolution is well illustrated in the many secondary invasions of the sea and the gradual transition from terrestrial to aquatic life that follow. Aquatic carnivorans are a particularly interesting group to study because they occupy an intermediate position in the transition from fully terrestrial to obligate aquatic animals and their morphology carries the obvious signature of the new selective pressures presented by amphibious life. Instead of the acquisition of novel aquatic adaptations, our study focused on a single loss. Our results reveal a waning importance of the sense of smell in aquatic carnivorans as reflected in reduced cribriform plate morphology. By studying cribriform plate morphology in fossil skulls, it will be possible

to work backwards in deep time and witness the gradual loss of olfactory anatomy in extinct and ancestral aquatic carnivorans.

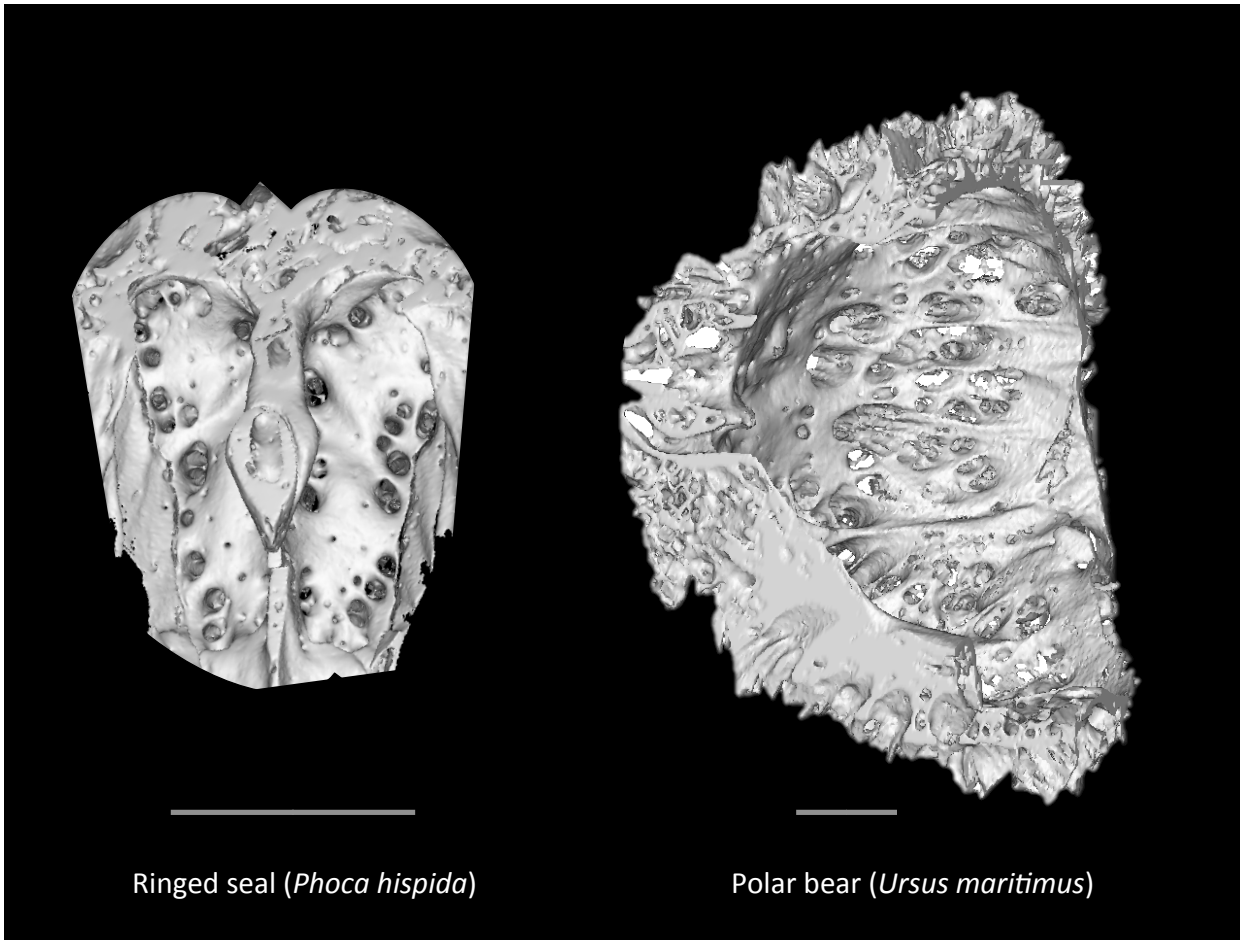

Figure 3-1. Cribriform plate (CP) in two arctoid carnivoran species. 3D models of CP bone constructed with Mimics imaging software. Left, the aquatic ringed seal (*Phoca hispida*) in posterior aspect as viewed from the brain case. Right, polar bear (*Ursus maritimus*) in oblique posterior aspect. Because the CP is spherical, the left half is removed for better visualization of the CP foramina.

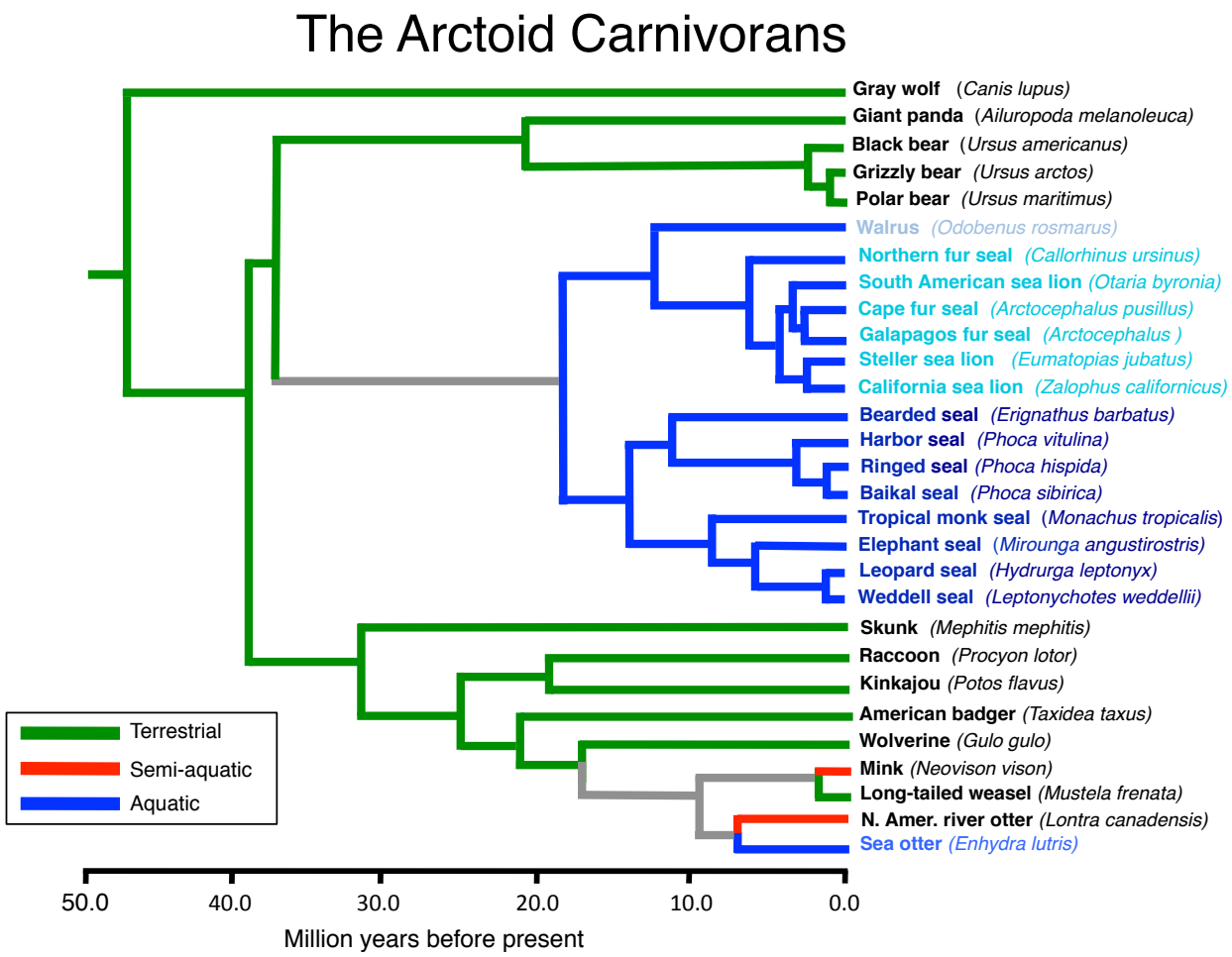

Figure 3-2. Estimated phylogenetic relationships of the sample species. Estimated tree compiled from molecular phylogenies (Koepfli et al., 2008; Meredith et al, 2011, Slater et al., 2012).

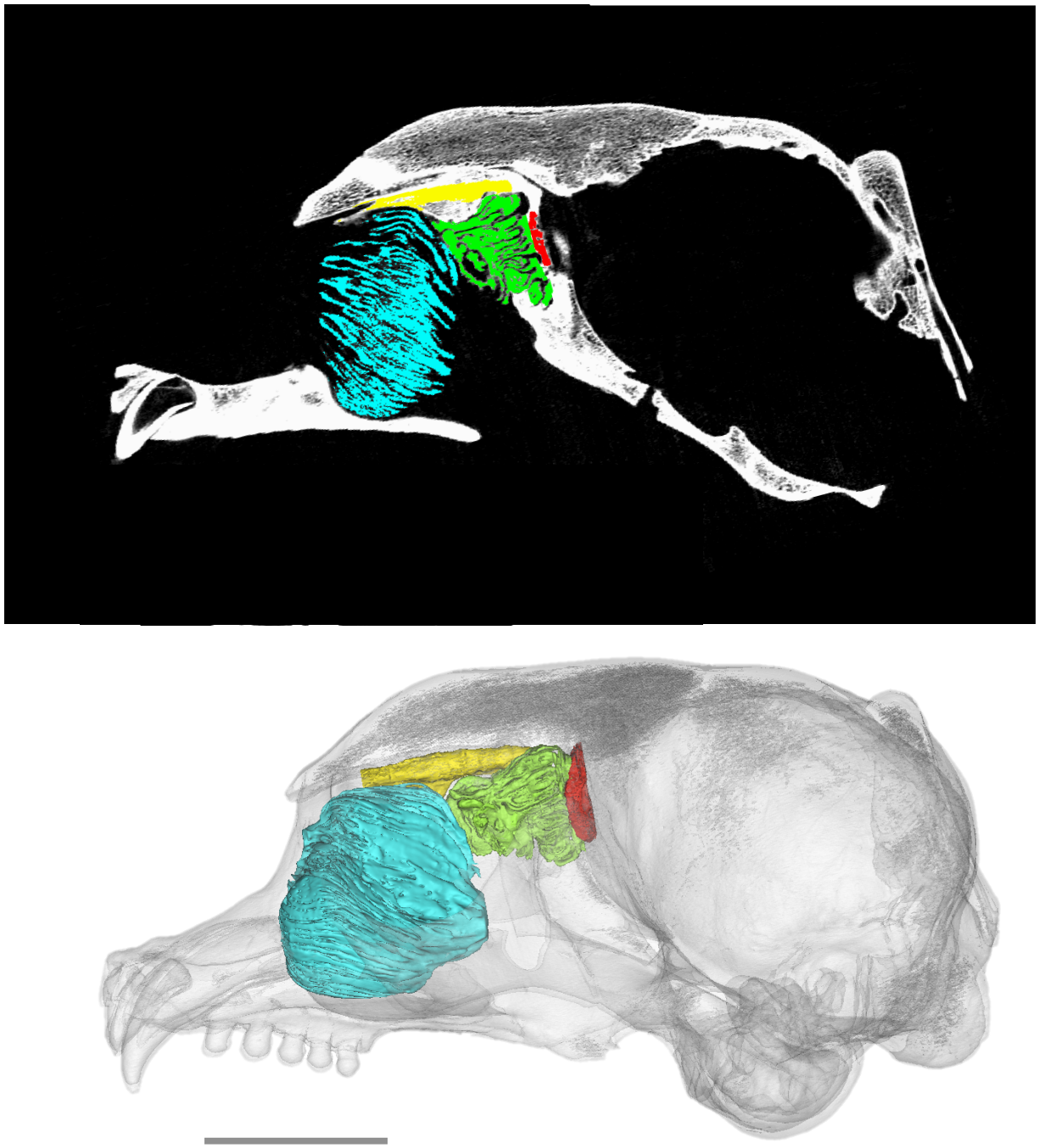

Figure 3-3. **Constructing 3D skull models.** Top: Sagittal section of a CT scan of a female Northern elephant seal (*Mirounga angustirostris*) skull. Individual morphological features are segmented. Bottom: volumetric renderings of skull features. Red: CP. Green: olfactory-related ethmoturbinals. Blue: respiratory maxilloturbinals. Scale bar: 50 mm.

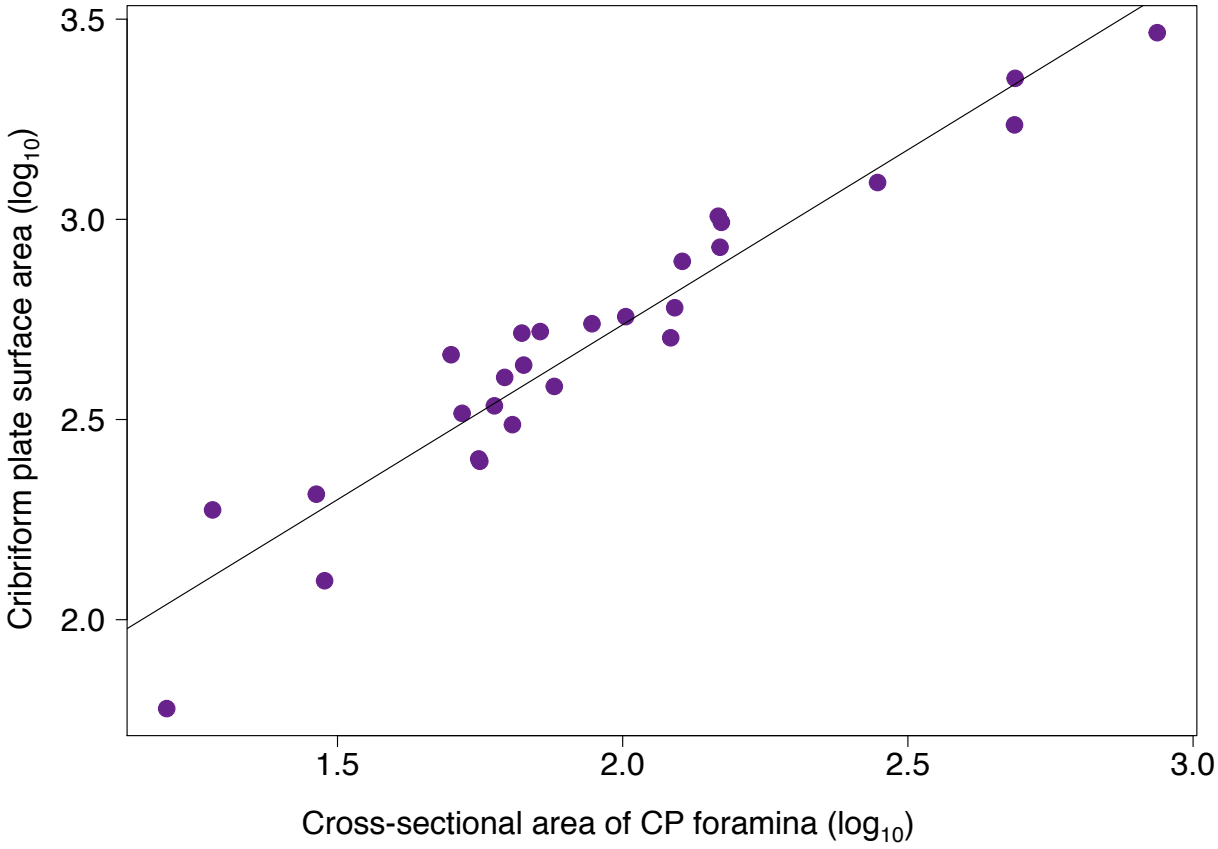

Figure 3-4. **Cribriform plate (CP) metrics.** Regression of CP surface area (mm) vs. total CP foramina area (mm) for all sample species (n = 28). Correlation: $r^2 = 0.91$, $P < 0.001$).

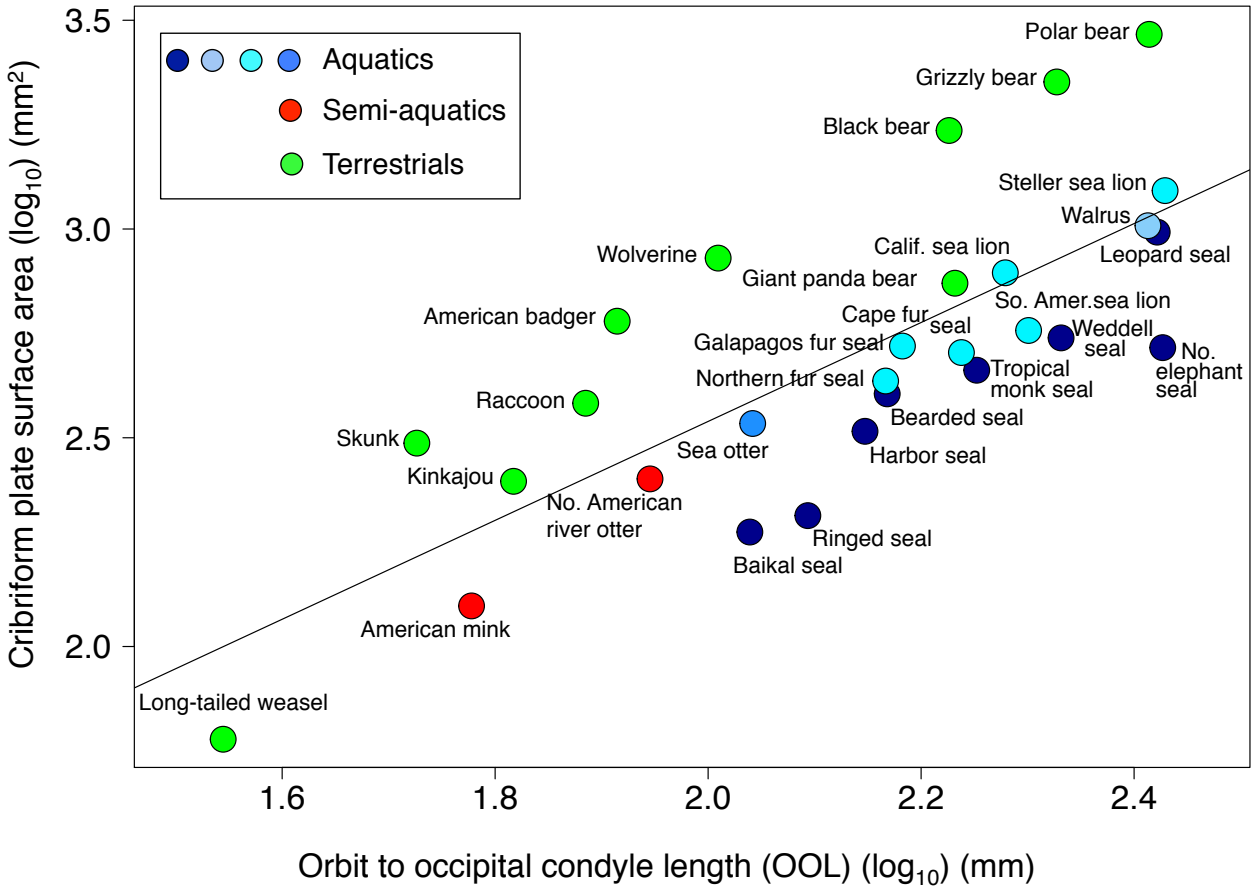

Figure 3-5. Log_{10}/Log_{10} plot of CP surface area vs orbit to occipital length (OOL) for arctoids from all habitats. Residuals from regression constitute relative CP size (RelCP) within the arctoids. All shades of blue: aquatics. Dark blue: Phocidae; Pale blue: Odobenidae; Turquoise: Otariidae; Royal blue: Mustelidae. Red: semi-aquatics. Green: terrestrials.

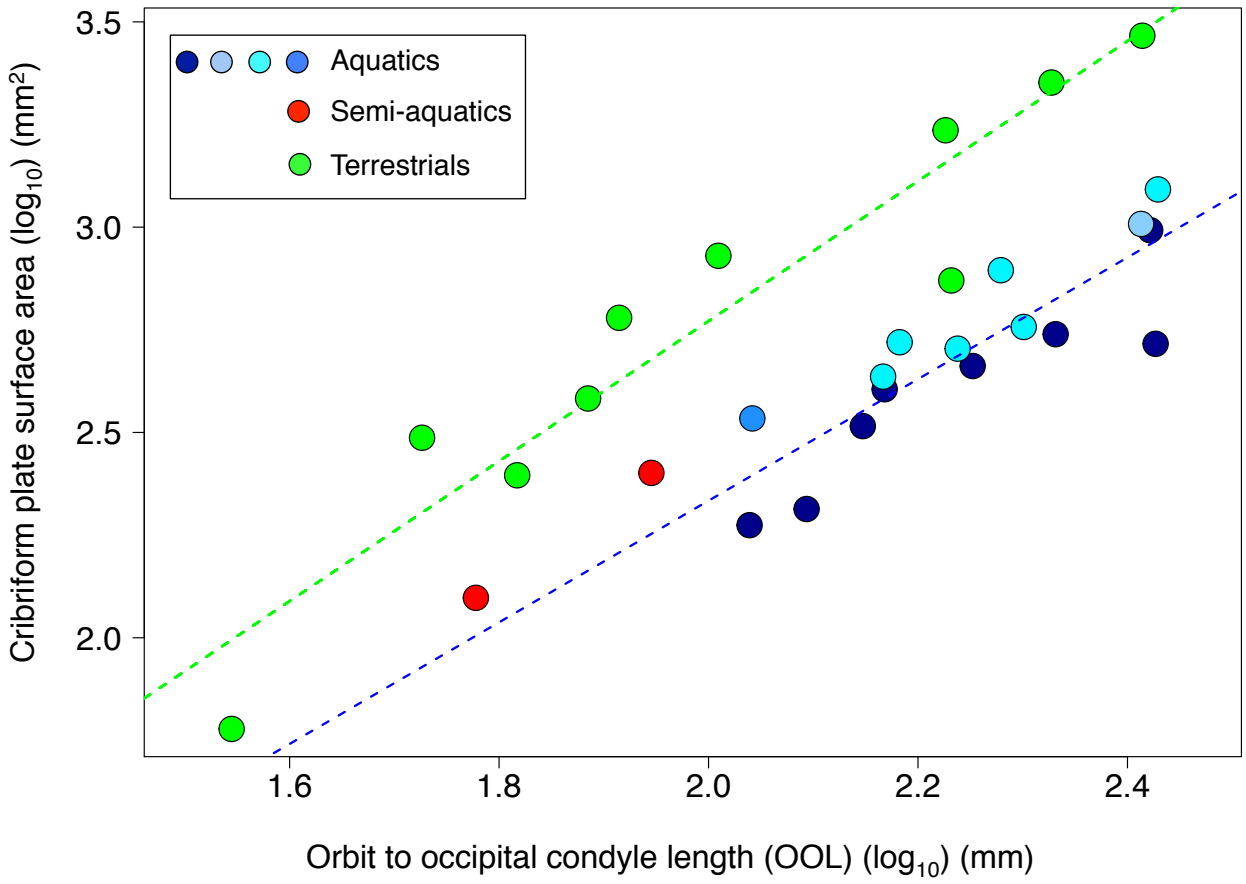

Figure 3-6. Log_{10}/Log_{10} plot of CP surface area vs OOL with regression lines per habitat. Green dashed line: least-squares regression line for terrestrials (n = 10). Blue line: least-squares regression line for aquatics (n = 16). Semi-aquatics were too few for a best-fit line.

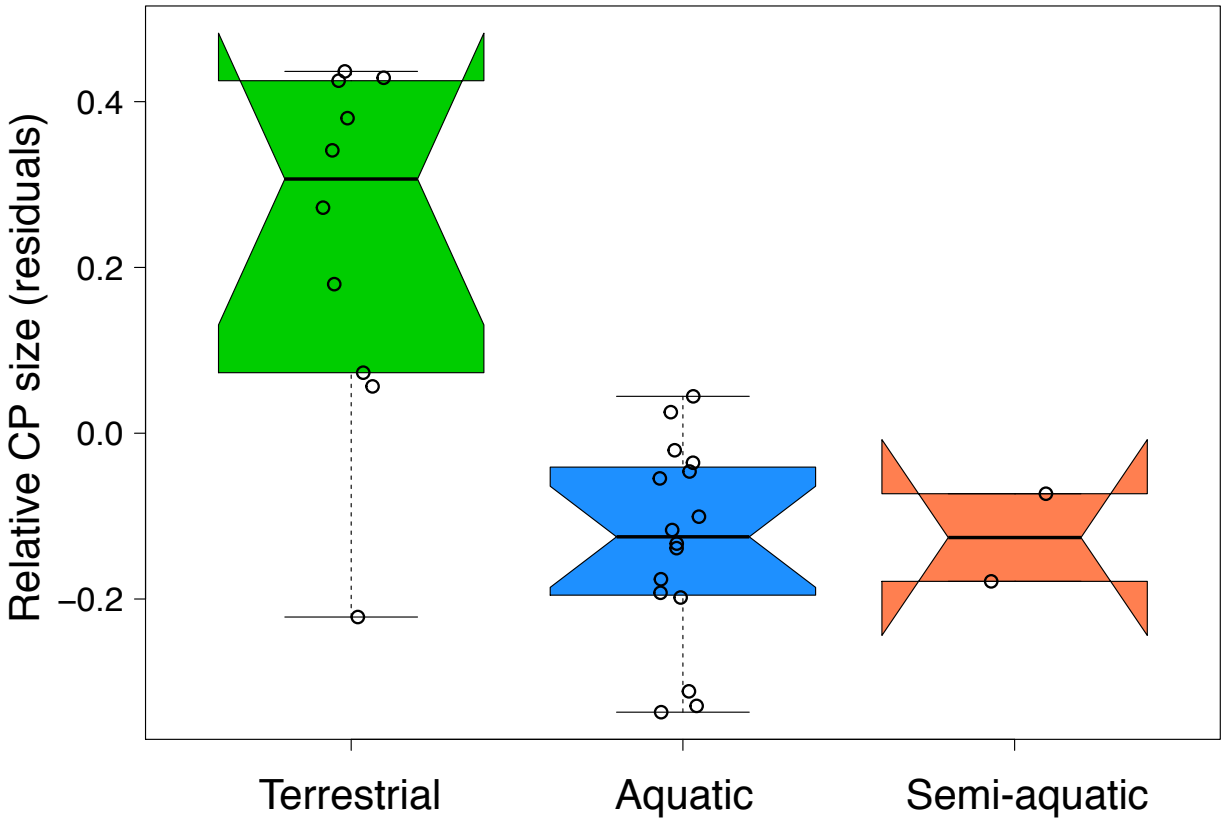

Figure 3-7. **Boxplot of RelCP by habitat among arctoid species.** Residuals from regression of $\log_{10}$ CP surface area on $\log_{10}$ OOL are compared between habitat groupings, terrestrial, semi-aquatic and aquatic. Open circles: mean RelCP value per species.

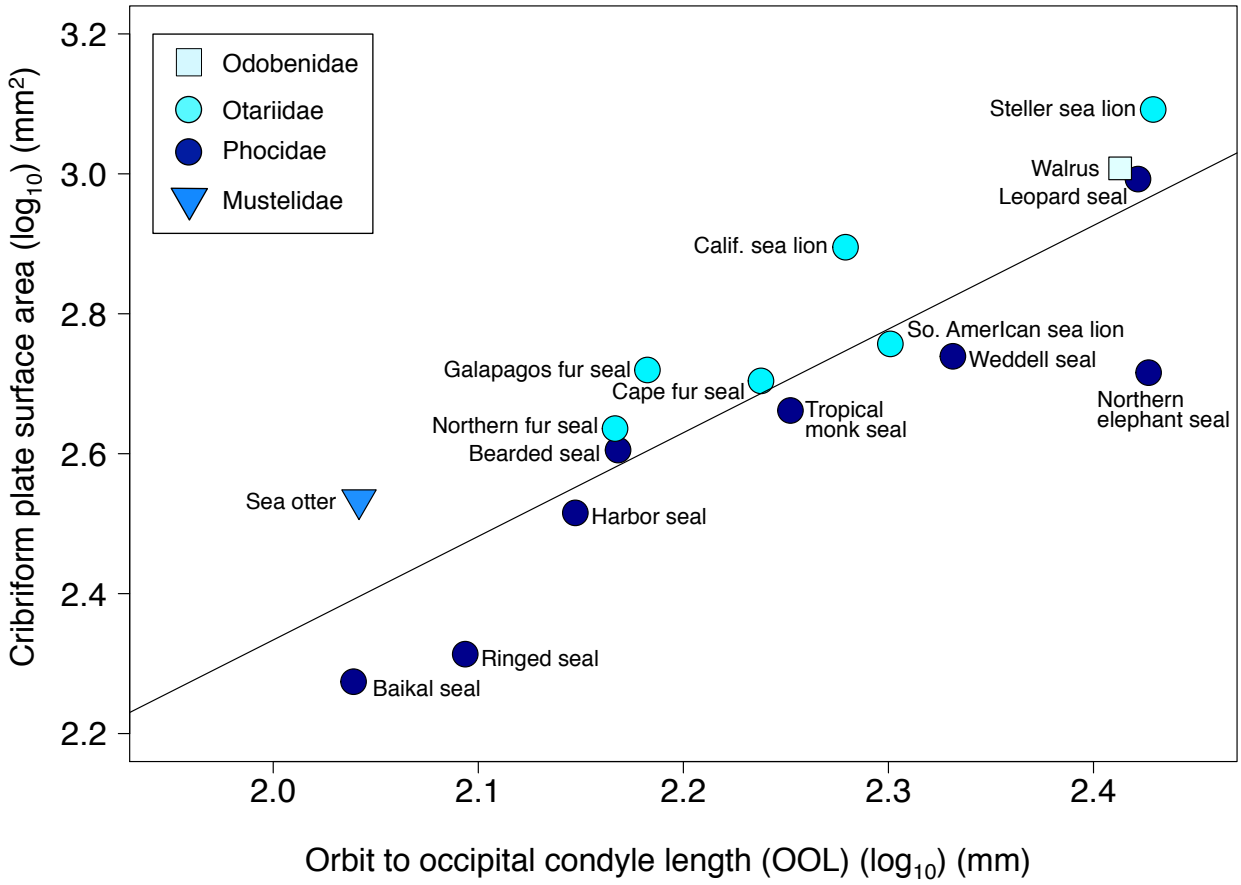

Figure 3-8. Log_{10}/Log_{10} plot of CP surface area vs OOL within aquatics. Residuals from regression constitute the relative CP size (RelCP) for aquatics that are used in subsequent analyses.

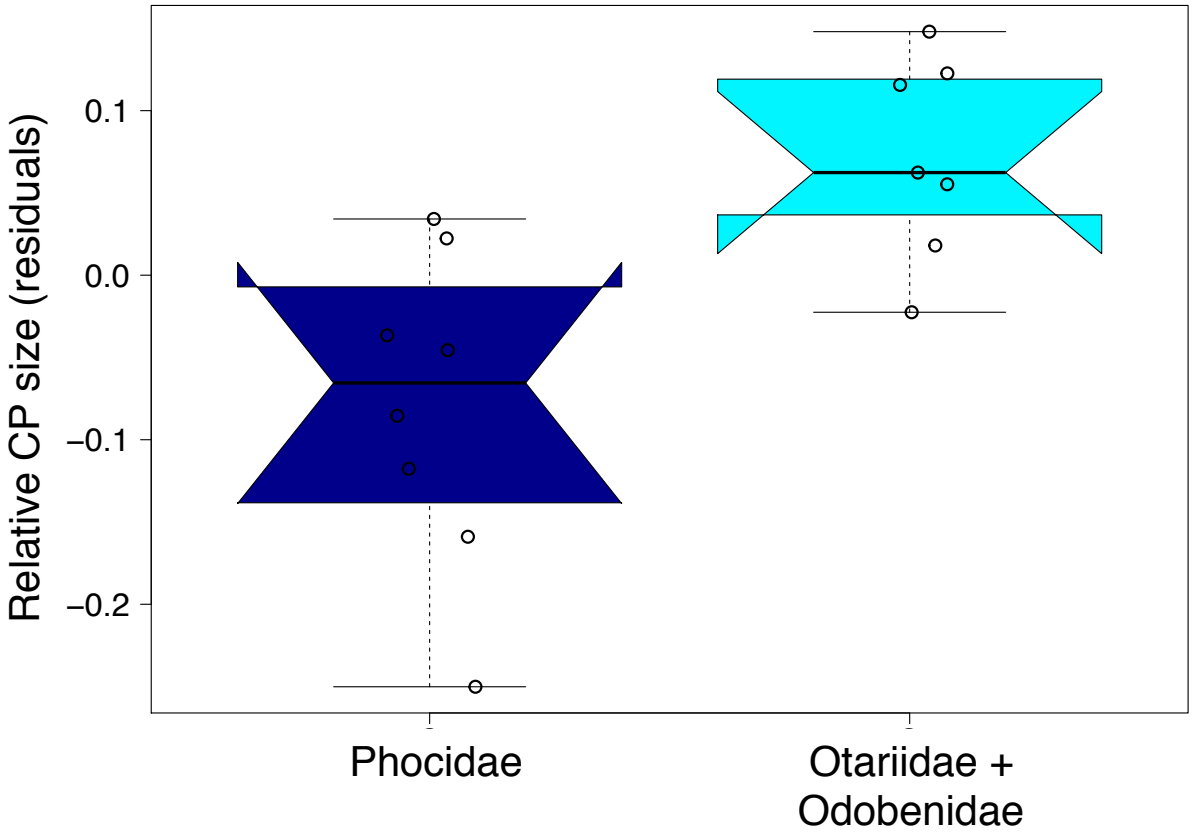

Figure 3-9. **Boxplot showing the role of phylogeny in RelCP within Pinnipedia.** RelCP are derived from residuals from the Log_{10}/ Log_{10} CP regression of CP surface area on OOL within aquatics. Phocidae (dark blue) species have on average significantly smaller RelCP than the group comprised of and Otariidae plus Odobenidae. Mustelidae was omitted as it has only one aquatic species.

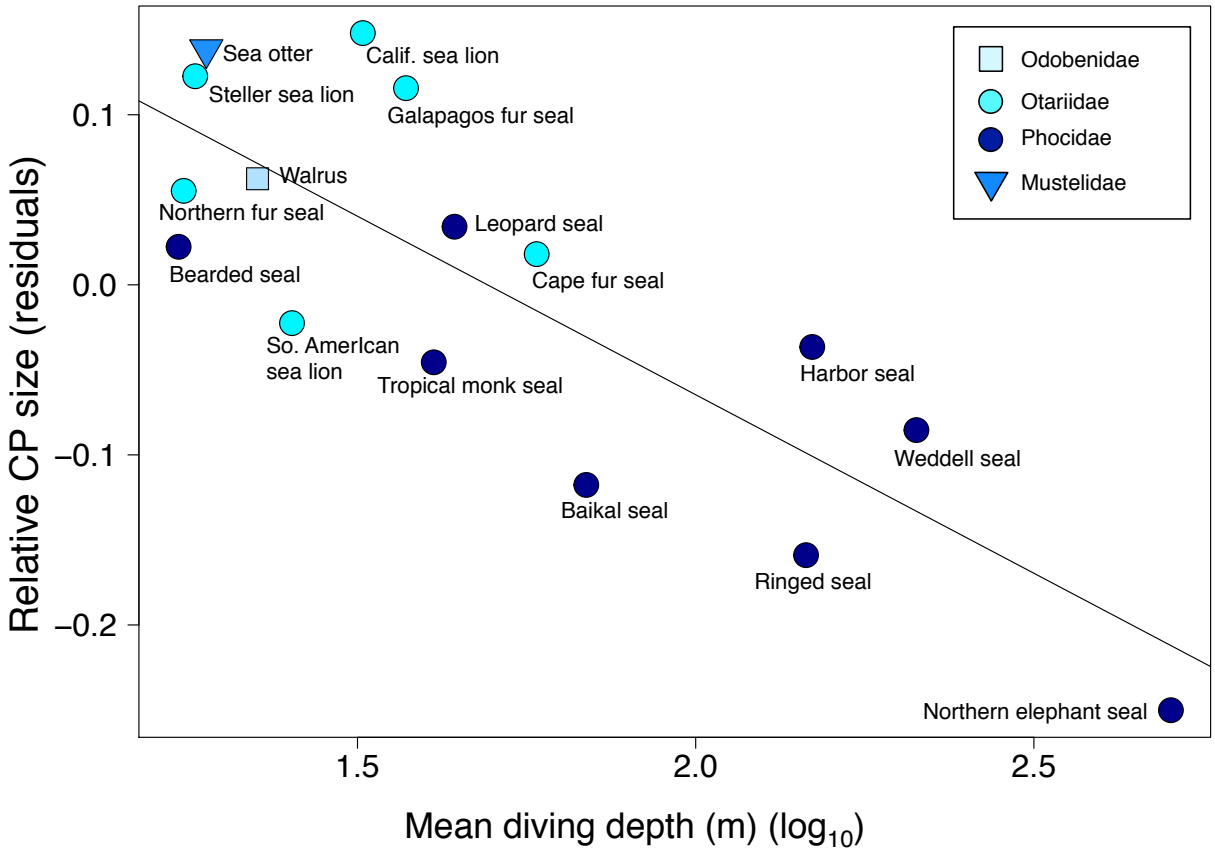

Figure 3-10. RelCP vs mean dive depth among all aquatics (log10). ($r^2 = 0.67$, $P < 0.0001$; PGLS $r^2 = 0.29$, $P = 0.03$).

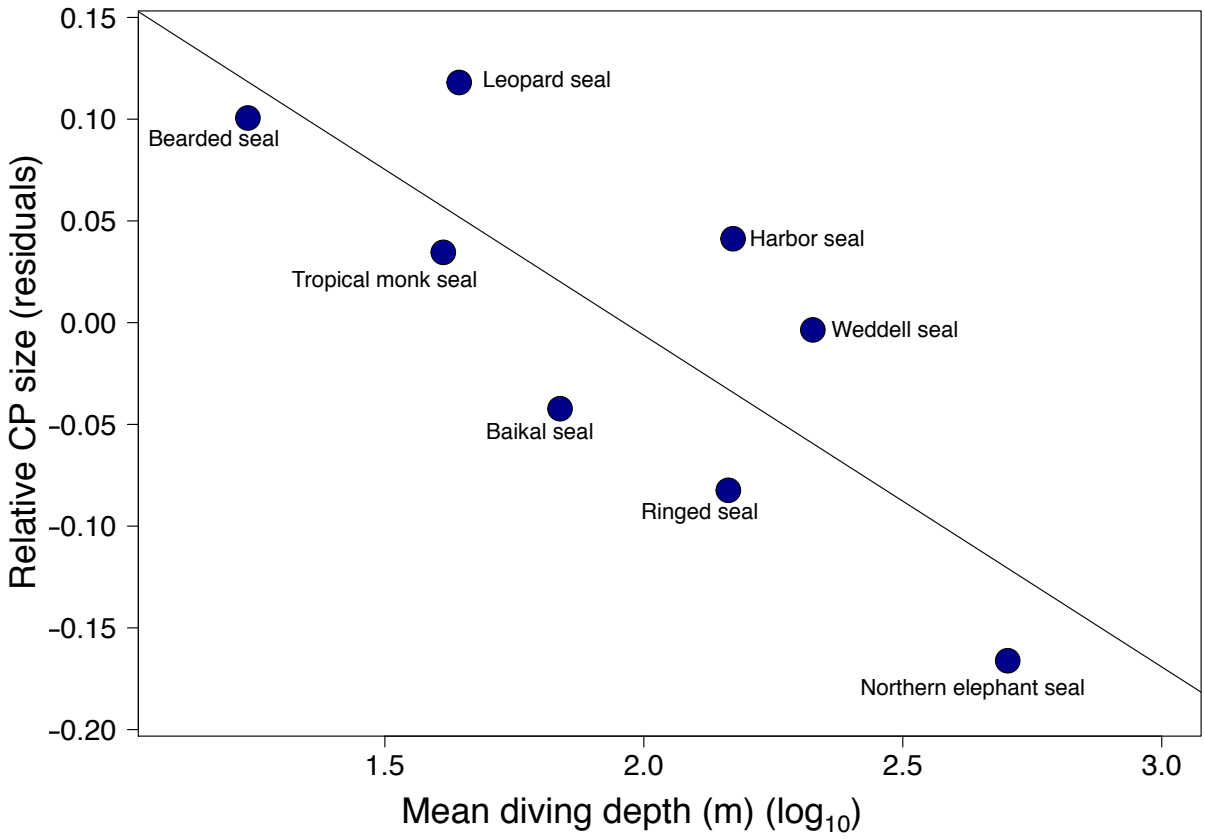

Figure 3-11. RelCP vs mean dive depth $_{(log10)}$ within phocids. ($r^2 = 0.64$, $P = 0.016$; PGLS $r^2 = 0.38$, P = NS).

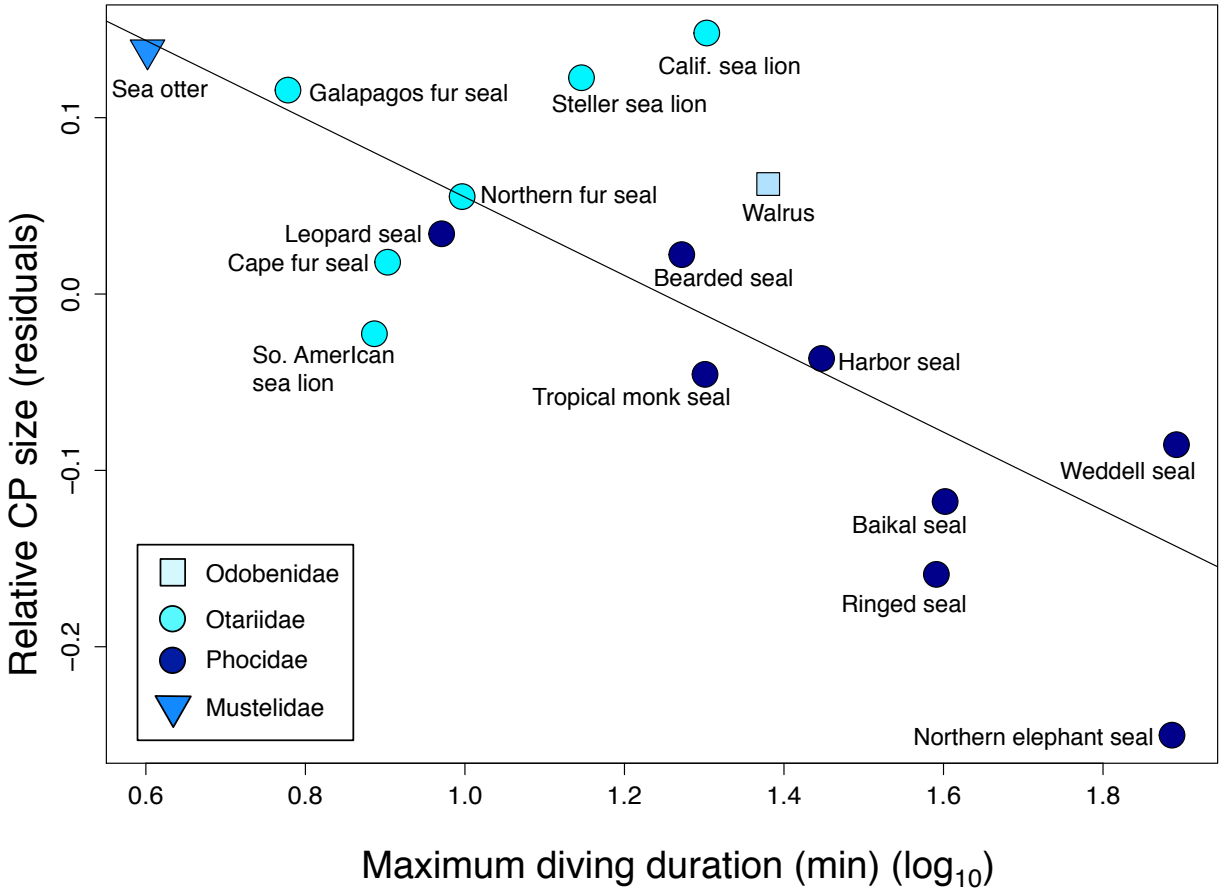

Figure 3-12. RelCP vs maximum dive duration (log10) among all aquatics. ($r^2 = 0.56$, $P = 0.0009$; PGLS $r^2 = 0.17$, P = NS).

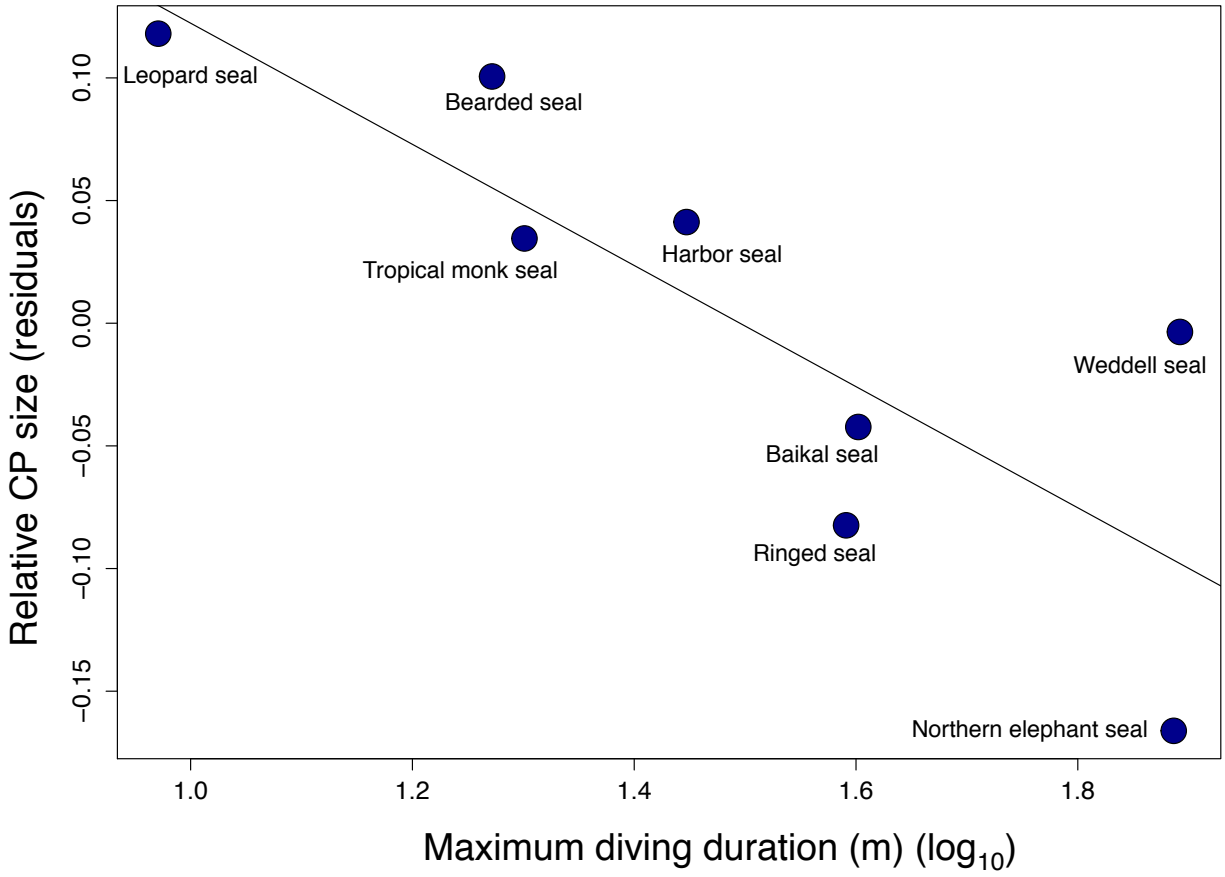

Figure 3-13. RelCP vs maximum dive duration (log10) within phocids. ($r^2 = 0.67$, $P = 0.0013$; PGLS $r^2 = 0.6$, $P = 0.02$).

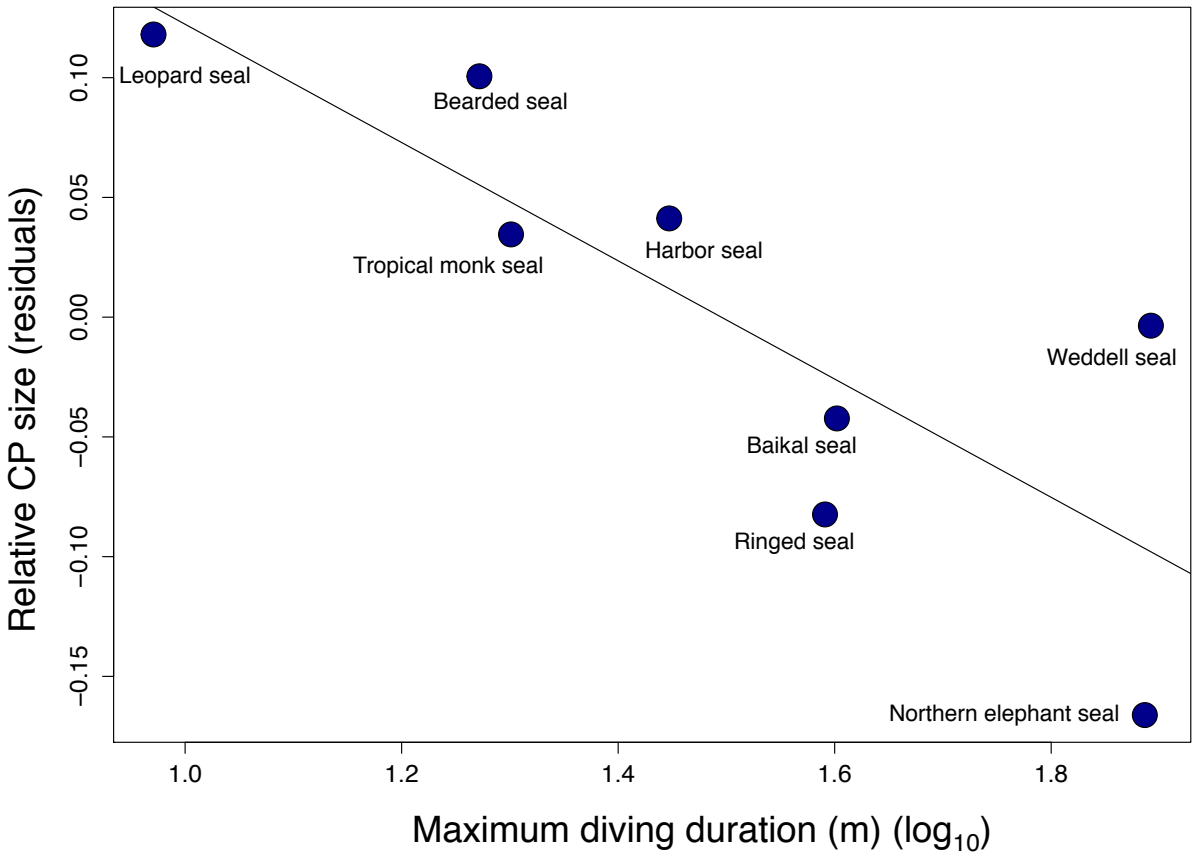

Figure 3-14. RelCP vs mean dive duration (log10) among all aquatics. ($r^2 = 0.58$, $P = 0.0006$; PGLS $r^2 = 0.42$, $P = 0.006$).

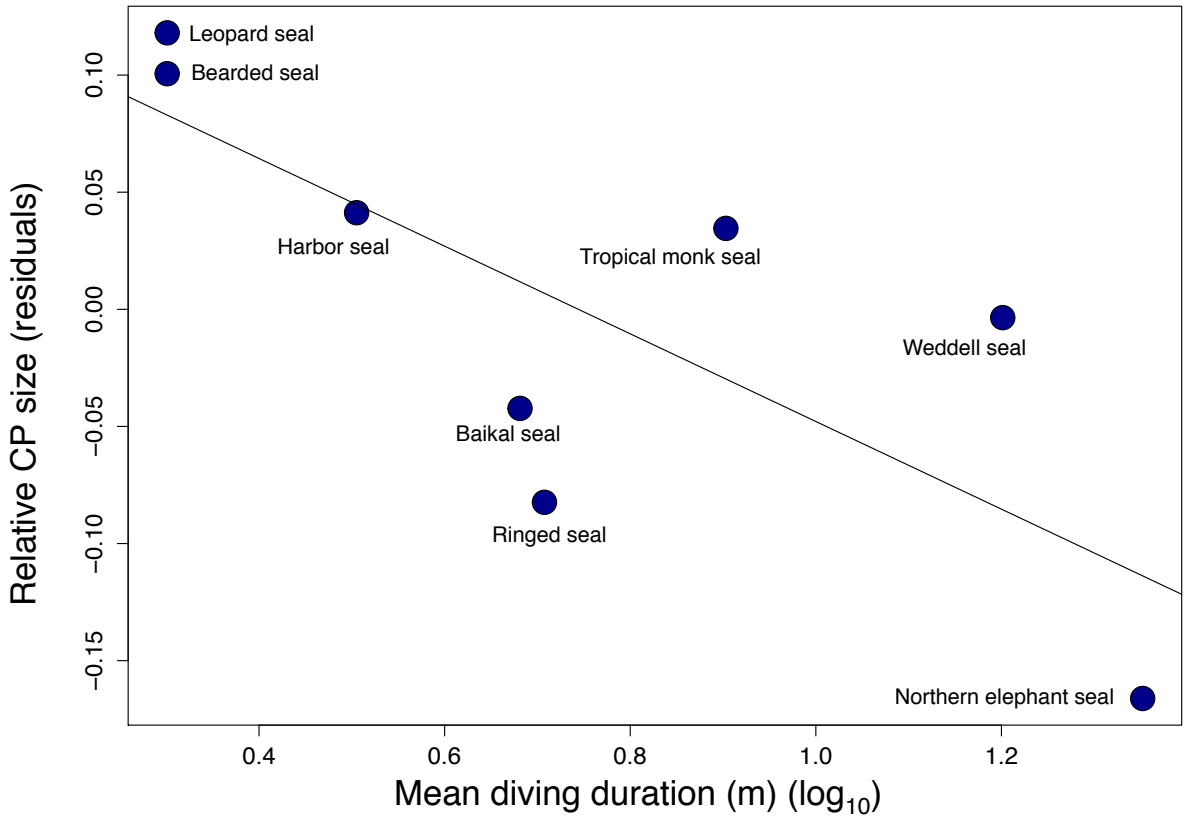

Figure 3-15. RelCP vs mean dive duration (log10) within phocids. ($r^2 = 0.59$, $P = 0.027$; PGLS $r^2 = 0.67$, $P = 0.012$).

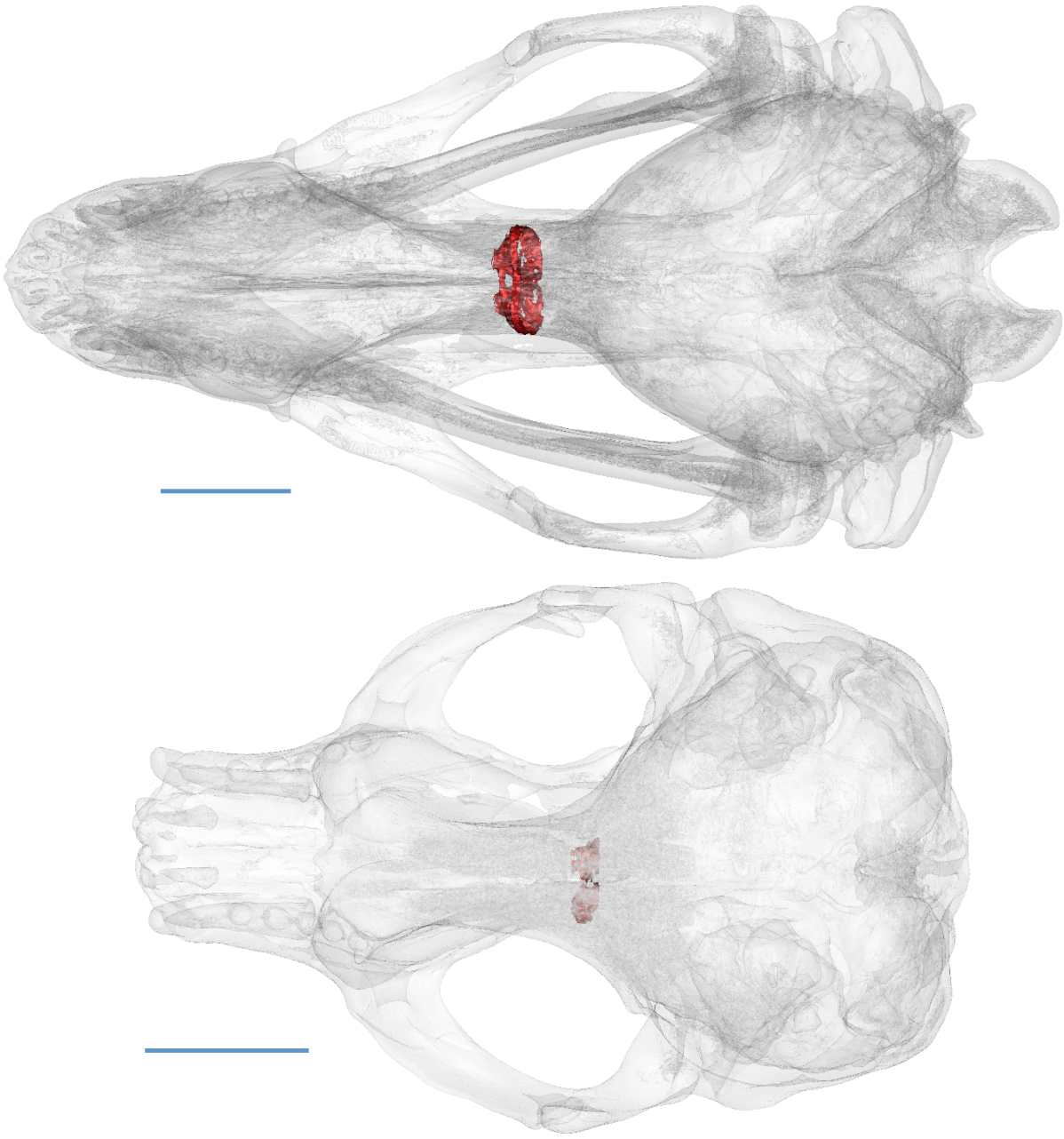

Figure 3-16. **CP morphology in shallow and deep diving phocids.** CP (red) in phocid skull models viewed dorsally. Above: the leopard seal (*Hydrurga leptonyx*), a relatively shallow diver; below: Female northern elephant seal (*Mirounga angustirostris*), a deep diver. Scale bar: 50 mm.

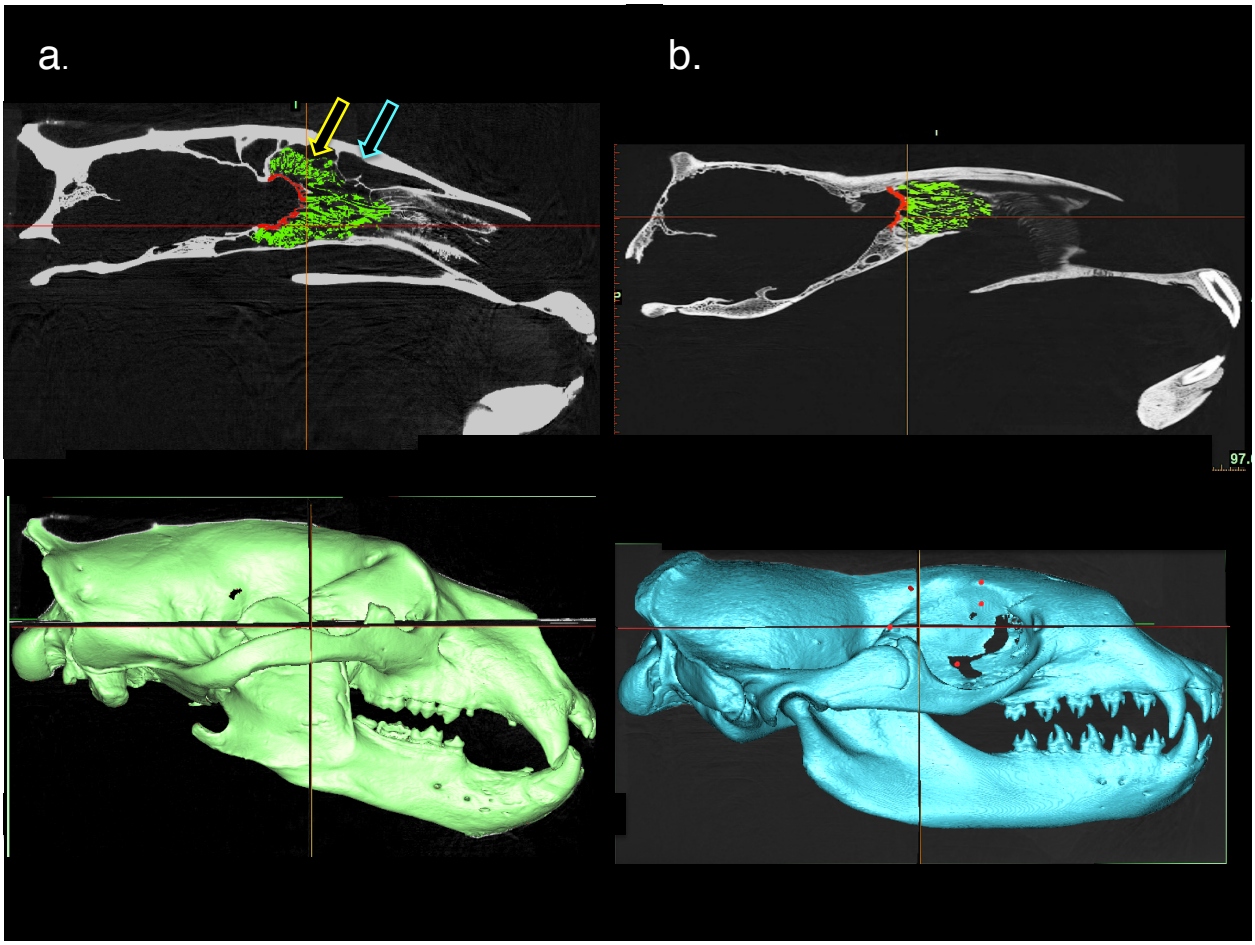

Figure 3-17. **Dorsal constraint on ethmoturbinals in aquatic carnivorans. Column a.:** Polar bear (*Ursus maritimus*). Top: sagittal section of CT scan. Frontal sinus (blue arrow) is present in terrestrial carnivorans. Ethmoturbinals (green) extend from CP (red) into sinuses (yellow arrow). **Column b.:** Leopard seal (*Hydrurga leptonyx*). Top: sagittal section of CT scan. Sinuses are absent in aquatic species and ethmoturbinals are absent dorsal to the CP.

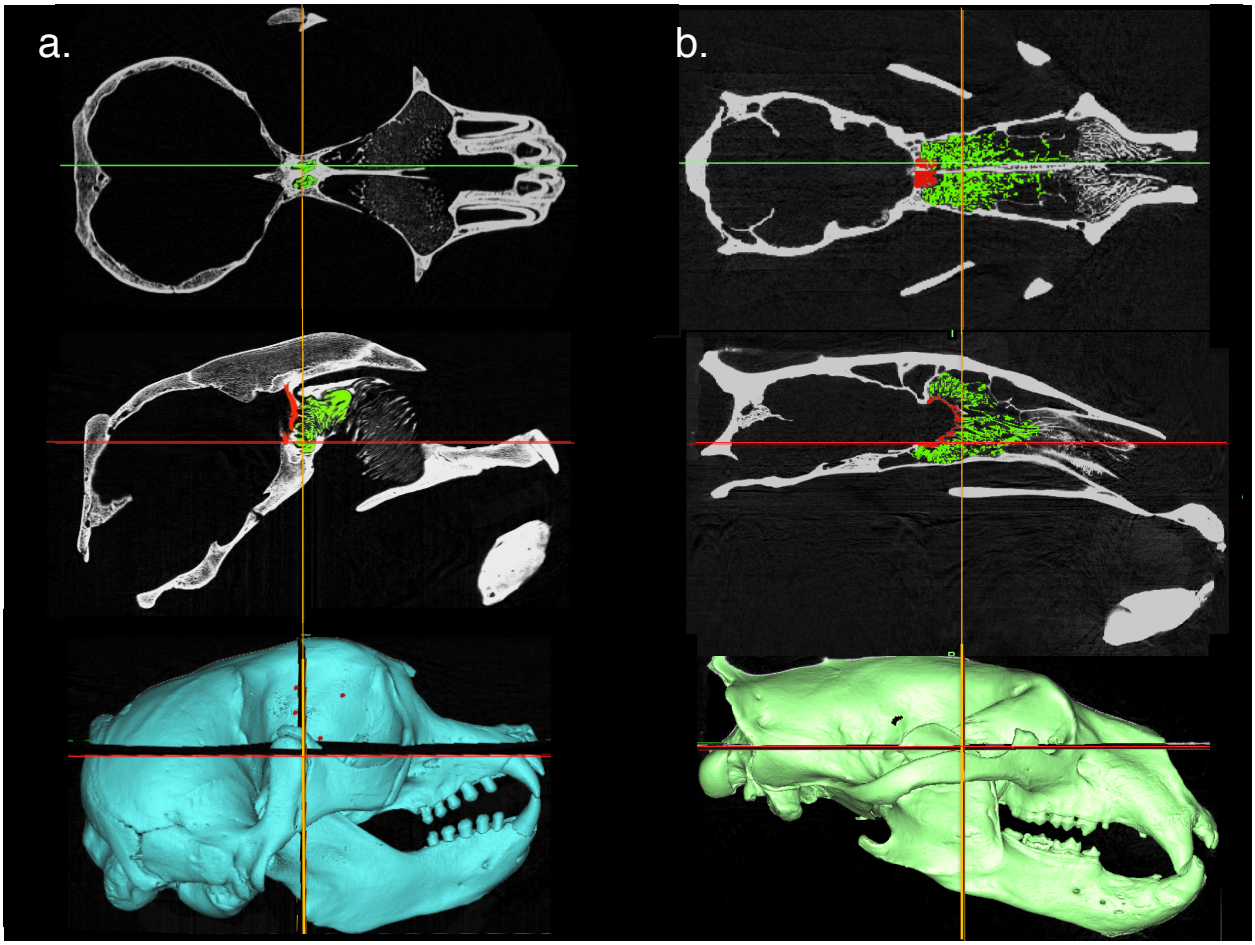

Figure 3.18. **Structural constraints on ethmoturbinals in aquatics. Column a,** Female northern elephant seal (*Mirounga angustirostris*). **Column b,** Polar bear (*Ursus maritimus*). **Top**: CT scan sectioned along horizontal axis (red line in center and bottom rows). Elephant seal's nasal cavity is laterally constricted between large orbits anterior to the CP (red) and contains few ethmoturbinals (green) in contrast to the polar bear's nasal cavity at this juncture. **Center**: Sagittal sections of CT scans are oriented relative to skull models below. Elephant seal ethmoturbinals are reduced ventral and anterior to CP compared with the polar bear due to the narrow interorbital space.

Table 3-1. **Morphological and ecological parameters for sample species.** CP, cribriform plate; OOL, orbit to occipital length; RelCP, relative cribriform plate size; Max., maximum.

Family	Species	Common name	CP surface area; species mean (mm^2)	OOL species mean (mm)	RelCP (all species)	RelCP (aquatics only)	RelCP (phocids only)	Max. dive depth (m)	Mean dive depth (m)	Max. dive duration (min)	Mean dive duration (min)	Sources of diving data
Phocidae												
	Erignathus barbatus	Bearded seal	402.875	147.29	-0.1331	0.0223	0.1006	288	17.2	18.7	2	Krafft et al., 2000
	Hydrurga leptonyx	Leopard seal	982.855	264.06	-0.0462	0.0342	0.1180	424.5	44	9.35	2	Kuhn et al., 2006
	Leptonychotes weddellii	Weddell seal	548.55	214.5	-0.1925	-0.0854	-0.0036	726	212	78	15.9	Shreer & Testa, 1996; Shreer & Kovacs, 1997
	Mirounga angustirostris	Northern elephant seal	519.807	267.22	-0.3289	-0.2501	-0.1662	1529	504.2	77	22.5	LeBoeuf et al., 1988; Delong & Stewart, 1991
	Monachus tropicalis	Tropical monk seal	458.943	178.74	-0.1761	-0.0456	0.0345	500	41	20	8	Delong et al., 1984; Parrish et al., 2000
	Phoca sibirica	Baikal seal	187.99	109.44	-0.3114	-0.1177	-0.0423	300	68.9	40	4.8	Stewart et al., 1996; Ponganis et al., 1997; Watanabe et al., 2004
	Phoca vitulina	Harbor seal	327.66	140.383	-0.1982	-0.0365	0.0412	508	148.7	28	3.2	Hastings et al., 2001
	Pusa hispida	Ringed seal	205.821	124.06	-0.3365	-0.1590	-0.0824	360	145.6	39	5.1	Teilman et al., 1999; Gjertz et al., 2000; Born et al., 2004
Otariidae												
	Arctocephalus galapagoensis	Galapagos fur seal	524.4	152.22	-0.0356	0.1156	NA	186	37.3	6	3.4	Kooyman & Trillmich, 1986
	Arctocephalus pusillus	Cape fur seal	505.92	172.92	-0.1168	0.0180	NA	204	58.2	8	2.9	Kooyman & Gentry, 1976; Arnould & Hindell, 2001
	Callorhinus ursinus	Northern fur seal	432.40	146.79	-0.1007	0.0552	NA	256	17.5	9.92	1.24	Ponganis et al., 1992; Sterling & Ream, 2004
	Eumatopias jubatus	Steller sea lion	1235.81	268.6	0.0445	0.1226	NA	328	18.2	14	1.1	Loughlin et al., 2003
	Otaria byronia	South American sea lion	571.405	199.96	-0.1387	-0.0225	NA	243	25.3	7.7	1.9	Werner & Campangna, 1995; Thompson et al., 1998
	Zalophus californianus	California sea lion	785.420	190.14	0.0254	0.1480	NA	544	32.2	20.1	1.9	Costa, et al., 2007
Odobenidae												
	Odobedus rosmarus	Walrus	1018.146	258.82	-0.0206	0.0624	NA	102	22.5	24	6	Fay, 1982; Gjertz et al., 2001
Mustelidae												
	Enhydra lutris	Sea otter	342.08	110.11	-0.0545	0.1384	NA	100	18.9	4	1.4	Bodkin et al., 2004; Yeates et al., 2007
	Gulo gulo	Wolverine	851.74	102.191	0.3801	NA	NA	NA	NA	NA	NA	NA
	Lontra canadensis	North American river otter	252.03	88.1904	-0.073	NA	NA	NA	NA	NA	NA	NA
	Mustela frenata	Long-tailed weasel	59.96	35.045	-0.2217	NA	NA	NA	NA	NA	NA	NA
	Neovison vison	American mink	125.09	59.96	-0.1787	NA	NA	NA	NA	NA	NA	NA
	Taxidea taxus	American badger	601.39	82.15	0.3412	NA	NA	NA	NA	NA	NA	NA
Procyonidae						NA	NA	NA	NA	NA	NA	NA
	Potos flavus	Kinkajoo	248.69	65.6583	0.0730	NA	NA	NA	NA	NA	NA	NA
	Procyon lotor	Raccoon	382.54	76.7354	0.1798	NA	NA	NA	NA	NA	NA	NA
Mephitidae						NA	NA	NA	NA	NA	NA	NA
	Mephitis mephitis	Striped skunk	307.00	53.27	0.2721	NA	NA	NA	NA	NA	NA	NA
Ursidae												
	Ailuropoda melanoleuca	Giant panda	741.58	170.52	0.0565	NA	NA	NA	NA	NA	NA	NA
	Ursus americanus	Black bear	1721.6075	168.377	0.4288	NA	NA	NA	NA	NA	NA	NA
	Ursus arctos	Grizzly bear	2250.22	212.528	0.42525	NA	NA	NA	NA	NA	NA	NA
	Ursus maritimus	Polar bear	2925.7249	259.514	0.43649	NA	NA	NA	NA	NA	NA	NA

Table 3-2. Summary statistics. Results from generalized least squares regressions (GLS), phylogenetic least squares regressions (PGLS), ANOVA and Tukey HSD post hoc tests performed on morphological, habitat and diving parameters. CP, cribriform plate; RelCP, relative cribriform plate; OOL, orbit to occipital length

Regression	*n*	r^2	*P* value	Slope	PGLS r^2	*P* value
CP metrics						
CP surface area (log_{10}) vs CP foramina cross-sectional area (log_{10}), all species	28	0.91	<0.0001	1.04		
CP vs body size proxy OOL						
CP surface area (log_{10}) vs OOL (log_{10}) in all species	28	0.58	<0.0001	1.18		
CP surface area (log_{10}) vs OOL (log_{10}) in aquatic species only	16	0.76	<0.0001	1.48		
CP surface area (log_{10}) vs OOL (log_{10}) in terrestrial species only	10	0.9	<0.0001	1.71		
Maximum diving depth						
RelCP vs Max Depth (log_{10}); all aquatics	16	0.39	0.01		<0.1	NS
RelCP vs Max Depth (log_{10}); phocids only	8	0.34	0.13		0.11	NS
Mean diving depth						
RelCP vs Mean Depth (log_{10}); all aquatics	16	0.67	<0.0001		0.29	0.03
RelCP vs Mean Depth (log_{10}); phocids only	8	0.64	0.016		0.37	NS
Maximum diving duration						
RelCP vs Max Duration (log_{10}); all aquatics	16	0.56	0.0009		0.17	NS
RelCP vs Max Duration (log_{10}); phocids only	8	0.67	0.013		0.6	0.02
Mean diving duration						
RelCP vs Mean Duration (log_{10}); all aquatics	16	0.58	0.0006		0.42	0.006
RelCP vs Mean Duration (log_{10}); phocids only	8	0.59	0.027		0.67	0.012

Pair-wise ANOVA	*n*	Tukey HSD post-hoc test *P* value	Phylogenetic ANOVA
Phylogeny and RelCP			
RelCP, Phocids vs Otariids	14	0.033	
RelCP, Phocids vs Otariids and Odobenid	15	0.009	
Habitat and RelCP			
RelCP, Aquatics vs Terrestrials	26	< 0.0001	< 0.0001
RelCP, Aquatics vs Semi-aquatics	18	0.99	0.33
RelCP, Terrestrials vs Semi-aquatics	12	0.019	0.26
Habitat and snout length			
Snount length, Aquatics vs Terrestrials	23	0.006	

Table 3-3. **Specimen sources and morphological data.** OOL, orbit to occipital length; CP, cribriform plate surface area; F, female; M, male; U, unknown sex. Museums and collections: H, Illinois State Museum; IZCA, Institute of Zoology of the Chinese Academy of Sciences; LACM, Museum of Natural History Los Angeles; MFWP, Montana Fish, Wildlife and Parks; MVZ, Museum of Vertebrate Zoology; SO, Southwest Fisheries: UCLA, Donald R. Dickey Collection, USNM, United States National Museum.

Species	Sex	ID number	OOL (mm)	CP (mm^2)	Habitat
Mephitis mephitis	M	USNM147553	56.49	334.6465	Terrestrial
Mephitis mephitis	F	UCLAJXS001	50.0481	279.3483	Terrestrial
Enhydra lutris	M	SO2951	113.93	363.128	Aquatic
Enhydra lutris	F	SO2853-97	106.29	321.03	Aquatic
Gulo gulo	M	USNM314885	103.6	889.5978	Terrestrial
Gulo gulo	F	USNM157327	100.7816	813.8828	Terrestrial
Lontra canadensis	M	UCLA15275	87.1432	223.285	Semi-aquatic
Lontra canadensis	F	UCLA18958	89.2375	280.7714	Semi-aquatic
Mustela frenata	M	USNM52702	38.54	70.4281	Terrestrial
Mustela frenata	F	USNM95054	31.55	49.4953	Terrestrial
Neovison vison	M	UCLA8488	59.96	125.0899	Semi-aquatic
Taxidea taxus	M	UCLA14841	78	558.6181	Terrestrial
Taxidea taxus	F	LACM45012	86.3	644.1695	Terrestrial
Potos flavus	M	USNM291066	66.7551	268.5371	Terrestrial
Potos flavus	F	LACM07241	64.5614	228.8372	Terrestrial
Procyon lotor	M	LACM52261	75.5338	353.0767	Terrestrial
Procyon lotor	F	LACM07241	77.937	412.0005	Terrestrial
Ailuropda melanoleuca	U	IZCAS6072	170.52	741.58	Terrestrial
Ursus americanus	M	USNM22070	178.74	2218.05	Terrestrial
Ursus americanus	F	USNM211397	129.7902	1339.3636	Terrestrial
Ursus americanus	M	MVZ162985	196.6	1607.409	Terrestrial
Ursus arctos	M	USNM82003	237.1369	2964.92	Terrestrial
Ursus arctos	F	USNM98062	205.6464	2317.9226	Terrestrial
Ursus arctos	U	MFWP113	194.8	1467.8174	Terrestrial
Ursus maritimus	F	MVZ123991	232.1	2453.5782	Terrestrial
Ursus maritimus	M	H001_51	266.7369	2800.1365	Terrestrial
Ursus maritimus	U	USNM275072	279.7043	3523.46	Terrestrial
Erignathus barbatus	M	LACM072575	139.56	337.599	Aquatic
Erignathus barbatus	F	LACM072576	155.01	468.15	Aquatic
Hydrurga leptonyx	M	USNM270326	254.23	992.4106	Aquatic
Hydrurga leptonyx	F	USNM269533	273.88	973.2998	Aquatic
Leptonychotes weddellii	F	MVZ127755	214.5	548.55	Aquatic
Mirounga	F	MVZ 184140	181.51	310.619	Aquatic

angustirostris					
Mirounga angustirostris	M	LACM054394	352.92	728.995	Aquatic
Monachus tropicalis	M	USNM100358	187.09	510.8872	Aquatic
Monachus tropicalis	F	USNM102527	170.38	406.998	Aquatic
Phoca sibirica	U	LACM52337	109.44	187.99	Aquatic
Phoca vitulina	U	UCLA1408	156.9	339.304	Aquatic
Phoca vitulina	M	LACM095963	125.21	294.997	Aquatic
Phoca vitulina	F	LACM31462	139.04	348.67	Aquatic
Pusa hispida	M	LACM54781	132.37	216.291	Aquatic
Pusa hispida	F	LACM22949	115.75	195.35	Aquatic
Arctocephalus galapagoensis	M	LACM031309	152.22	524.4	Aquatic
Arctocephalus pusillus	M	LACM052358	190.35	614.918	Aquatic
Arctocephalus pusillus	F	LACM052359	155.49	396.923	Aquatic
Callorhinus ursinus	M	LACM052343	144.56	453.18	Aquatic
Callorhinus ursinus	F	LACM054630	149.01	411.629	Aquatic
Eumetopias jubatus	M	LACM052314	295.39	1475.2	Aquatic
Eumetopias jubatus	F	LACM052316	241.81	996.411	Aquatic
Otaria byroni	M	LACM095756	237.95	681.189	Aquatic
Otaria byroni	F	LACM095771	161.96	461.62	Aquatic
Zalophus californianus	M	UCLA252	214.3	868.2482	Aquatic
Zalophus californianus	F	LACM95730	155.72	599.4903	Aquatic
Zalophus californianus	M	UCLA1118	200.39	888.52	Aquatic
Odobenus rosmarus	F	UCLA2471	258.82	1018.146	Aquatic

References

Amo, L., Rodríguez-Gironés, M. Á. & Barbosa, A. Olfactory detection of dimethyl sulphide in a krill-eating Antarctic penguin. *Mar. Ecol. Prog. Ser.* **474,** 277–285 (2013).

Berta, A., Sumich, J. L. & Kovacs, K. M. *Marine Mammals: Evolutionary Biology*. (Academic Press, 2015).

Bird, D. J., Amirkhanian, A., Pang, B. & Van Valkenburgh, B. Quantifying the cribriform plate: influences of allometry, function, and phylogeny in Carnivora. *Anat. Rec. (Hoboken).* **297,** 2080–2092 (2014).

Born, E. W., Teilmann, J., Acquarone, M. & Riget, F. F. Habitat use of ringed seals (Phoca hispida) in the North Water area (North Baffin Bay). *Arctic* 129–142 (2004).

Buhl, E. H. & Oelschläger, H. A. Ontogenetic development of the nervus terminalis in toothed whales - Evidence for its non-olfactory nature. *Anat. Embryol. (Berl).* **173,** 285–294 (1986).

Burton, R. K. & Koch, P. L. Isotopic tracking of foraging and long-distance migration in northeastern Pacific pinnipeds. *Oecologia* **119,** 578–585 (1999).

Costa, D. P., Kuhn, C. & Weise, M. Foraging ecology of the California sea lion: Diet, diving behavior, foraging locations, and predation impacts on fisheries resources. *Calif. Sea Grant Coll. Progr.* (2007).

Costa, D. P., Kuhn, C. & Weise, M. Foraging ecology of the California sea lion: Diet, diving behavior, foraging locations, and predation impacts on fisheries resources. (2007).

Costa, D. P. *et al.* Accuracy of ARGOS locations of pinnipeds at-sea estimated using fastloc GPS. *PLoS One* **5,** (2010).

Craven, B., Paterson, E. G. & Settles, G. S. The fluid dynamics of canine olfaction: unique nasal airflow patterns as an explanation of macrosmia. *J. R. Soc. Interface* **7,** 933–43 (2009).

Curtis, A. A., Lai, G., Wei, F. & Van Valkenburgh, B. Repeated loss of frontal sinuses in arctoid carnivorans. *J. Morphol.* **276,** 22–32 (2015).

Dacey, J. W. H. & Wakeham, S. G. Oceanic dimethylsulfide: production during zooplankton grazing on phytoplankton. *Science (80-.).* **233,** 1314–1317 (1986).

Davis, R. W. & Weihs, D. Locomotion in diving elephant seals: physical and physiological constraints. *Philos. Trans. R. Soc. Lond. B. Biol. Sci.* **362,** 2141–2150 (2007).

Debey, L. B. & Pyenson, N. D. Osteological correlates and phylogenetic analysis of deep diving in living and extinct pinnipeds: What good are big eyes? *Mar. Mammal Sci.* **29,** 48–83 (2012).

DeLong, R. L., Kooyman, G. L., Gilmartin, W. G. & Loughlin, T. R. Hawaiian monk seal diving behavior. *Acta Zool. Fenn.* **172,** 129–131 (1984).

Delong, R. L. & Stewart, B. S. Diving Patterns of Northern Elephant Seal Bulls. *Mar. Mammal Sci.* **7,** 369–384 (1991).

Deméré, T. A., Berta, A. & Adam, P. J. Chapter 3: Pinnipedimorph evolutionary biogeography. *Bull. Am. Museum Nat. Hist.* 32–76 (2003).

England, D. R. & Dillon, L. S. Cerebrum of sea otter. *Texas J. Sci.* **24,** 221 (1972).

Ewer, R. F. *The carnivores*. (Cornell University Press, 1973).

Farbman, A. I. *Cell biology of olfaction*. **27,** (Cambridge University Press, 1992).

Fay, F. H. Ecology and Biology of the Pacific Walrus, *Odobenus rosmarus divergens* Illiger. *North Am. Fauna* 1–279 (1982). doi:10.3996/nafa.74.0001

Folkow, L. P., Blix, A. S. & Eide, T. J. Anatomical and functional aspects of the nasal mucosal and ophthalmic retia of phocid seals. *J. Zool.* **216,** 417–436 (1988).

Fritz, S. A., Bininda-Emonds, O. R. P. & Purvis, A. Geographical variation in predictors of mammalian extinction risk: Big is bad, but only in the tropics. *Ecol. Lett.* **12,** 538–549 (2009).

Gittleman, J. L. *Carnivore behavior, ecology, and evolution*. (Springer Science & Business Media, 2013).

Gjertz, I., Kovacs, K. M., Lydersen, C. & Wiig, Ø. Movements and diving of adult ringed seals (Phoca hispida) in Svalbard. *Polar Biol.* **23,** 651–656 (2000).

Gjertz, I., Griffiths, D., Krafft, B. A., Lydersen, C. & Wiig, Ø. Diving and haul-out patterns of walruses Odobenus rosmarus on Svalbard. *Polar Biol.* **24,** 314–319 (2001).

Graziadei, P. P. C. & Graziadei, G. A. M. Neurogenesis and plasticity of the olfactory sensory neurons. *Ann. N. Y. Acad. Sci.* **457,** 127–142 (1985).

Harrison, R. J. & Kooyman, G. L. General physiology of the pinnipedia. *Behav. Physiol. Pinnipeds. Appleton-Century-Crofts, New York, NY* 211–296 (1968).

Hastings, K. K., Small, R. J., Simpkins, M. A. & Swain, U. G. Dive behavior of adult and subadult harbor seals from Kodiak Island and Southeast Alaska. *Harb. Seal Investig.*

Alaska. Annu. Rep. NOAA Award NA87FX0300. Alaska Dep. Fish Game, Div. Wildl. Conserv. Anchorage, AK 184–208 (2001).

Hayden, S. *et al.* Ecological adaptation determines functional mammalian olfactory subgenomes. *Genome Res.* **20,** 1–9 (2010).

Kastak, D. & Schusterman, R. J. In-air and underwater hearing sensitivity of a northern elephant seal (*Mirounga angustirostris*). *Can. J. Zool.* **77,** 1751–1758 (1999).

Koepfli, K. P. *et al.* Multigene phylogeny of the Mustelidae: Resolving relationships, tempo and biogeographic history of a mammalian adaptive radiation. *BMC Biol.* **6,** 10 (2008).

Kooyman, G. L., Gentry, R. L. & Urquhart, D. L. Northern fur seal diving behavior: a new approach to its study. *Science.* **193,** 411–412 (1976).

Kooyman, G. L. & Trillmich, F. Diving behavior of Galapagos sea lions in *Fur seals* (1986).

Kooyman, G. & Ponganis, P. The physiological basis of diving to depth: Birds and Mammals. *Annu. Rev. Physiol*. 1998.60:19-32.

Kowalewsky, S., Dambach, M., Mauck, B. & Dehnhardt, G. High olfactory sensitivity for dimethyl sulphide in harbour seals. *Biol. Lett.* **2,** 106–109 (2006).

Krafft, B. A., Lydersen, C., Kovacs, K. M., Gjertz, I. & Haug, T. Diving behaviour of lactating bearded seals (Erignathus barbatus) in the Svalbard area. *Can. J. Zool.* **78,** 1408–1418 (2000).

Kröger, R. H. H. & Katzir, G. Comparative anatomy and physiology of vision in aquatic tetrapods. *Sensory evolution on the threshold—adaptations in secondarily aquatic vertebrates.* (University of California Press, Berkeley,, 2008).

Kuhn, C. E. *et al.* Diving physiology and winter foraging behavior of a juvenile leopard seal (Hydrurga leptonyx). *Polar Biol.* **29,** 303–307 (2006).

LeBoeuf, B. J., Costa, D. P., Huntley, A. C. & Feldkamp, S. D. Continuous, deep diving in female northern elephant seals, *Mirounga angustirostris*. *Can. J. Zool. Can. Zool.* **66,** 446–458 (1988).

Levenson, D. H. & Schusterman, R. J. Dark Adaptation and Visual Sensitivity in Shallow and Deep-Diving Pinnipeds1. *Mar. Mammal Sci.* **15,** 1303–1313 (1999).

Loughlin, T. R., Sterling, J. T., Merrick, R. L., Sease, J. L. & York, A. E. Diving behavior of immature Steller sea lions (*Eumetopias jubatus*). *Fish. Bull.* **101,** 566–582 (2003).

Lowell, W. R. & Flanigan, W. F. Marine Mammal Chemoreception. *Mamm. Rev.* **10,** 53–59 (1980).

Marshall, C. D., Amin, H., Kovacs, K. M. & Lydersen, C. Microstructure and innervation of the mystacial vibrissal follicle-sinus complex in bearded seals,(*Erignathus barbatus;* Pinnipedia*:* Phocidae). *Anat. Rec. Part A Discov. Mol. Cell. Evol. Biol.* **288A,** 13–25 (2006).

Meredith, R. W. *et al.* Impacts of the Cretaceous Terrestrial Revolution and KPg extinction on mammal diversification. *Science* **334,** 521–4 (2011).

Negus, V. The Comparative Anatomy of the Nose and Paranasal sinuses. Livingstone. (1958).

Nevitt, G. Olfactory foraging in Antarctic seabirds: A species-specific attraction to krill odors. *Mar. Ecol. Prog. Ser.* **177,** 235–241 (1999).

Nevitt, G. A., Veit, R. R. & Kareiva, P. Dimethyl sulphide as a foraging cue for Antarctic procellariiform seabirds. *Nature* **376,** 680 (1995).

Nordøy, E. S. & Blix, A. S. Movements and dive behaviour of two leopard seals (*Hydrurga leptonyx)* off Queen Maud Land, Antarctica. *Polar Biol.* **32,** 263–270 (2008).

Nowak, R. M. *Walker's Mammals of the World*. **1,** (JHU Press, 1999).

Odend'hal, S. & Poulter, T. C. Pressure Regulation in the Middle Ear Cavity of Sea Lions: A Possible Mechanism. *Science (80-.).* **153,** 768–769 (1966).

Oelschläger, H. H. a & Buhl, E. H. Development and rudimentation of the peripheral olfactory system in the harbor porpoise *Phocoena phocoena* (Mammalia: Cetacea). *J. Morphol.* **184,** 351–360 (1985).

Orme, D. The caper package: comparative analysis of phylogenetics and evolution in R. *R Package version* **5,** (2013).

Parrish, F. A., Craig, M. P., Ragen, T. J., Marshall, G. J. & Buhleier, B. M. Identifying diurnal foraging habitat of endangered Hawaiian monk seals using a seal-mounted video camera. *Mar. Mammal Sci.* **16,** 392–412 (2000).

Pauly, D., Trites, A. W., Capuli, E. & Christensen, V. Diet composition and trophic levels of marine mammals. *Ices J. Mar. Sci.* **55,** 467–481 (1998).

Peterson, R. S. & Bartholomew, G. A. The natural history and behavior of the California sea lion. *Soc. Mammal. Spec. Pub* (1967).

Peterson, R. S. & Bartholomew, G. A. *The natural history and behaviour of the California sea lion*. (1967).

Pihlström, H. Comparative anatomy and physiology of chemical senses in aquatic mammals. *Sens. Evol. Threshold Adapt. Second. Aquat. Vertebr.* 95–109 (2008).

Pihlström, H., Fortelius, M., Hemilä, S., Forsman, R. & Reuter, T. Scaling of mammalian ethmoid bones can predict olfactory organ size and performance. *Proc. Biol. Sci.* **272,** 957–962 (2005).

Ponganis, P. J., Gentry, R. L., Ponganis, E. P. & Ponganis, K. V. Analysis of swim velocities during deep and shallow dives of two northern fur seals, Callorhinus ursinus. *Mar. Mammal Sci.* **8,** 69–75 (1992).

Ponganis, P. J., Kooyman, G. L., Baranov, E. A., Thorson, P. H. & Stewart, B. S. The aerobic submersion limit of Baikal seals, Phoca sibirica. *Can. J. Zool.* **75,** 1323–1327 (1997).

Reidenberg, J. S. Anatomical adaptations of aquatic mammals. *Anat. Rec.* **290,** 507–513 (2007).

Repenning, C. A. Adaptive Evolution of Sea Lions and Walruses. **25,** 251–259 (1976).

Repenning, C. A. Underwater hearing in seals: functional morphology. *Funct. Anat. Mar. Mamm.* **1,** 307–331 (1972).

Riedman, M. L. & Estes, J. a. The Sea Otter (Enhydra lutris): Behavior , Ecology , and Natural History. *Biol. Rep.* **90,** 1–136 (1990).

Ross, G. J. B. Nuzzling behaviour in captive Cape fur seals Gestation periods and age of sexual maturity of some African antelopes. (1970).

Rowe, T. B., Eiting, T. P., Macrini, T. E. & Ketcham, R. A. Organization of the olfactory and respiratory skeleton in the nose of the gray short-tailed opossum *Monodelphis domestica*. *J. Mamm. Evol.* **12,** 303–336 (2005).

Scheffer, V. B. *Seals, sea lions, and walruses: a review of the Pinnipedia*. (Stanford University Press, 1958).

Scholander, P. F. Experimental investigations on the respiratory function in diving mammals and birds. (2009).

Schreer, J. F. & Kovacs, K. M. Allometry of diving capacity in air-breathing vertebrates. *Can. J. Zool. Can. Zool.* **75,** 339–358 (1997).

Schreer, J. F., Kovacs, K. M. & Hines, R. J. O. Comparative diving patterns of pinnipeds and seabirds. *Ecol. Monogr.* **71,** 137–162 (2001).

Schreer, J. F. & Testa, J. W. Classification of Weddell seal diving behaviour. *Mar. Mammal Sci.* **12,** 227–250 (1996).

Slater, G. J., Harmon, L. J. & Alfaro, M. E. Integrating fossils with molecular phylogenies improves inferences of trait evolution. *Evolution.* **66,** 3931–3944 (2012).

Sousa, R., Dias, S. & Antunes, C. Subtidal macrobenthic structure in the lower lima estuary, NW of Iberian Peninsula. *Ann. Zool. Fennici* **44,** 303–313 (2007).

Stephens, R. J., Beebe, I. J. & Poulter, J. C. Innervation of the vibrissae of the California sea lion, Zalophus californianus. *Anat. Rec.* **176,** 421–442 (1973).

Sterling, J. T. & Ream, R. R. At-sea behavior of juvenile male northern fur seals (*Callorhinus ursinus*). *Can. J. Zool.* **82,** 1621–1637 (2004).

Stewart, B. S., Petrov, E. a, Baranov, E. a, Timonin, a & Ivanov, M. Seasonal movements and dive patterns of juvenile Baikal seals, Phoca sibirica. *Mar. Mammal Sci.* **12,** 528–542 (1996).

Stirling, I. The social evolution of mating systems in pinnipeds. *Adv. study Mamm. Behav.* **7,** 489–527 (1983).

Teilmann, J., Born, E. W. & Acquarone, M. Behaviour of ringed seals tagged with satellite transmitters in the North Water polynya during fast-ice formation. *Can. J. Zool.* **77,** 1934–1946 (1999).

Thompson, D., Duck, C. D., McConnell, B. J. & Garrett, J. Foraging behaviour and diet of lactating female southern sea lions (Otaria flavescens) in the Falkland Islands. *J. Zool.* **246,** 135–146 (1998).

Van Valkenburgh, B. Skeletal and dental predictors of body mass in carnivores. *Body size Mamm. Paleobiol. Estim. Biol. Implic.* **18,** 1–205 (1990).

Van Valkenburgh, B. *et al.* Aquatic adaptations in the nose of carnivorans: evidence from the turbinates. *J. Anat.* **218,** 298–310 (2011).

Watanabe, Y., Baranov, E. A., Sato, K., Naito, Y. & Miyazaki, N. Foraging tactics of Baikal seals differ between day and night. *Mar. Ecol. Prog. Ser.* **279,** 283–289 (2004).

Welsch, U. & Riedelsheimer, B. Histophysiological observations on the external auditory meatus, middle, and inner ear of the Weddell seal (Leptonychotes weddelli). *J. Morphol.* **234,** 25–36 (1997).

Werner, R. & Campagna, C. Diving behaviour of lactating southern sea lions (Otaria flavescens) in Patagonia. *Can. J. Zool.-Rev. Can. Zool.* **73,** 1975–1982 (1995).

Wyss, A. R. The walrus auditory region and the monophyly of pinnipeds. *Amer. Museum Novit.* (1987).